

THESIS FOR THE DEGREE OF DOCTOR OF PHILOSOPHY (PHD)

**Exploring the diverse cellular functions of the proteasome activator  
PA200**

by Douda Abdenour

Supervisor: Dr. Tar Krisztina



UNIVERSITY OF DEBRECEN  
DOCTORAL SCHOOL OF MOLECULAR MEDICINE

DEBRECEN, 2021

# TABLE OF CONTENTS

<b>TABLE OF CONTENTS</b> .....	<b>2</b>
<b>ABBREVIATIONS</b> .....	<b>5</b>
<b>INTRODUCTION</b> .....	<b>8</b>
<b>REVIEW OF THE LITERATURE</b> .....	<b>10</b>
Proteolysis .....	10
<i>Lysosome mediated protein degradation</i> .....	11
<i>Autophagy</i> .....	11
<i>Macroautophagy</i> .....	11
<i>Microautophagy</i> .....	12
<i>CMA</i> .....	12
<i>Proteasome mediated protein degradation</i> .....	13
Structure and function of proteasome.....	15
<i>The 20S proteasome: The Proteolytic Core</i> .....	15
<i>Tissue-specific proteasomes</i> .....	17
<i>The activator families of the proteasome</i> .....	18
<i>The 19S regulatory subunit (PA700/RP)</i> .....	18
<i>The 11S regulators: PA28<math>\alpha\beta</math> and PA28<math>\gamma</math> (REG)</i> .....	19
<i>The Proteasome activator 200 kDa (PA200)</i> .....	20
<i>The structure of PA200</i> .....	21
<i>Biological functions of the PA200/Blm10 family</i> .....	24
<i>DNA double-strand breaks (DSBs) repair</i> .....	24
<i>The degradation of acetylated histones</i> .....	26
<i>The role of the Blm10/PA200 family in the maintenance of mitochondrial integrity</i> .....	27
<i>Cardiovascular disease and fibrosis</i> .....	27
<i>The role of PA200/Blm10 in aging</i> .....	28
Mitochondria .....	29
<i>Mitochondrial dynamics</i> .....	30
<i>The mitochondrial fission and fusion machinery</i> .....	32
<i>Outer membrane fission by Drp1</i> .....	32
<i>Inner membrane fission by S-OPA1 and MTP18</i> .....	32
<i>Outer membrane fusion by mitofusins</i> .....	33
<i>Inner membrane fusion by OPA1</i> .....	33
<i>Mitochondrial bioenergetics</i> .....	36
<i>Mitochondrial respiratory chain inhibitors</i> .....	38
<i>Diseases related to mitochondrial dysfunctions</i> .....	39
Cross-talk between the UPS and mitochondria .....	41
<b>AIMS</b> .....	<b>43</b>
<b>MATERIALS AND METHODS</b> .....	<b>44</b>
<i>Chemical and reagents</i> .....	44
<i>Antibodies</i> .....	45
<i>Cell culture</i> .....	46

<i>Downregulation of PSME4/PA200</i> .....	46
<i>Antibiotic titration and selection of shPA200 cells</i> .....	47
<i>Cell lysis and protein measurement</i> .....	48
<i>Subcellular fractionation</i> .....	48
<i>RNA extraction</i> .....	48
<i>Reverse transcription and cDNA synthesis</i> .....	49
<i>Quantitative Real-Time PCR</i> .....	49
<i>Chromatin Immunoprecipitation (ChIP)</i> .....	51
<i>ChIP-Seq analysis</i> .....	52
<i>Mitochondrial live staining in high content screening (HCS) system</i> .....	52
<i>Mitochondrial morphology analysis</i> .....	53
<i>Measurements of mitochondrial membrane potential (<math>\Delta\Psi_m</math>)</i> .....	53
<i>Measurement of reactive oxygen species (ROS)</i> .....	54
<i>Sulforhodamine B (SRB) assay</i> .....	54
<i>Lactate dehydrogenase (LDH) assay</i> .....	55
<i>Cell cycle assay</i> .....	55
<i>Human phospho-kinase array analysis</i> .....	56
<i>SDS-PAGE and Western blot</i> .....	56
<i>Glycolysis and mitochondrial bioenergetics measurements</i> .....	57
<i>Protein carbonyl assay</i> .....	58
<i>RNA sequencing (RNA-seq) and RNA-Seq data analysis</i> .....	58
<i>Functional analysis of RNA-Seq data</i> .....	59
<i>Statistical analysis</i> .....	59
<b>RESULTS</b> .....	<b>60</b>
<i>Stable depletion of PSME4/PA200 in SH-SY5Y human neuroblastoma cells</i> .....	60
<i>Depletion of PA200 in neuroblastoma cells increases the expression of necrotic and apoptotic markers upon rotenone treatment</i> .....	62
<i>PA200 is over recruited to promoter regions of genes involved in cell cycle, metabolism, and protein modification processes</i> .....	65
<i>PA200 binds to and is distributed on promoters depending on the mitochondrial status</i> .....	67
<i>Study the expression of genes whose promoters are enriched in the anti-PA200 ChIP</i> .....	69
<i>PA200 affects cell cycle in a mitochondrial inhibitor dependent manner</i> .....	70
<i>PA200 regulates the expression of genes involved in cell proliferation and response to stress</i> .....	72
<i>PA200 knockdown leads to reduced c-Jun and phospho-c-Jun following rotenone administration</i> .....	73
<i>PA200-deficient cells exhibit mitochondrial dysfunction</i> .....	80
<i>PA200 knock-down reduces mitochondrial ETC biogenesis</i> .....	82
<i>Cells stably depleted of PA200 shift from OXPHOS to glycolysis</i> .....	84
<i>PA200-deficient cells exhibit fused mitochondrial morphology upon selective mitochondrial inhibitor treatment</i> .....	86
<i>Effects of PA200 depletion on genes related to mitochondrial dynamics</i> .....	90
<i>PA200-deficient cells demonstrate stabilized L-OPA1 isoform upon oligomycin treatment</i> .....	92
<i>Loss of PA200 increases ROS production and oxidized proteins upon mitochondrial stress</i> .....	94
<i>PA200 influences mitochondrial membrane potential (<math>\Delta\Psi_m</math>)</i> .....	96

**DISCUSSION.....97**  
**SUMMARY.....106**  
**KEYWORDS .....107**  
**ACKNOWLEDGMENT.....108**  
**REFERENCES .....109**  
**APPENDIX .....130**

## ABBREVIATIONS

2-DG	2-deoxy-D-glucose
AAA	ATPases Associated with a variety of cellular Activities
AAs	amino acids
AD	Alzheimer's disease
ADP	adenosine diphosphate
AKT	protein kinase B
ALS	amyotrophic lateral sclerosis
AMPK	AMP-activated protein kinase
ATG	autophagy-related
ATP	adenosine triphosphate
A $\beta$	amyloid- $\beta$ peptides
BRD	bromodomain
BSA	bovine serum albumin
ChIP	chromatin immunoprecipitation
ChIP-seq	chromatin immunoprecipitation sequencing
CI	NADH ubiquinone oxidoreductase
CII	succinate dehydrogenase
CIII	cytochrome c oxido-reductase
CIV	cytochrome c oxidase
CMA	Chaperone-mediated autophagy
CP	core particle
Cryo-EM	cryo-electron micrographs
Cu/Zn SOD	copper/zinc superoxide dismutase
Cyt <i>c</i>	cytochrome <i>c</i>
DEGs	differentially expressed genes
DGE	differential gene expression
dKO	double knockout
DMEM	Dulbecco's Modified Eagle's Medium
DMSO	dimethyl sulfoxide
Drp1	dynamain-related protein 1
DSBs	DNA double-strand breaks
DTT	Dithiothreitol
DUB	Deubiquitinase enzymes
ECAR	extracellular acidification rate
ECL	enhanced chemiluminescence
EDTA	Ethylenediamine tetraacetic acid
EGTA	ethylene glycol tetraacetic acid
ER	Endoplasmic reticulum
ES	embryonic stem
ETC	electron transport chain
FACS	fluorescence-activated single cell sorting
FAs	fatty acids
FBS	fetal bovine serum
FCCP	carbonyl cyanide-4 (trifluoromethoxy) phenylhydrazone

FDR	false discovery rate
Fis1	mitochondrial fission protein 1
GO	gene ontology
GPX	glutathione peroxidase
GSH	glutathione
GTP	guanosine triphosphate
H <sub>2</sub> O	water
H <sub>2</sub> O <sub>2</sub>	hydrogen peroxide
H <sub>2</sub> O <sub>2</sub>	hydrogen peroxide
HbYX	hydrophobic tyrosine-other
HCS	high content screening
HD	Huntington's disease
HEAT	Huntingtin - elongation factor 3 -PR65/A subunit of PP2A - lipid kinase TOR
HR	HEAT repeat
Hsc70	heat shock cognate protein 70
HSP90	heat shock protein 90
IMM	inner mitochondrial membrane
IMS	intermembrane space
INF $\gamma$	interferon gamma
IPF	idiopathic pulmonary fibrosis
IR	ionizing radiation
JNK	c-Jun N-terminal kinases
KO	knockout
LAMP	lysosome-associated membrane protein
LDH	lactate dehydrogenase
LG	L-glutamine
L-OPA1	long isoform of optic atrophy 1
MAD	mitochondria-associated degradation
MEF	murine embryonic fibroblast
Mff	mitochondrial fission factor
MFN1	mitofusin 1
MFN2	mitofusin 2
MHC I	class I major histocompatibility complex
MiD49	mitochondrial dynamics proteins of 49 kD
MiD51	mitochondrial dynamics proteins of 51 kD
MITOL	MITOchondrial ubiquitin Ligase
mtDNA	mitochondrial DNA
MTP18	mitochondrial protein 18 kDa
mtROS	mitochondrial reactive oxygen species
MULAN	Mitochondrial Ubiquitin Ligase Activator of NF-kB
N-Htt	N-terminal Huntingtin fragments
NO	nitric oxide
O <sup>2-</sup>	superoxide
OCR	oxygen consumption rate
OD	Optical Density
OMA1	Overlapping with the M-AAA Protease 1 Homolog
OMM	outer mitochondrial membrane

ONOO <sup>-</sup>	peroxynitrite
OPA1	optic atrophy 1
OSCP	sensitivity-conferring protein
OXPPOS	oxidative phosphorylation
PA200	proteasome activator 200 kDa
PA200 <sup>Δ/Δ</sup>	PA200 knockout mice
PBS	phosphate buffer saline
PCNA	proliferating cell nuclear antigen
PCR	Polymerase chain reaction
PD	Parkinson's disease
PE	Phosphatidyl ethanolamine
phLF	primary human lung fibroblasts
PI	propidium-iodide
PS	penicillin/streptomycin
PVDF	Hydrophilic polyvinylidene fluoride
Q	ubiquinone
QH2	ubiquinol
REG	regulator
RIPA	Radioimmunoprecipitation assay
ROS	reactive oxygen species
RP	regulatory particle
RT-qPCR	real-time quantitative PCR
SD	standard deviation
SDS	sodium dodecyl sulfate
SDS-PAGE	sodium dodecyl sulfate-polyacrylamide gel electrophoresis
shRNA	short hairpin RNA
S-OPA1	short isoform of optic atrophy 1
SRB	sulforhodamine b
T	Threonine
T/E	Trypsin/EDTA
TCA	Trichloroacetic acid
TCAC	tricarboxylic acid cycle
TGF-β1	transforming growth factor
TMRE	tetramethylrhodamine ethyl ester
TSS	transcription start sites
Ub	ubiquitin
Ublc	ubiquitin-like conjugation
ULK1	unc-51-like kinase 1
UPS	ubiquitin-proteasome system
VPS34	class III phosphatidylinositol 3-kinase
WT	wild type
Y	Tyrosine
YME1L	Yeast Mitochondrial AAA Metalloprotease Like 1 ATPase
ΔpH	proton gradient
ΔΨ <sub>m</sub>	mitochondrial membrane potential

## INTRODUCTION

The proteasome activator PA200 is one of the activator subunits of the proteasomes. PA200 binds to the 20S proteasome core and enhances degradation of peptides in a ubiquitin and ATP independent manner. PA200 was identified at the first time in bovine testis (Ustrell et al., 2002), then its homologs were described in worm (*Caenorhabditis elegans*), yeast (*Saccharomyces cerevisiae*), and plants (*Arabidopsis thaliana*) (Book et al., 2010; Ustrell et al., 2002). Bioinformatics analysis of PA200 amino acid sequence revealed that PA200 entirely consists of 32 HEAT-Like motif repeats, which form at the tertiary structure an asymmetric dome-like structure with major and minor lobes (Kajava et al., 2004; Ortega et al., 2005). At the protein and mRNA levels, three PA200 isoforms were identified in eukaryotic cells; PA200-I; ~ 190 kDa, PA200-II; ~ 140 kDa and, PA200-III; ~ 130 kDa (Blickwedehl et al., 2007; Ustrell et al., 2002). Only PA200 I isoform can bind to the 20S proteasome core to form single (PA200-20S) or double capped (PA200-20S-PA200) proteasome complexes. Biochemical characteristics of PA200 are fully understood, however, to date, the biological functions of PA200 are more controversial. PA200 has structural and functional particularities that candidate this protein to have other important functions in addition to its role in proteolysis machinery. PA200 is entirely reached with HEAT-like motif repeats which are typically associated with protein-protein recognition, suggested that PA200 may have a role as an adaptor protein. Furthermore, PA200 binds to 20S and enhances the axial gate opening like all other proteasome activators, however, the mechanism of substrate delivery into 20S catalytic chamber remains unclear. Additionally, it has been reported that the affinity of PA200 to 20S proteasomes is the lowest with a percentage of 1-2% compared to 20S-19S (15-25%) and 20S-11S (5-10%) proteasome complexes in different cell types (Sahu & Glickman, 2021). Notably, some cell types do not show the interaction of PA200 and the 20S proteasome, such as cardiac muscle cells in mice (Gomes et al., 2006). This suggests that PA200 may have other functions than an activator of the ubiquitin-proteasome system (UPS) that needs further investigation.

The first proposed biological function of PA200, in addition to its role as proteasome activator, was that the protein is involved in repair of DNA double-strand breaks (DSBs) (Ustrell et al., 2002). However, the exact molecular mechanisms of PA200 in the DNA DSBs repair process remain unclear. PA200 knockout mice show a defect in male fertility but not females, and this phenomenon was explained as an impairment in the DNA DSBs repair machinery in meiotic cells upon deletion

of PA200 during spermatogenesis. The authors argue that if we consider PA200 as an essential factor in DNA DSBs repair, we expect to see the same phenotypes of mice-deficient of well-known DNA DSBs repair factors in PA200<sup>Δ/Δ</sup> mice. Deletion of these factors leads to both male and female sterility, which was not observed in the PA200<sup>Δ/Δ</sup> female mice (Khor et al., 2006). In the same context, it has been reported that proteasome activity in sperm of PA200<sup>Δ/Δ</sup> mice is strongly reduced only in the double knockout (dKO) mice of *PSME3* and *PSME4* (encoding for PA28γ and PA200, respectively), but not a single *PSME4* KO mouse (Huang et al., 2016). It is known that PA200 is highly expressed in testis compared to all other tissues and its deletion did not show any major effect on proteasome activity, unlike PA28γ. This suggests that PA200 influences the spermatogenesis process with another mechanism that is not related to the proteolytic machinery. It has been shown that loss of Blm10 (yeast ortholog of PA200) leads to impaired mitochondrial respiration and an increase in oxidative stress sensitivity (Tar et al., 2014). More interestingly, Blm10 expression level increased upon switching from fermentation to oxidative metabolism (Lopez et al., 2011), which suggests the possible role of PA200 in oxidative phosphorylation machinery and overall metabolism. Furthermore, recent studies demonstrated that PA200 knockout mice exhibit muscle fiber atrophy and accelerated aging (Jiang et al., 2020). The accelerated aging in PA200-deficient mice could be aging-related to mitochondrial dysfunction, which is a common factor of aging and aging-related neurodegenerative disorders.

Almost all the above-discussed functions of PA200 were related to proteasome activity without providing an exact molecular mechanism behind it. Furthermore, the possible role of PA200 in the pathophysiology of diseases through the maintenance of cell survival, mitochondrial integrity, and metabolism is undetermined. In the present study, we investigated the possible new cellular functions of PA200, in the SH-SY5Y cell line, using chromatin immunoprecipitation (ChIP) followed by ChIP-sequencing (ChIP-seq) analysis and global transcriptomic analysis approaches. My main research work focused on the effects of PA200 on cell survival, mitochondrial integrity and metabolism under normal condition and upon mitochondrial stress.

# REVIEW OF THE LITERATURE

## Proteolysis

All proteins are sooner or later subjected to proteolysis, regardless of their cellular functions, half-life, biochemical, and structural properties (Minina et al., 2017). However, the ways how proteins are degraded by either partial digestion (limited proteolysis) or complete digestion (digestive proteolysis) are different. In eukaryotic cells, two major processes carry out digestive proteolysis: The UPS and autophagy are constitutively involved in the turnover of cellular proteins (Fig. 1). In general, proteasomes specifically degrade proteins tagged with ubiquitin (Ub) and with a short half-life (Tomko & Hochstrasser, 2013). Unlike the UPS, autophagy is responsible for the degradation of long half-lived proteins and other types of macromolecules such as lipids, nucleic acids, and carbohydrates (Ciechanover, 2005).

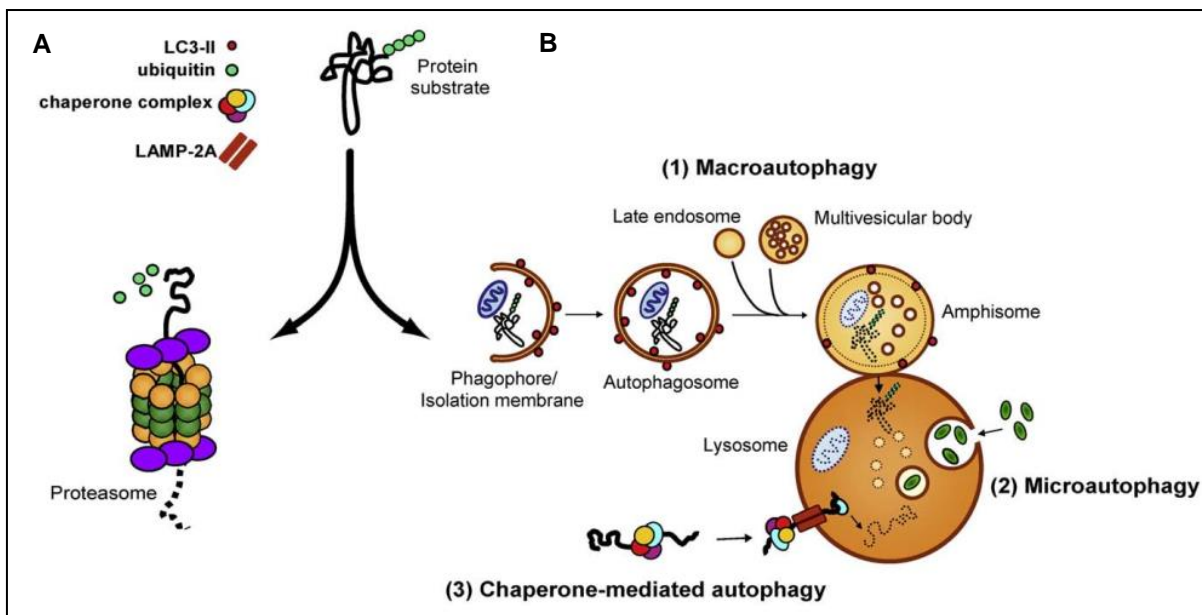


**Figure 1. Cellular proteolytic systems: ‘The UPS and the autophagy-lysosomal system’.** (A) Short-lived, polyubiquitin-tagged proteins are usually degraded by the 26S proteasome. Some ubiquitinated proteins can also be degraded by the autophagy-lysosomal system. (B) The autophagy-lysosomal system is comprised of three classes (1) Defective organelles and protein aggregates are degraded by macroautophagy by the formation of autophagosomes that are delivered to the lysosome, (2) Small cytosolic substrates are directly engulfed by lysosomes and degraded by microautophagy, and (3) Chaperone-mediated autophagy (CMA), specifically targets cytosolic substrates that are associated with a specific chaperone complex and translocated into the lysosome through the lysosome-associated membrane protein (LAMP)-2A receptor. (Nedelsky et al., 2008)

## **Lysosome mediated protein degradation**

### **Autophagy**

Autophagy is a lysosome-dependent self-digestion process; it serves as a balancer of cellular energy at critical times during development and response to stress (Glick et al., 2010; Mizushima et al., 2008). Autophagy plays a crucial role in removing aggregated and misfolded proteins, eliminating defective organelles, such as peroxisomes, endoplasmic reticulum (ER), and mitochondria, as well as cleaning intracellular pathogens (Glick et al., 2010; Mizushima et al., 2008). The autophagy substrates are delivered into the lysosomal lumen via three different pathways and based on that the autophagy process is classified into three forms; macroautophagy, microautophagy, and chaperone-mediated autophagy (CMA) (Fig. 1) (Kaushik & Cuervo, 2012; Li et al., 2012; Majeski & Fred Dice, 2004; Mortimore & Reeta Pösö, 1986).

Macroautophagy is the most widely studied and best-characterized type of autophagy (Yang & Klionsky, 2010). It can selectively degrade defective organelles including depolarized mitochondria and protein aggregates mediated by autophagosome formation and finely fused with lysosomes for degradation. Macroautophagy is considered a key regulator of organelle and protein quality control in eukaryotes (Wang & Robbins, 2014). Unlike macroautophagy, microautophagy is a direct lysosomal degradative process. It occurs by internalization of soluble intracellular components via invagination of the lysosomal membrane to assure their degradation (Li et al., 2012). Another selective autophagy -lysosome mediated protein degradation pathway was identified only in mammalian cells, known as CMA. This class of autophagy specifically degrades cytosolic proteins with a particular pentapeptide. Furthermore, it is capable to identify a single cytosolic protein and directing it to lysosomes (Arias & Cuervo, 2011)

### **Macroautophagy**

Macroautophagy is divided into five successive steps; it begins with the induction step, which is a response to therapeutic or metabolic stress. This phase is mediated by the Unc-51 like autophagy activating kinase 1 (ULK1). The second step is the initiation of phagophore formation (nucleation); this phase is triggered by a protein complex containing class III phosphatidylinositol 3-kinase (VPS34). In the elongation phase, the phagophore starts to expand to sequester a cargo and form a structure called the autophagosome. The formation of autophagosome is mediated by two

ubiquitin-like conjugation (Ublc) systems (Atg8 coupled with the membrane lipid phosphatidyl ethanolamine (PE) (Atg8–PE), and the Atg12–Atg15). After cargo formation, it will fuse with the lysosome for degradation. Once the autophagosome is fused with the lysosome, the degradation step starts immediately by a wide range of hydrolases that break down all materials in the lysosomal lumen. (Abada & Elazar, 2014; Galluzzi et al., 2017; Yang & Klionsky, 2010)

### **Microautophagy**

Microautophagy occurs also in five steps, starting with invagination and autophagy tube elongation followed by vesicle formation, extension, scission, degradation, and recycling (Li et al., 2012). Briefly, starvation conditions trigger the initiation of membrane invagination and autophagy tube formation. The invagination occurs after lateral redistribution of lipids and local exclusion of large transmembrane proteins on particular parts of the lysosome membrane, which create smooth areas with a very low content of transmembrane proteins. This step is adenosine triphosphate (ATP)-dependent (Li et al., 2012; Sattler & Mayer, 2000). Two Ublc systems participate in the initiation of the microautophagy process; first, it is mediated by the E1-like enzymes (Atg7 and Atg8), and the second by an E2-like enzyme (Atg3, and cysteine protease Atg4) (Doelling et al., 2002). Next, invagination naturally occurs due to low protein incorporation at the top of the autophagic tube, and this step ends by the formation of a microautophagy vesicle (Müller et al., 2016). The vesicle expansion is mediated by several enzymes and Ublc systems. After the formation of the microautophagy vesicle and expansion, the vesicle is released (scission from autophagic tubes) into the lysosome lumen for degradation. At the end of the process, the vesicle is degraded by hydrolysis (Epple et al., 2001).

### **CMA**

The mechanism of CMA is different compared to macroautophagy and microautophagy which both direct the cytosolic cargo to the lysosomal lumen by vesicles. However, CMA delivers its target substrate by cytosolic chaperones and co-chaperones (Bejarano & Cuervo, 2010). Briefly, the cytosolic heat shock cognate protein 70 (Hsc70) recognizes the CMA-targeting motif in the cytosolic protein substrate. The substrate-Hsc70co-chaperones complex then is delivered into the lysosomal membrane and interacts with the CMA receptor, called LAMP-2A. The protein substrate starts to unfold and translocates to the lumen of the lysosome across the CMA translocation

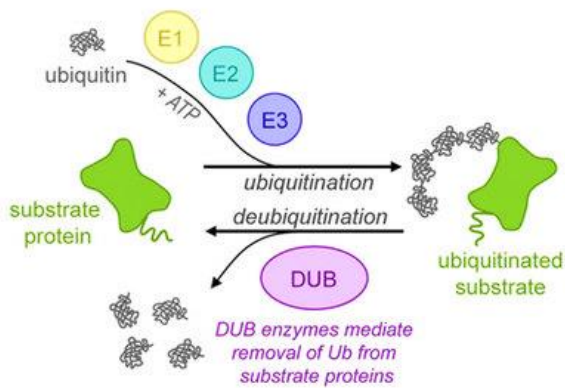
complex and a luminal form of Hsc70 (Lys-hsc70). The degradation occurs rapidly and immediately (Bejarano & Cuervo, 2010; Cuervo, 2011).

### **Proteasome mediated protein degradation**

Proteolysis through the UPS is believed to occur with short-lived proteins that are involved in a variety of basic cellular processes, such as modulation of ion channels, cell cycle via cyclin degradation, eliminate of aged housekeeping proteins, and antigen-presenting processes (Myung et al., 2001; Schwartz & Ciechanover, 1999). Unlike autophagy, which is based on specific or non-specific lysosomal degradation of cytosolic cargo containing target proteins, the UPS degrades its target proteins with exquisite specificity (Myung et al., 2001). The selective recognition of specific cytosolic substrates by 26S (19S-20S proteasome complex) is ensured by the ubiquitination machinery, in an ATP-dependent manner (Schwartz & Ciechanover, 1999). The covalent binding of ubiquitin molecules to target substrates acts as an opsonization molecule that facilitates the recognition of ubiquitinated proteins as a signal for degradation by the 26S proteasome (Myung et al., 2001). The ubiquitination process consists of several enzymatic steps that modulate the target protein by covalently adding ubiquitin molecules to specific sites (Maupin-Furlow, 2012). Ubiquitin activating enzymes or E1s are responsible for activating and binding ubiquitin in a two-step reaction in an ATP-dependent manner. E2s or ubiquitin-conjugating enzymes transfer the ubiquitin from E1 to the active site Cys residue of E2. E3s or ubiquitin ligases perform the last step of the cascade. One of the hundreds of E3s catalyzes the reaction by forming an isopeptide bond between a Lys residue of the target protein and a Gly residue at the C-terminal end of the ubiquitin. Ubiquitin proteins themselves contain seven Lys residues therefore they serve as ideal targets for ubiquitination to give rise to various polyubiquitin chain compositions. The chain is extended by attaching the next ubiquitin moiety to a Lys residue within the first ubiquitin.

Increasing evidence demonstrates that the position of ubiquitinated Lys determines the ultimate fate of the substrate protein. The most common type of linkages are the Lys48-linked (K48) chains that target the substrate protein for proteasomal degradation (Maupin-Furlow, 2012; Schwartz & Ciechanover, 1999) (Fig. 2).

### A Substrate ubiquitination



### B Substrate processing by the 26S proteasome

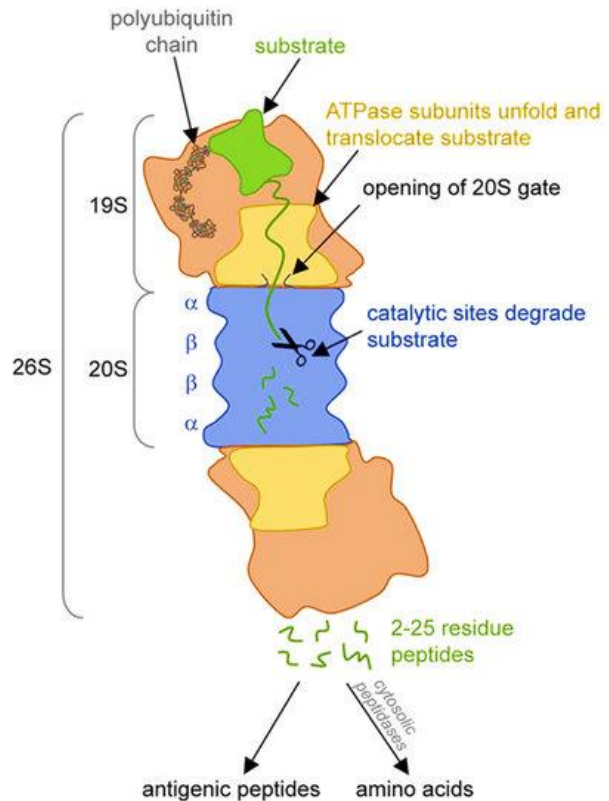


**Figure 2. 26S proteasome-mediated protein degradation.** (A) Simplified model of substrate ubiquitination by ubiquitin conjugation system modulated by E1, E2, and E3 enzymes that ensure the activation of ubiquitin, conjugation, and ligation to the protein substrates, respectively. This process requires ATP hydrolysis. The ubiquitinated substrate is a signal for protein degradation. (B) Processing of ubiquitinated substrate by the 26S proteasome starts by recognition through 19S regulatory subunit of 20S proteasome. Substrate unfolding, internalization of the unfolded protein substrate, and finally degradation in the catalytic chamber of the 20S proteasome. The degradation process by the 26S proteasome is ATP-dependent. (Thibaudeau & Smith, 2019)

## Structure and function of proteasome

### The 20S proteasome: The Proteolytic Core

Proteasomes are large multi-enzyme complexes present in the cytosol and nucleus of eukaryotic cells (Rivett, 1998). The UPS can be also present in the extra cellular space (Sixt & Dahlmann, 2008). The main function of proteasomes is to maintain intracellular protein homeostasis by preventing the accumulation of damaged and misfolded proteins (Finley, 2009). The proteasome system is involved in the regulation of important cellular processes, such as cell cycle, apoptosis, signal transduction, transcription, DNA repair, and antigen presentation (Pickart & Cohen, 2004). The proteasome is composed of the 670-kDa 20S core particle (CP). The 20S consists of 28 protein subunits organized into four stacked rings with each ring composed of seven  $\alpha$  - or seven  $\beta$  - subunits ( $\alpha_7\beta_7\beta_7\alpha_7$ ) (Groll et al., 1997; Löwe et al., 1995) (Fig 3). The proteolytic sites of the proteasome are possessed by the N termini of  $\beta$  subunits. Three out of seven subunits are catalytically active, cleaving the proteins after acidic ( $\beta_1$ ), basic ( $\beta_2$ ), or hydrophobic ( $\beta_5$ ) residues (Finley et al., 2016; Seemüller et al., 1995). The catalytic activities include caspase-like, trypsin-like, and chymotrypsin-like activities, respectively (Bochtler et al., 1999; Kish-Trier & Hill, 2013). The function of the  $\alpha$  -subunits is to stabilize the proteasome complex (Bochtler et al., 1999). Furthermore, the N-termini of the  $\alpha$ - subunits form the 20S proteasome gate with a 13 Å° central pore preventing non-specific protein degradation (Groll et al., 2000).

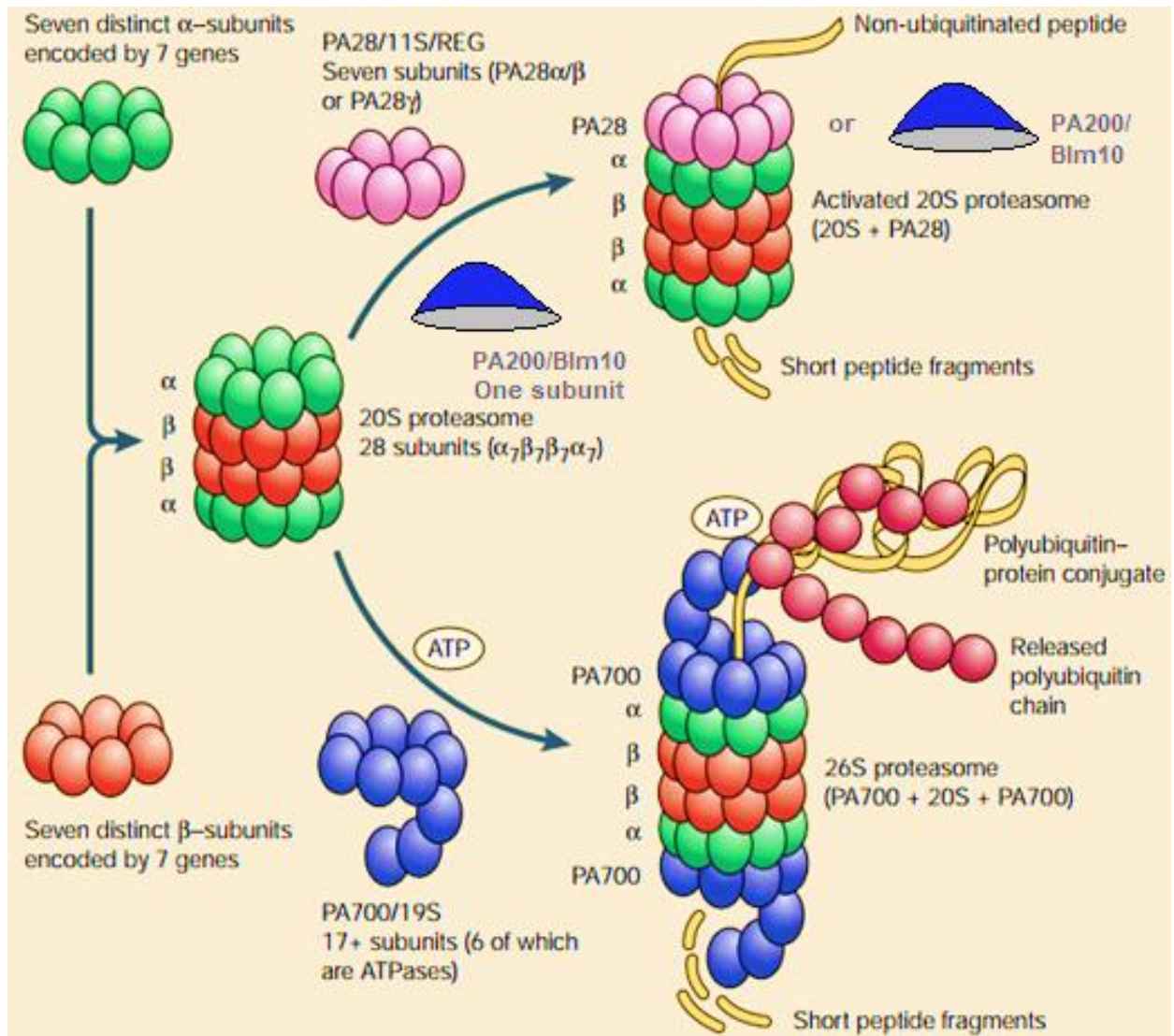


**Figure 3. Composition and organization of the proteasome complexes and their regulatory subunits.** The catalytic core of the proteasome (20S) consists of 28 subunits. The barrel-shaped structure of the 20S is formed by four heptameric rings stacked axially; the two inner rings are composed of seven different  $\beta$ -subunits holding the catalytic sites. The outer rings are composed of 7 different  $\alpha$ -subunits, which serve as an anchor for 20S regulators. The 20S core can assemble with different regulatory subunits, including the PA700 (19S), PA28 (11S), and the PA200/Blm10 families. The binding of these regulators facilitates the access of substrates to the catalytic chamber of the 20S. This process could be ATP and ubiquitin-dependent in the case of 19S binding or ATP and ubiquitin-independent in the case of 11S or PA200/Blm10 regulators binding. Modified from (McNaught et al., 2001)

## Tissue-specific proteasomes

In mammals, the constitutive catalytic subunits of 20S CP ( $\beta 1$ ,  $\beta 2$ , and  $\beta 5$ ) are susceptible to replacement with other variants, based on tissue specificity and extracellular stimuli (Qian et al., 2013; Stadtmueller & Hill, 2011). Three tissue-specific proteasomes are known in mammalian cells; the immunoproteasome which is characterized by the presence of the catalytic  $\beta$ -subunits  $\beta 1i$ ,  $\beta 2i$ , and  $\beta 5i$  subunits (“i” is for immunoproteasome) (Dahlmann, 2016; Groettrup et al., 2010) (Fig 4). These variants are expressed mainly in the cells of the immune system, such as monocytes and lymphocytes. Upon viral or bacterial infection, more than 90% of the ordinary proteasomes are replaced by immunoproteasome (Barton et al., 2002; Khan et al., 2001). This inducible type of proteasome has a lack in cleavage-specificity after hydrophobic and basic residues, which is represented by low catalytic activity after acidic residues and enhanced cleavage after hydrophobic residues (Groettrup et al., 2010). The products of  $\beta i$ -subunits have high affinity toward class I major histocompatibility complex (MHC I). (Gaczynska et al., 1993; Silva et al., 2012). Another tissue-specific proteasome is the thymoproteasome. Encoding a specific catalytic  $\beta$ -subunit named  $\beta 5t$  (“t” for thymus). The 20S CP of the thymoproteasome is composed of  $\beta 1i$ ,  $\beta 2i$ , and  $\beta 5t$  instead of  $\beta 1$ ,  $\beta 2$ , and  $\beta 5$  (Groettrup et al., 2010; Khan et al., 2001) (Fig 4). Unlike the immunoproteasome, the  $\beta 5t$  subunit has a low catalytic activity to cleave after hydrophobic residues. The peptides produced by thymoproteasome activity have a very low affinity to MHC-I, which is involved in the T cell selection (positive selection of CD8+ T cells) and maturation in the thymus (Murata et al., 2007; Tomko & Hochstrasser, 2013). Another proteasome subpopulation is known as spermatoproteasome, which is exclusively found in male germ cells. It is only expressed in spermatids and mature sperms. The  $\alpha 4$  -subunit is replaced with an alternate core subunit,  $\alpha 4s$ /PSMA8 in mammals (Uechi et al., 2014). Moreover, two alternate  $\alpha$ -subunits,  $\alpha 4T1$  and  $\alpha 4T2$ , are found in *Drosophila* (Yuan et al., 1996).

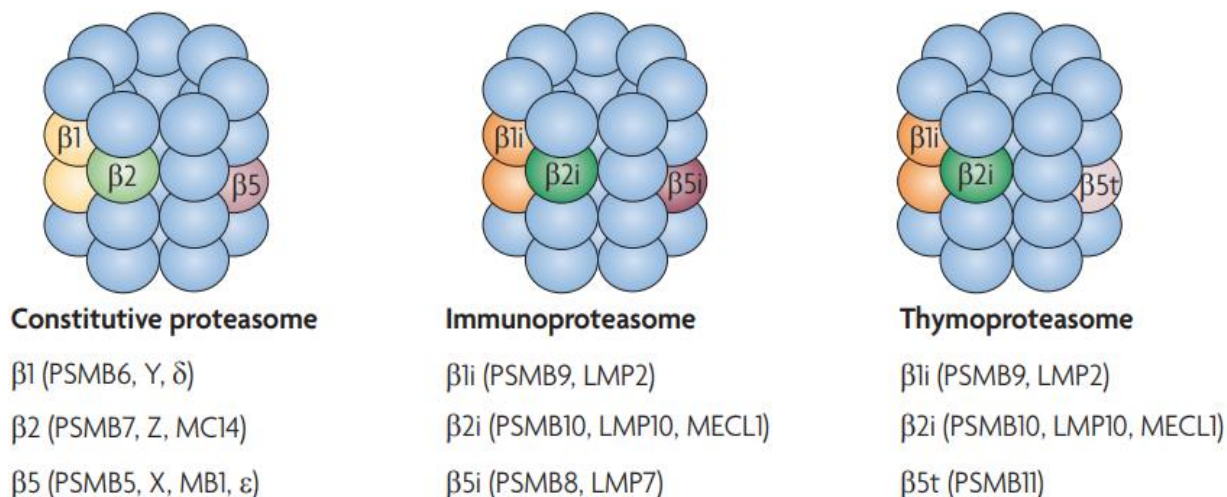


**Figure 4. Tissue-specific proteasome isoforms.** The active site of the constitutive proteasome is characterized by  $\beta 1$ ,  $\beta 2$ , and  $\beta 5$  subunits with chymotrypsin-, caspase-, and trypsin-like activities. The proteolytic subunits of the immunoproteasome are  $\beta 1i$ ,  $\beta 2i$ , and  $\beta 5i$  with a strongly decreased caspase-like activity, and an increased chymotrypsin-like activity, compared to the constitutive proteasome. The proteolytic thymoproteasome subunits are  $\beta 1i$ ,  $\beta 2i$ , and  $\beta 5t$  with a decreased chymotrypsin-like activity. (Groettrup et al., 2010)

## The activator families of the proteasome

### The 19S regulatory subunit (PA700/RP)

The 20S CP itself can degrade unfolded and small peptides in an ATP- and ubiquitin-independent manner with a low proteolytic capacity (Baugh et al., 2009). Therefore, the association of the proteasome with regulatory subunits (activators) is necessary for fully functional proteasome and specific protein degradation. The regulatory subunits provide the gate opening and the access of substrates to the central proteolytic chamber of the 20S (Peth et al., 2009). Three different families of activators regulate the 20S gate opening (Stadtmueller & Hill, 2011). The 19S or regulatory particle/RP/PA700 is a highly conserved activator in eukaryotic cells (archaeal; PAN and eubacterial; ARC/Mpa homologs). It binds to one or both sides of the 20S CP to form a high molecular weight complex named 26S (19S - 20S) and 30S proteasome (19S - 20S - 19S) (Rechsteiner, 1998; Stadtmueller & Hill, 2011), which represent 15-25 % and 5-15 % of total proteasomes complexes, respectively (Fig 5) (Sahu & Glickman, 2021). The 26S or 30S consist of two sub-complexes, the base, and the lid. (Glickman et al., 1998). Six out of ten subunits of the base (Rpt1-Rpt6) are ATPases and they belong to the AAA family (ATPases Associated with a

variety of cellular Activities), which is responsible for the gate opening and conducts substrates into the 20S CP proteasome (Finley, 2009). The other base subunits are non-ATPase subunits (Rpn1, Rpn2, Rpn10, and Rpn13), playing a role in substrate recognition. Rpn1 and Rpn2 serve as docking sites for Ub processing factors that interact with ubiquitinated substrates and the proteasome at the same time. Rpn10 and Rpn13 bind directly to polyubiquitinated substrates (Elsasser et al., 2004; Rosenzweig et al., 2012). The lid consists of eight non-ATPase subunits (Rpn3, Rpn5–9, Rpn11, Rpn12, and Rpn15 (Dss1/Sem1)). The lid ensures the assembly of 19S and serves as an enzyme that deubiquitinates the ubiquitin-tagged substrates. Deubiquitination is mediated by the highly conserved metalloprotease deubiquitinase enzyme, DUBRpn11 (Yao & Cohen, 2002). The binding of the C terminal of the 19S to the  $\alpha$  ring of the 20S leads to open the gate and facilitates substrate degradation (Bochtler et al., 1999).

### **The 11S regulators: PA28 $\alpha\beta$ and PA28 $\gamma$ (REG)**

The PA28 activator or 11S regulator (REG) is involved in a ubiquitin and ATP independent substrate degradation (Dubiel et al., 1992). The activator is present in eukaryotic cells except for yeast and with less conservation between species (Stadtmueller & Hill, 2011). PA28 represents 2-10 % of total proteasome complexes (Fig 5) (Sahu & Glickman, 2021). Reports showed that PA28 activators are involved in the degradation of oxidized proteins (Pickering & Davies, 2012). In eukaryotic cells, PA28 has three members, two hetero-heptameric subunits PA28 $\alpha\beta$  mainly distributed in the cytosol (Huber & Groll, 2017), however, the homo-heptameric subunits PA28 $\gamma$  are constitutively expressed in the nucleus (Orlowski & Wilk, 2000). Furthermore, the combination of PA28  $\alpha$  and  $\beta$  is more efficient at the activation of proteasome, compared to the PA28  $\alpha$  and  $\gamma$  combination. Mild stress or interferon gamma (INF $\gamma$ ) induces the expression of PA28 $\alpha\beta$ , but not PA28 $\gamma$  (Tanahashi et al., 2000). The PA28 $\alpha\beta$  activator with the 19S forms a hybrid immunoproteasome involved in MHC I ligand generation and controlling the quality of peptides released (Tanahashi et al., 2000), suggesting the protective role of PA28 $\alpha\beta$  and the immunoproteasome during infection and oxidative stress conditions (Johnston-Carey et al., 2016). The function of the PA28 $\gamma$  is different compared to the PA28 $\alpha\beta$  isoform. Several reports demonstrated that REG $\gamma$ /PA28 $\gamma$  involved in the degradation of some natively unfolded proteins, RNA splicing, DNA repair, and cell cycle (Levy-Barda et al., 2011; Murata et al., 1999; Zannini et al., 2008).

## The Proteasome activator 200 kDa (PA200)

In addition to the well-known proteasome activators PA700 (19S) and PA28 (11S REG), a new proteasome activator with a molecular weight of 200 KDa (PA200) was identified in bovine testis (Ustrell et al., 2002). PA200 alternatively binds to the 20S proteasome to promote ubiquitin- and ATP-independent peptide degradation (Ustrell et al., 2002). PA200-20S represents 1-2% of total proteasome complexes (Fig 5) (Sahu & Glickman, 2021). The orthologs of PA200 exist in worm (*Caenorhabditis elegans* with 29% similarity), yeast (*Saccharomyces cerevisiae* with 17% similarity), and plants (*Arabidopsis thaliana* with 22 % similarity) (Book et al., 2010; Ustrell et al., 2002). The functional particularity of PA200, compared to other activators, is similar to PA28 $\alpha\beta$  and PA28  $\gamma$  regarding the ubiquitin and ATP independent degradation of substrates and the inability to degrade full-length proteins (Ustrell et al., 2002). PA200 is involved in several cellular processes including DNA repair, spermatogenesis, and mitochondrial inheritance (Khor et al., 2006; Sadre-Bazzaz et al., 2010; Ustrell et al., 2002), however, the molecular details behind many of these functions are not clear.

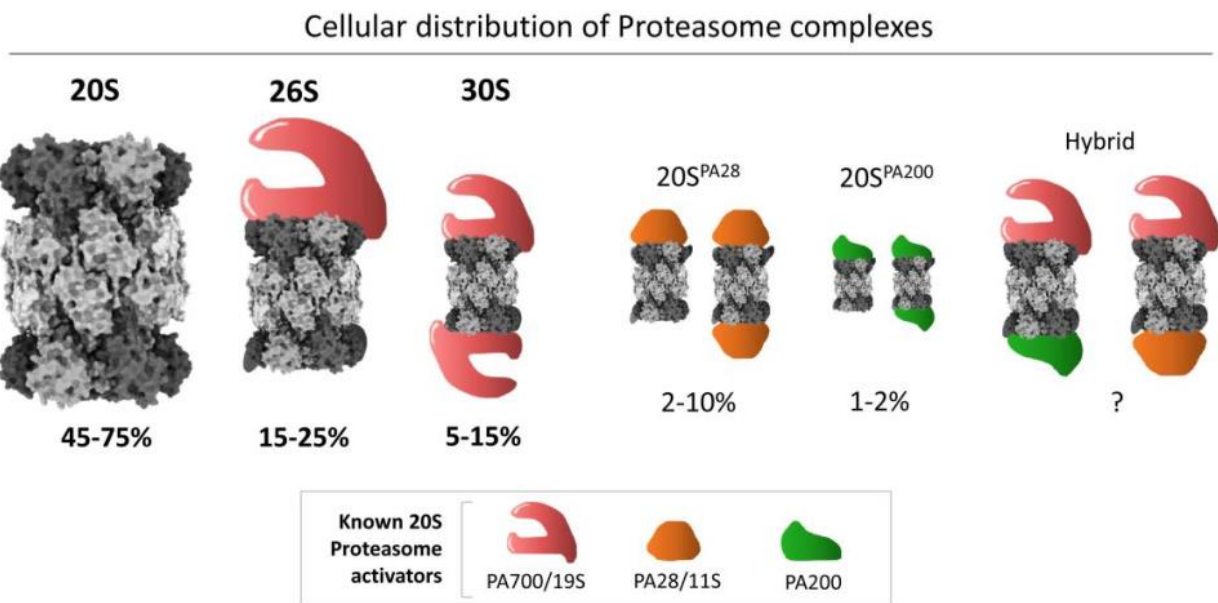


**Figure 5. Cellular distribution of mammalian proteasome complexes.** The 20S proteasomes present usually as free form with 45-75% of total proteasome complexes. The holoenzyme 26S and 30S present the majority of proteasome active forms with 5-25 %, compared to PA28-20S and PA200-20S forms with 5-10% and 1-2%, respectively. The formation of hybrid proteasome complexes, 26S-PA200 and 26S-PA28, are variable depending on cell type and extracellular stimulus. (Sahu & Glickman, 2021)

## **The structure of PA200**

PA200 was identified as a component of slow-migration of an active form 20S proteasome (Hoffman et al., 1992). The human PA200 activator consists of 1,843 amino acid residues with a theoretical molecular weight of 200 kDa. Western blot analysis of murine tissues demonstrates that PA200 is broadly expressed in mammalian tissues with a high expression level in testis (Ustrell et al., 2002).

Structural prediction methods and bioinformatic analysis revealed that PA200 is entirely formed by 32 HEAT-Like motif repeats (Huntingtin - elongation factor 3 -PR65/A subunit of PP2A - lipid kinase TOR) (Kajava et al., 2004; Ortega et al., 2005). The first characterization of PA200-20S interaction was assessed using electron microscopy. The data disclosed that PA200 binds either one or both sides of the 20S CP (Fig 6). Cryo-electron micrographs (cryo-EM) of the singly-bound PA200-20S complex at the 23 Å resolution have an asymmetric dome-like structure with major and minor lobes. PA200 binds to all  $\alpha$  subunits except the  $\alpha 7$  subunit (Fig 6) (Ortega et al., 2005). Three isoforms of PA200 were identified in eukaryotic cells; PA200 I with a molecular weight of ~ 190 kDa, PA200 II with a molecular weight of ~ 140 kDa, and the PA200 III with a molecular weight of ~ 130 kDa. The PA200 I isoform can bind only to 20S proteasomes (Blickwedehl et al., 2007; Ustrell et al., 2002). PA200 I isoform is present in the cytosol either as soluble, proteasome unbound, or as proteasome bound form (Blickwedehl et al., 2007).

Blm10, the yeast ortholog of PA200 (originally named BLM3p) (Doherty et al., 2004), was described as a nuclear CP assembly protein, which binds to nascent CP and controls a late stage of nuclear CP maturation (Fehlker et al., 2003). PA200 and Blm10 share only 17% of sequence identity. This percentage of similarity is concentrated at the C-terminal residues, however, the function of the proteins seems to be conserved. PA200 and Blm10 bind to proteasomes as a single polypeptide chain with a horseshoe-like shape (Schmidt et al., 2005) (Fig 6). The binding of PA200 and Blm10 activators to CP causes opening of the axial channel and promotes the peptidase activity of the proteasome (Iwanczyk et al., 2006; Schmidt et al., 2005; Ustrell et al., 2002) (Fig 6).

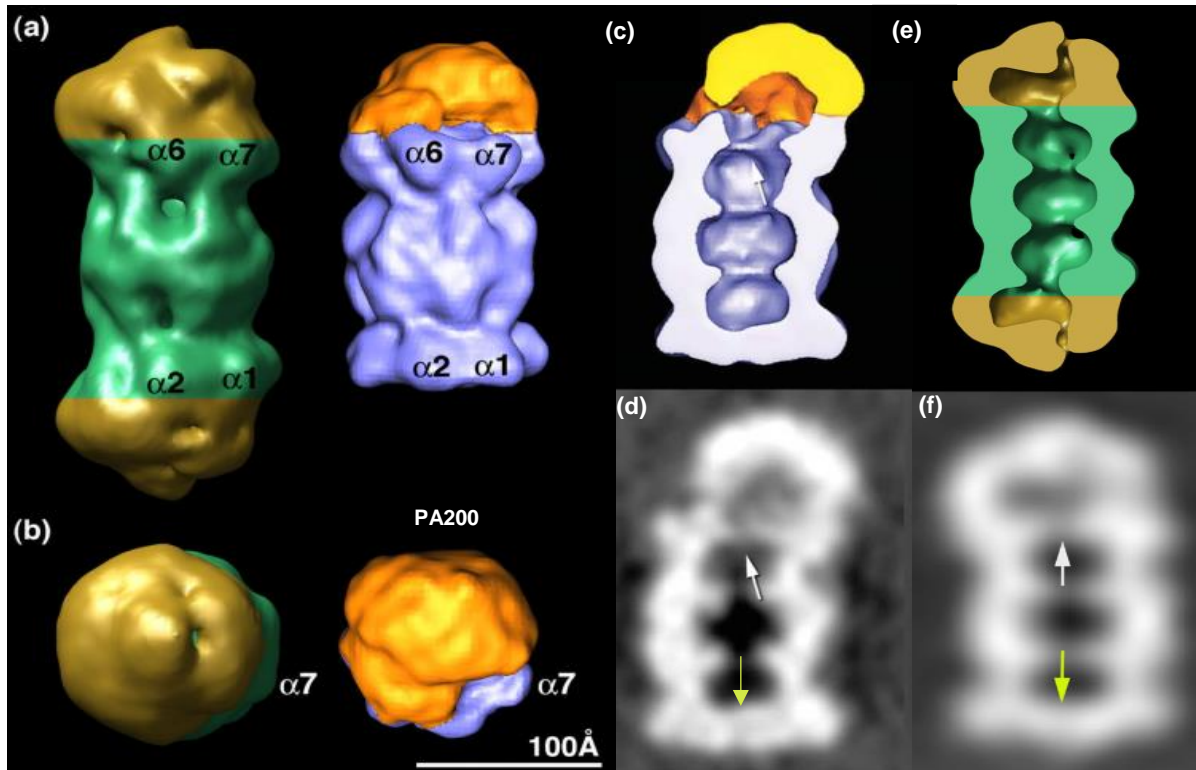


**Figure 6. Three-dimensional reconstruction of bovine PA200-20S and the yeast Blm10-20S-Blm10 complexes.** (a) Side views of PA200-20S and Blm10-20S-Blm10 complexes revealed the dome-like structure of PA200 ((right)/Blm10 (left)). (b) Surface representation of the axial view of the 20S capped either with PA200 (right) or Blm10 (left). The axial view of PA200-20S complexes shows the non-symmetrical dome-like structure of PA200 that binds to all  $\alpha$  subunits except  $\alpha$ -7. (c) And (e) Sharp cut of the surface representing the recombinant structure of PA200 (c) and Blm10 (e). The binding of activators creates an internal cavity, which communicates with the catalytic chamber of the 20S. (d) and (f) Central section of the density maps of the PA200-20S (left panel) and Blm10-20S (right panel) complexes. The binding of activators to the 20S significantly reduces the density in the center of the  $\alpha$ -rings (white arrows), compared to the free  $\alpha$  rings (yellow arrow). Modified from (Iwanczyk et al., 2006; Ortega et al., 2005)

The molecular mechanistic comparison between 26S and Blm10 on  $\alpha$ -subunits positioning revealed that the 26S gate opening is due to repositioning of all 7  $\alpha$ - subunits of the proteasomes to form a large gate (Förster et al., 2003). The rearrangement of  $\alpha$ -subunit binding with Blm10, however, prevents the formation of a normal gate structure (Fehlker et al., 2003).

PA200 interacts with the proteasome via two interacting regions; the first interaction site involves the C-terminal residue of PA200 (<sup>1838</sup>SPCYYA<sup>1843</sup>) and includes a HbYX motif (hydrophobic tyrosine-other). The HbYX motif interacts with the interface of  $\alpha$ 5 and  $\alpha$ 6 subunits (Toste Rêgo & da Fonseca, 2019). The second anchor region is formed by an extended PA200 loop that is formed by residues 561–576 docks, which tightly bind into the interface of  $\alpha$ 1- $\alpha$ 2 subunits (Toste Rêgo & da Fonseca, 2019). The dome-like structure of PA200 caps the 20S core particle using its C-terminal HbYX motif to rearrange the  $\alpha$ -subunits to partially open the 20S gate. The direct binding of PA200 onto the  $\alpha$  ring opening results in the inner chamber of the proteasome considerably closed. Thus, it restricts the access of the proteolytic active site to small peptides and unfolded proteins (Toste Rêgo & da Fonseca, 2019). Moreover, the atomic model comparison of the active site in the 20S and 20S-PA200 complexes revealed that among the three important  $\beta$ -subunits that are involved in the catalytic activity, only the S1 pocket in the  $\beta$ 2 subunit exhibits wider movement. However,  $\beta$ 1 and  $\beta$ 5 showed more narrowness sites and that can reduce the accessibility to the substrate. These findings explain the increase of trypsin-like activity ( $\beta$ 2) after PA200 binding and in parallel slight inhibition of the caspase- and chymotryptic-like activities ( $\beta$ 1 and  $\beta$ 5, respectively) (Toste Rêgo & da Fonseca, 2019). In addition to the structural investigation of the recombinant 20S-PA200, non-protein cryo-EM densities revealed that the second groove of PA200 consists of a cluster of positively charged residues assigned to PA200-bound inositol phosphates (Lin et al., 2020; Toste Rêgo & da Fonseca, 2019). Further structural analysis of PA200/Blm10 proteins revealed the presence of bromodomain (BRD)-like (BRDL) domain that binds specifically to acetylated histones. Compared to well-known human BRD families, PA200/Blm10 BRD-like domain does not share any sequence homology with any known BRDs, however, structurally it resembles BRDs (Guan et al., 2020; Qian et al., 2013).

## **Biological functions of the PA200/Blm10 family**

### **DNA double-strand breaks (DSBs) repair**

PA200 functionally is more like PA28  $\alpha\beta$  and PA28 $\gamma$  activators than the 19S regulator (Ustrell et al., 2002). PA200 activator enhances the trypsin-like catalytic activity of the proteasome in a ubiquitin- and ATP-independent manner to degrade peptides, but not full-length proteins (Toste Rêgo & da Fonseca, 2019; Ustrell et al., 2002). The first biological role of PA200 in addition to its minor role in proteolysis was described as a cytoprotective protein that is involved in DNA repair by degrading specific substrates (Ustrell et al., 2002).

Transcriptomic analysis of yeast exposed to several DNA damaging agents (bleomycin and methyl methane sulfonate) revealed an increase of mRNA expression of Blm10 by 5 folds (Jelinsky et al., 2000). Blm10 binds to Sir4P, one of the proteins that accumulated on the chromatin during DNA damage (Ho et al., 2002). The authors speculated that PA200/Blm10 has a role in DNA repair. The properties of PA200 make the protein a good candidate to be involved in the process. First, the mRNA and protein level of PA200 is high in testis, where DNA DSBs occur with high frequency. Second, PA200 is abundant in the nucleus and form nuclear foci similar to many DNA repair factors in response to  $\gamma$ -irradiation (Schultz et al., 2000; Ustrell et al., 2002, 2005).

The PA200/Blm10 family serves as proteasome activators that enhance the proteasomal activity for small peptides, but not full-length proteins. It was hypothesized that Blm10 serves as an adaptor protein when it binds to Sir4P during DNA DSBs repair, and it recruits the 26S proteasome that degrades proteins and histones to ensure the accessibility of DNA DSBs repair factors to damaged sites (Ustrell et al., 2002).

Data obtained from PA200 knockout mice revealed that there is no effect of PA200 deletion on mouse embryonic development. Furthermore, exposing PA200 $\Delta\Delta$  embryonic stem (ES) cells to either ionizing radiation (IR) or bleomycin does not show any sign of sensitization (Khor et al., 2006). The authors concluded that PA200 does not contribute to the DNA repair process under the defined experimental work conditions (Khor et al., 2006). Surprisingly, PA200 $\Delta\Delta$  male mice show a defect in fertility due to impaired spermatogenesis and haploid spermatid maturation (Khor et al., 2006). Other reports demonstrated that only double knockout (dKO) mice of *PSME3* and *PSME4* (encoding for PA28 $\gamma$  and PA200, respectively) are completely infertile, but not the single KO ones

(Huang et al., 2016). The sperm of dKO mice is morphologically similar to the wild type (wt) mice, however, it has remarkable defects in motility (Huang et al., 2016). Furthermore, proteasome activity was abolished and an increased level of oxidative damage was detected in sperms of dKO mice (Huang et al., 2016). Transcriptomic screening of dKO mice revealed an increase in the expression of proteins involved in oxidative stress response (Huang et al., 2016).

Khor et al. speculated that, if PA200 is an essential factor in DNA DSBs repair, they were expected to see the same effects of deletion of well-known DNA DSBs repair factors, such as Dmc1 or Msh5, in PA200-deficient mice. These factors are required for the repair of DSBs generated during meiosis (Edelmann et al., 1997; Pittman et al., 1998). The deletion of these two factors leads to male and female sterility, which is not seen in the PA200<sup>Δ/Δ</sup> female mice (Khor et al., 2006). Furthermore, DNA DSBs repair occurs constitutively in the immune system cells during the maturation of B and T lymphocytes (Bassing et al., 2002; Chaudhuri & Alt, 2004). Mice deficient of one protein related to the DNA DSBs repair leads to defects in lymphocyte development, which again was not shown in the PA200<sup>Δ/Δ</sup> mice. Both lymphocyte development and immunoglobulin classes in PA200<sup>Δ/Δ</sup> are similar to wt mice. (Khor et al., 2006).

*In vitro* studies demonstrate that PA200-proteasomes are accumulated on the chromatin in response to IR (Blickwedehl et al., 2007). The authors mention that DNA repair occurs mainly in 4 to 6 h, and they suggest that PA200-proteasome foci are formed at the late stage of DNA repair to degrade proteins involved in DNA DSBs repair (Blickwedehl et al., 2007). Moreover, mutation but not deletion of PA200/Blm10 leads to radiation sensitivity (Schmidt et al., 2005). This result is similar to the results from ES cells, derived from PA200-null mice, which do not show an apparent increase in sensitivity to IR (Khor et al., 2006), thus, PA200 has no direct effect on DNA DSBs repair (Blickwedehl et al., 2007).

Other reports showed that PA200 deficient cells exhibit impairment in long-term survival upon IR exposure (Blickwedehl et al., 2012). This effect is reversed after the addition of glutamine in excess. However, in a glutamine-free medium, PA200 depleted cells exhibit a high rate of proliferation, compared to control cells (Blickwedehl et al., 2012). This data suggests that cells deficient of PA200 have a defect in glutamine homeostasis (Blickwedehl et al., 2012).

## The degradation of acetylated histones

long-term exposure of murine embryonic fibroblasts (MEF) to low concentration of hydrogen peroxide ( $H_2O_2$ ) enhances the expression of PA200 and PA28 $\alpha\beta$  activators (Pickering & Davies, 2012). The capacity of the proteasome to degrade oxidized proteins, such as histones and hemoglobin, however, is enhanced in the presence of the PA28 activator, but not PA200 (Pickering & Davies, 2012). *In vitro* combination of PA200 and 20S CP at appropriate concentrations leads to the inhibition of the activity of the proteasome against oxidized proteins and native hemoglobin but not native histones (Pickering & Davies, 2012). The authors suggest that, unlike PA28y, PA200 is not responsible for the turnover of oxidized protein, but may be involved in DNA repair through the degradation of histone proteins (Pickering & Davies, 2012).

The investigation of the turnover of histones during spermatogenesis and DNA repair revealed that 4% of histones or variants are retained in nucleosomes of mature sperms (Hammoud et al., 2009). Furthermore, the accumulation of histones or their delayed degradation leads to inefficiency in transcriptional machinery and increased DNA damage (Singh et al., 2009). PA200-deficient mice exhibit an accumulation of core histones in elongated spermatids and that leads to apoptosis. The authors speculated that PA200 is involved in a tightly regulated process of acetylated histone degradation (Qian et al., 2013). Notably, acetylated histones are involved in numerous cellular processes, including transcription, DNA repair by relaxing chromatin upon stress-induced DNA DSBs (Campos & Reinberg, 2009), and spermatogenesis (Gaucher et al., 2010). In yeast, the DNA DSBs repair process is required for the removal of core histones that are present in the vicinity of DNA-damaged sites (Tsukuda et al., 2005). Qian et al, showed that during DNA DSBs repair, PA200/Blm10 proteins enhance the proteasomal degradation of acetylated core histones mediated by BRD-like regions of PA200/Blm10. The authors speculated that the PA200/Blm10 mediated degradation of acetylated histones facilitates the access of DNA repair proteins to the DNA damage site (Qian et al., 2013).

In contrast, studies demonstrated that the formation of Blm10 double-capped CP complex (Blm10-CP-Blm10) inhibits the proteasome activity (Lehmann et al., 2008; Sadre-Bazzaz et al., 2010), while the asymmetric CP-Blm10 complex shows active proteasome. The authors speculated that Blm10 is probably a proteasome inhibitor or essential factor for proteasome assembly. Furthermore, peptidomics analyses of wt and *blm10A* strains do not show any significant

differences in the intracellular peptides between the two strains (Dasgupta et al., 2016). This data suggested that the absence of Blm10 does not cause a major change in the level of cellular peptides.

### **The role of the Blm10/PA200 family in the maintenance of mitochondrial integrity**

Other reports demonstrate that Blm10 is important for the maintenance of mitochondrial function with no remarkable changes in mitochondrial morphology (Sadre-Bazzaz et al., 2010). However, Tar et al. showed that loss of Blm10 increased mitochondrial fission through the stabilization of the Dnm1 protein level (Tar et al., 2014). Furthermore, Blm10 deletion leads to impaired mitochondrial respiration and increased sensitivity to oxidative stress. Blm10 expression level increased upon switch from fermentation to oxidative metabolism (Lopez et al., 2011).

### **Cardiovascular disease and fibrosis**

Studies demonstrated that the expression of PA200 is regulated by miR-29b at the mRNA level. Replacement of synthetically engineered miR-29b leads to reduced PA200 protein level, assembly with the proteasome, and peptide activity (Jagannathan et al., 2015). Besides, a report showed that lovastatin, a drug used to treat hypercholesterolemia, has a direct effect on proteasome-mediated oxidative stress (Wang et al., 2017). Lovastatin induces the overexpression of miR-29b which in turn abolishes the expression of *PSME4*, the gene for PA200. In a cardiovascular disease model, lovastatin treatment leads to reduced PA200 protein level and PA200-proteasome complex, besides that has diminished oxidative stress which prevents endothelial dysfunction and minimizes the multiple cardiovascular risk factors (Wang et al., 2017). The authors related the reduction of proteasome activity to the lovastatin-induced PA200 silencing; however, the mechanism of oxidative stress diminution upon lovastatin treatment is not clear. The involvement of PA200 in the pathomechanism of diseases was primarily investigated in patients with idiopathic pulmonary fibrosis (IPF) (Welk et al., 2019). PA200 was highly expressed in myofibroblasts and hyperplastic basal cells in the fibrotic tissue of the IPF patients. Furthermore, the increased PA200 protein level was accompanied by PA200-proteasome complex formation in fibrotic tissues (Welk et al., 2019). Transient depletion of PA200 in primary human lung fibroblasts (phLF) strongly promotes myofibroblast differentiation. On the other hand, treatment of phLF cells with transforming growth factor (TGF)- $\beta$ 1 leads to up-regulation of PA200 and promotes myofibroblast differentiation. This contradicted the function of PA200 in fibroblast differentiation, raising the proposition that up-

regulation of PA200 upon TGF- $\beta$ 1 may acts a negative regulator of TGF- $\beta$ 1-induced myofibroblast differentiation (Welk et al., 2019). The mechanism of the inhibitory effects of PA200 on myofibroblast differentiation and induced fibrosis in patients suffering from IPF remains unclear.

### **The role of PA200/Blm10 in aging**

Another recent report has demonstrated that PA200/Blm10 is related to cellular aging, mediated by DNA damage and dysfunction of proteasome activity. The authors showed that the level of PA200 but not the 20S proteasomes and the PA28 family decreased in MEF cells during aging (Chen et al., 2020). Inversely, the authors mention that overexpression of BLM10 in the yeast-aging model prevents the aging hallmarks and maintains the activity of the proteasome. This suggests that the aging-dependent decline in proteasome activity is primarily caused by the reduced protein levels of PA200 /Blm10 (Chen et al., 2020) and that PA200/Blm10 proteins antagonize aging. A recent study has also demonstrated that mutation in the acetyl binding region of PA200 interrupts the degradation of acetylated histones, suggesting that the degradation of histones requires acetylation (Jiang et al., 2020). Furthermore, deletion of PA200 dramatically altered transcription during aging by inducing an overall change in the disposition of transcriptional hallmarks (H3K4me3 and H3K56ac) (Jiang et al., 2020). Also, PA200 deficient mice exhibit anxiety-like behavior, defects in the immune system, and accelerated aging (Jiang et al., 2020). The PA200-proteasomes mediated degradation of acetylated histone directly modulates the distribution of transcription hallmarks that controls the transcriptional machinery in different promoter regions (Jiang et al., 2020).

Neuronal aging and neurodegenerative diseases are related to each other. Recently, it has been shown that PA200/Blm10 family mediates the degradation of mutant N-terminal Huntingtin fragments (N-Htt) with 103 glutamines (Htt103Q). Furthermore, a pull-down assay shows that PA200 binds to N-Htt. The loss of Blm10 in yeast or PA200 in human cells results in increased mutant N- Htt aggregate formation and elevated cellular toxicity, the authors related the increase of insoluble N-Htt aggregates upon depletion of PA200 and deletion of Blm10 in yeast to the impairment of proteasome activity (Aladdin et al., 2020).

## Mitochondria

Mitochondria or the powerhouse of the cells are one of the important organelles in eukaryotic cells. The essential function of mitochondria is to supply ATP through oxidative phosphorylation (OXPHOS) and produce approximately 90% of the cellular energy (Chance et al., 1979; McBride et al., 2006).

Mitochondria consist of the mitochondrial matrix, a folded inner mitochondrial membrane (IMM) that holds the assembled electron transport chain (ETC). The IMM forms cristae, an inter membrane space (IMS), and an outer mitochondrial membrane (OMM) (Rambold & Pearce, 2018; Tilokani et al., 2018). Unlike other organelles, the mitochondria have their genome (mitochondrial DNA; mtDNA), which is comprised of 16,569 base pairs that encode for 2 ribosomal RNAs, 22 transfer RNAs, and 13 proteins for ETC subunits (Jornayvaz & Shulman, 2010). The remaining proteins (1000-1500 proteins) involved in the mitochondrial biogenesis and activity are encoded by the nuclear genome. These proteins contain a mitochondrial localization signal for efficient delivery of the polypeptide to mitochondria (Baker et al., 2007).

In mammalian cells, the number of mitochondria ranges between 200 to 2000 mitochondria per cell (Pieczenik & Neustadt, 2007). The mitochondrial mass and its location depend on the cell type and the rate of metabolic activity (Piquereau et al., 2013). In somatic cells, mitochondria do not function as a single organelle, indeed, they operate together through mitochondrial dynamics. In addition to energy production (ATP), the mitochondria are involved in several intracellular processes including the maintenance of intracellular  $\text{Ca}^{2+}$  homeostasis (signaling pathways), generation of reactive oxygen species (ROS), proliferation, cell migration, and regulation of apoptosis (Kamer & Mootha, 2015; McBride et al., 2006; Rambold & Pearce, 2018). All these processes are managed based on the mitochondrial architecture, which continuously undergoes coordinated cycles of fission and fusion (Liesa et al., 2009).

## **Mitochondrial dynamics**

Gene screening and live-cell imaging have disclosed that the mitochondria are highly dynamic. Mitochondrial dynamics overall are resumed by the balance of mitochondrial fission and fusion, cristae remodeling, mitochondrial number, distribution, and the expression pattern of the genes that control these processes (Liesa et al., 2009; Pernas & Scorrano, 2016). Mitochondria continuously undergo fission and fusion cycles to control the distribution, size, and shape of the mitochondrial network (Tilokani et al., 2018) (Fig. 7). The maintenance of equilibrium between mitochondrial function, morphology, and cellular homeostasis is mediated by a heterogeneous group of proteins that coordinate their activities (Lee & Yoon, 2016). Mitochondrial number and distribution are controlled by the fission machinery, as well as a response to changes in energetic cellular needs (Bereiter-Hahn, 1990) (Fig. 7). However, fusion occurs to ensure mitochondrial preservation, biochemical homogeneity, regulation of mtROS levels, and exchange of mutated mtDNAs (Pernas & Scorrano, 2016; Vafai & Mootha, 2012). Furthermore, mitochondrial dynamics and intracellular metabolism are connected. ATP deprivation and starvation conditions drive mitochondria to interconnect with each other to form an elongated mitochondrial network (Gomes et al., 2011; Mitra et al., 2009) (Fig.7). Long tubular forms of mitochondria ensure energy restoration and the exchange of metabolites (Gomes et al., 2011). On the contrary, mitochondrial fission is promoted by access to nutrients (Jheng et al., 2012) (Fig. 7).

# Mitochondrial dynamics

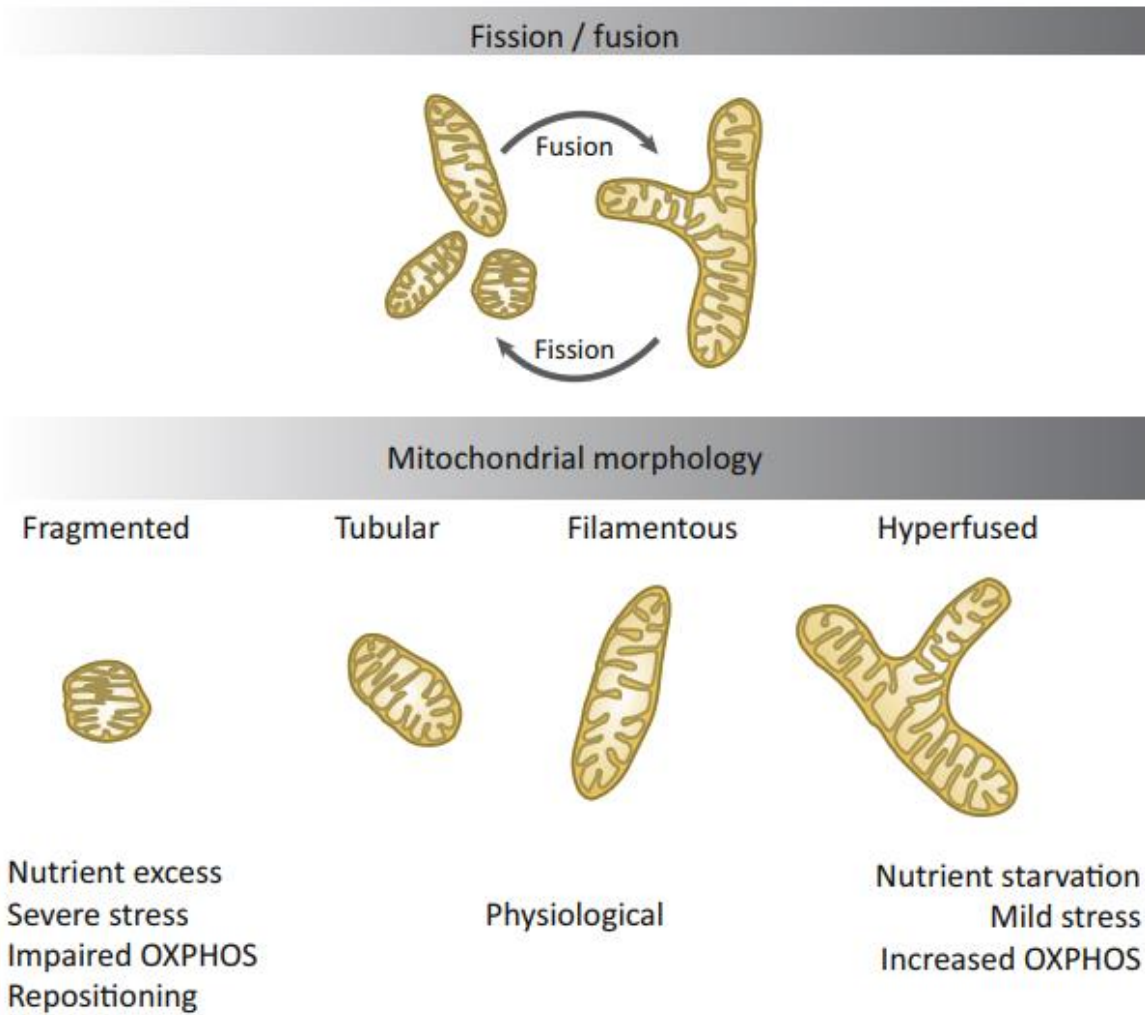


**Figure 7. Mitochondrial morphology in different conditions.** Mitochondria are dynamic organelles continuously enrolled in fission and fusion cycles depending on the nutrient availability, cell cycle stage, and extracellular stimuli. (Rambold & Pearce, 2018)

## **The mitochondrial fission and fusion machinery**

### **Outer membrane fission by Drp1**

The mitochondrial fission and fusion machinery are tightly regulated by a family of GTP-dependent dynamin-related proteins (Kasahara & Scorrano, 2014).

The central protein that mediates mitochondrial OMM fission is the large GTPase dynamin-related protein 1 (Drp1) (Ingerman et al., 2005; Nakamura et al., 2006). Drp1 assembles into oligomeric spirals in OMM and promotes mitochondrial division at specific points. The binding of Drp1 on mitochondria is mediated by OMM receptors including the mitochondrial dynamics proteins of 51 and 49 kD (MiD51 and MiD49), the mitochondrial fission protein 1 (Fis1), and the mitochondrial fission factor (Mff) (Labbé et al., 2014). Furthermore, the earlier stage of Drp1 oligomerization is controlled by the ER and actin (Friedman et al., 2011; Manor et al., 2015). Once Drp1 is recruited to the OMM, the structural conformation of Drp1 changes via GTP binding and hydrolysis resulting in membrane constriction and scission (Fig. 8B).

### **Inner membrane fission by S-OPA1 and MTP18**

The machinery of IMM fission is not fully understood. Several reports disclosed that the short isoform of optic atrophy 1 (S-OPA1) (Anand et al., 2014) and the mitochondrial protein 18 kDa (MTP18) proteins have a crucial role in the IMM fission process (Tondera et al., 2005). S-OPA1 is generated from L-OPA isoform cleavage by Yeast Mitochondrial AAA Metalloprotease Like 1 ATPase (YME1L) and Overlapping with the M-AAA Protease 1 Homolog (OMA1) (Anand et al., 2013). Deletion of YME1L and OMA1 leads to the reduction of S-OPA1 isoform in IMM and promotes permanent mitochondrial fusion. Also, deletion of MTP18 leads to hyperfused mitochondria which suggest its direct or indirect role in the fission machinery (Tondera et al., 2005). On the other hand, overexpression of MTP18 enhances Drp1 recruitment to mitochondrial fission, the molecular mechanism behind the role of MTP18 in IMM fission remains unclear (Wai & Langer, 2016).

## **Outer membrane fusion by mitofusins**

Similar to mitochondrial fission, mitochondrial fusion occurs also in both membranes, IMM and OMM, mediated by dynamin-like GTPases. First, OMM fusion is controlled by mitofusin1 and mitofusin 2 (MFN1 and MFN2) in mammals (H. Chen et al., 2003; Koshiba et al., 2004) (Fig. 8A). MFNs ensure the maintenance of the reticular formation of the mitochondrial network. The C-termini of MFN 1 and 2 are anchored to the OMM while the N-termini possess the catalytic GTP-binding domains. Depending on the GTP hydrolysis, the allosteric conformation of MFN 1 and 2 are changed to form homo- or heterodomain interactions to mediate the OMM fusion (Koshiba et al., 2004) (Fig. 8A). Furthermore, MFN2 modulates the ER-mitochondria interaction to ensure the exchange of  $\text{Ca}^{2+}$  ions between the two organelles (De Brito & Scorrano, 2008; Friedman et al., 2011). Moreover, MFNs play a crucial role in the mitophagy process (Tanaka et al., 2010). Loss of MFNs leads to an impairment of both OMM and IMM fusion ( Song et al. 2009).

## **Inner membrane fusion by OPA1**

IMM fusion is mediated by the dynamin-like GTPase, OPA1 protein (Cipolat et al., 2004; Wong et al., 2000). OPA1 is anchored to the IMM via its transmembrane N-termini while the GTPase active domain is exposed to IMS. In mammals, splicing of OPA1 produces different OPA1 isoforms including L-OPA1 a and b. The cleavage of L-OPA1 isoforms by the metalloendopeptidase OMA1 and the i-AAA ATP-dependent metalloprotease YME1L1 generates the S-OPA1 isoforms which are named as c, d, and e (Anand et al., 2014). After L-OPA cleavage, a portion of S-OPA1 isoforms are present as a soluble form in IMS (Ishihara et al., 2006). Activities of OMA1 and YME1L are modulated by ATP abundance and extracellular stimuli (Fig. 8C). On other hand, mitochondrial depolarization, ATP depletion, and increased ROS production were associated with OMA1 and YME1L activation (Anand et al., 2014; Baker et al., 2014). The activity of OMA1 at physiological conditions is limited, but constitutively cleaves L-OPA1 at S1 (Quirós et al., 2012). Notably, even in conditions where OMA1 is overexpressed, the catalytic activity of OMA1 is low. However, different stress stimuli promote overactivation of OMA1 associated with the conversion of L-OPA1 to S-OPA1 by cleavage of L-OPA1 into S1 and S3, the accumulation of S-OPA1 isoforms causes excess mitochondrial fission (Anand et al., 2014) (Fig. 8C). YME1L ensures the proteolytic cleavage of L-OPA1 in S2 (Anand et al., 2014; Quirós et al., 2012). Stress-induced OMA1 activation not only leads to conversion of L-OPA1 to S-OPA1 but also promotes

autocatalytic proteolysis of OMA1. This action is a crucial auto-negative feedback of OMA1 to ensure the formation of a fused mitochondrial network again upon mitigation of stress (Baker et al., 2014). In addition to the regulation of IMM fusion, OPA1 regulates the cristae morphology (Olichon et al., 2003), for proper assembly of ETC supercomplex, and maintenance of mtDNA and mitochondrial respiration (Burté et al., 2015; Liesa et al., 2009; Zorzano & Claret, 2015).

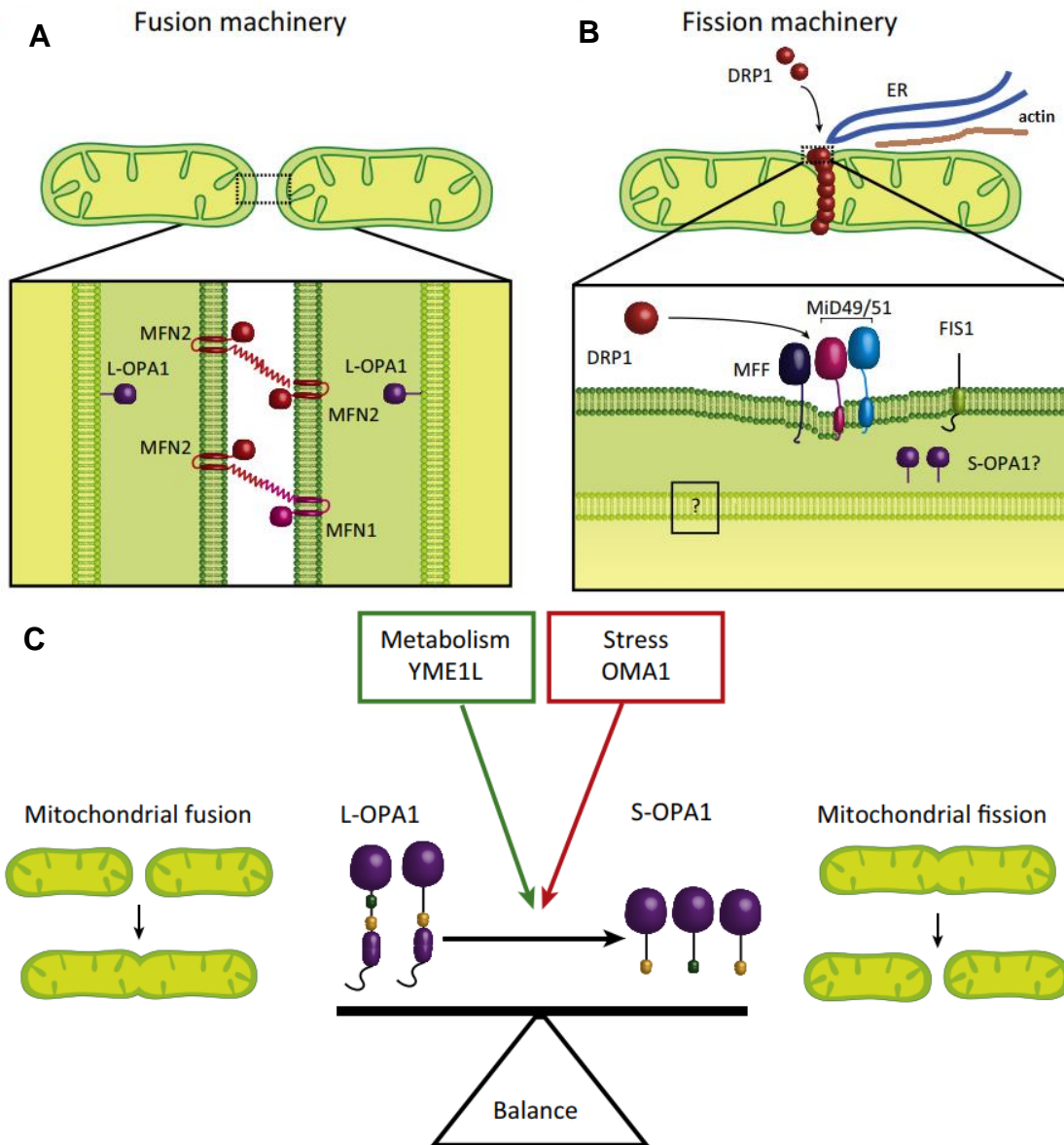


**Figure 8. Mitochondrial fusion and fission machinery.** (A) Mitochondrial fusion starts by the fusion of OMM (dark green) mediated by homo- and heterotypic interactions between MFN1 and MFN2 (red), followed by IMM (light green) fusion regulated by L-OPA1 (purple) (B) Mitochondrial fission starts by the recruitment of Drp1 (red) at the site of fission in OMM and is mediated by ER-actin (blue-brown) and Fis1, the receptor of Drp1, Mff, and MiD49/51. IMM fission is mediated by S-OPA1 isoform. (C) The activities of OMA1 and YME1L are regulated by responses to stress and metabolic stimuli, respectively. The mitochondrial network is maintained by the balanced formation of L- and S-OPA. The stressed conditions lead to OMA1 hyperactivation, thereby accumulation of S-OPA1 and access to mitochondrial fragmentation. Modified from (Wai & Langer, 2016).

## Mitochondrial bioenergetics

Mitochondria play a crucial role in the maintenance of cell metabolism through the coordination of cell adaptability to critical conditions, such as oxidative stress, starvation, and DNA damage (Vyas et al., 2016). Thus, the mitochondria are multifunctional organelles. Cells generating their energy starting from primary energy sources such as carbohydrates, amino acids, and fatty acids (FAs). The energy is stored in chemical bonds of ATP and GTP (Walsh et al., 2018) (Fig. 9). The consumed fuels are metabolized to provide sample metabolites such as pyruvate, amino acids (glutamine), and FAs, and then delivered into the mitochondrial matrix for the tricarboxylic acid cycle (TCAC). The electrons produced from TCAC are conserved as two forms NADH and FADH<sub>2</sub> (electron donors) (Mitchell, 1961). Then the electrons are transferred from, NADH and FADH<sub>2</sub> to pass along through the ETC in the IMM. The ETC consists of four enzymatic complexes; NADH ubiquinone oxidoreductase (CI), succinate dehydrogenase (CII), cytochrome *c* oxidoreductase (CIII), and cytochrome *c* oxidase (CIV) that are embedded in the IMM (Whitehall & Greaves, 2020) (Fig. 9).

Electrons from NADH are transferred to CI, then to the lipid-soluble ubiquinone (Q) to form ubiquinol (QH<sub>2</sub>) (Hinkie et al., 1991). The reduced QH<sub>2</sub> shuttles the electrons through the mitochondrial membrane to CIII. CIII transfers the electrons to cytochrome *c* (Cyt *c*) mediated by cytochrome *b* (Hatefi, 1985). Cyt *c* carries the electrons (2<sup>-e</sup>) to the final complex; CIV, which catalyzes the irreversible reduction of O<sub>2</sub>, to form H<sub>2</sub>O (Hatefi, 1985). Movement of electrons from the CI to CIII is coupled with the pumping of four protons into the IMS, similar from CIII to cytochrome *c* which is coupled with the pumping of two protons into the IMS (Hinkie et al., 1991). FADH<sub>2</sub> carries the electrons directly to CII, and then they pass to CIII through the Q-lipoprotein. Interestingly, the energy of electron transfer from FADH<sub>2</sub> to Q is not sufficient for proton pumping (Hinkie et al., 1991). The pumped protons in the IMS create mitochondrial membrane potential ( $\Delta\Psi_m$ ). The proton gradient ( $\Delta pH$ ) and  $\Delta\Psi_m$  create the transmembrane potential of hydrogen ions. The  $\Delta pH$  force in the IMS promotes the motility of complex V (ATP synthase) to ensure the electrochemical gradient equilibrium across the IMM. This force is used for the phosphorylation of adenosine diphosphate (ADP) to ATP (Hatefi, 1985). The primary metabolites used for mitochondrial ATP generation are pyruvate, FAs, or amino acids (AAs) with a different process of catabolism, but all carbon material pass through the TCAC. Mitochondria are also a part of the intracellular biogenesis of a vast variety of metabolites such as cholesterol, glucose, nucleotides,

heme (Ahn & Metallo, 2015; Sano et al., 1959), FAs (Hiltunen et al., 2009), AAs (Yang et al., 2016). Furthermore, the mitochondria have a crucial role in calcium homeostasis (Gunter et al., 2004), the modulation of ROS production (Loschen et al., 1971), and induction of apoptosis (Liu et al., 1996).

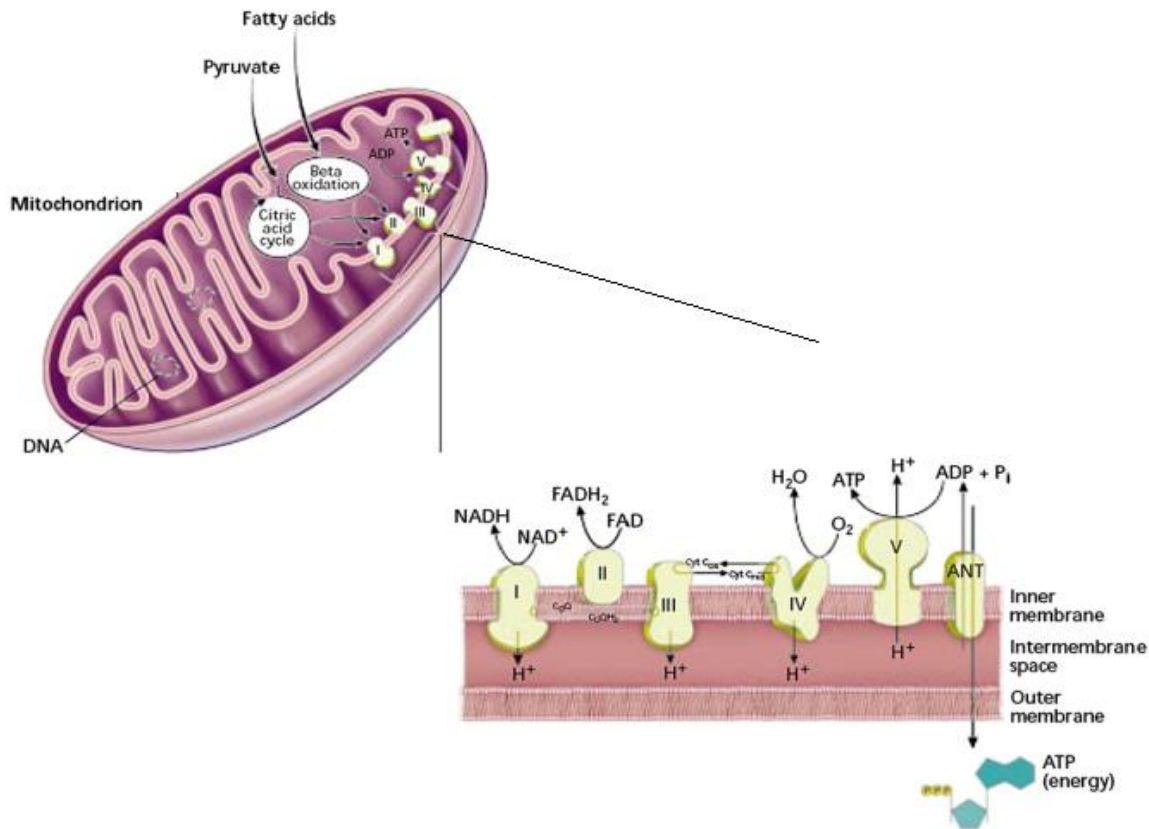


**Figure 9. Mitochondria; the main place of ATP production.** Metabolites, such as pyruvate and FAs, are carried into the mitochondrial matrix mediated by specific transporters. FAs pass through beta-oxidation cycles, however, pyruvate via pyruvate dehydrogenase complex enters the TCAC. Electrons that carry high energy produced from the TCAC are captured by the electron carriers NAD<sup>+</sup> and FAD, to form NADH and FADH<sub>2</sub>. FADH<sub>2</sub> and NADH, each deliver the electrons into the ETC. High-energy electrons pass through ETC complexes and are coupled with protons. The proton gradient between the IMS and the matrix creates a force that changes the structure of the protein assembly of the CV accompanied by the transformation of ADP and inorganic phosphate to ATP. Modified from (Pieczenik & Neustadt, 2007)

## Mitochondrial respiratory chain inhibitors

Rotenone is a natural hydrophobic pesticide. *In vivo* studies demonstrated that rotenone induces the pathological symptoms of PD in animal models (Betarbet et al., 2000). Furthermore, treatment of SH-SY5Y cell line with rotenone is used as an *in vitro* model for PD. Rotenone inhibits the mitochondrial CI by blocking the electron transport between the NADH dehydrogenase and coenzyme Q (Gutman et al., 1968). Thus, rotenone inhibits the oxidative phosphorylation process and induces high ROS production (Radad et al., 2006). Reports revealed that rotenone induces apoptosis in several mammalian cells such as SH-SY5Y cells (Newhouse et al., 2004) and human breast cancer cells (MCF-7 ) (Deng et al., 2010), through the JNK and p38 signaling pathway.

Antimycin A is an antibiotic that was used for the first time as an antifungal compound. Similar to rotenone, antimycin A is a potent inhibitor of aerobic respiration. Antimycin A inhibits the CIII of ETC by preventing the transfer of electrons between cytochromes *b* and *c* (Campo et al., 1992; Van Ark & Berden, 1977). It has been shown that Antimycin A induces ROS production and depletion of glutathione (GSH) content in HeLa cells, thus, inhibits cell growth and induces apoptosis (Woo et al., 2007). another report argue that the antimycin-induced cell death is not due to an increase in ROS production but due to the strongly depleted GSH level (Y. H. Han et al., 2008).

Oligomycin is another inhibitor of the oxidative phosphorylation process, unlike rotenone and antimycin A, oligomycin inhibits the phosphorylation step rather than the ETC. oligomycin inhibits specifically the F<sub>0</sub>F<sub>1</sub>-ATP synthase, thereby blocks the ATP production. Studies demonstrated that HepG2 cells treated with oligomycin increased ROS production and cytosolic Ca<sup>2+</sup>, however, SK-Hep-1 cells respond to oligomycin by enhanced migration (Chang et al., 2009). Reports demonstrated that the high rate of invasion and migration induced by oligomycin treatment in lung cancer cells is due to the increase of phosphorylated (p) protein kinase B (AKT) and p AMP-activated protein kinase (AMPK). (Han et al., 2018). Furthermore, oligomycin has been shown to induce apoptosis in human lymphoblastoid cells (Wolvetang et al., 1994).

Rotenone, oligomycin, and antimycin A are used as a positive control of mitochondrial oxidative phosphorylation disorders, and as *in vitro* model to study aging-associated diseases (Wolvetang et al., 1994).

## **Diseases related to mitochondrial dysfunctions**

The majority of mitochondrial-related diseases, such as neurodegenerative, cardiovascular diseases, cancer, and aging-related mitochondrial function, are caused by dysregulation of ROS production (Wei et al., 1998). In normal cellular respiration, mitochondria consume approximately 85 % of cellular oxygen to produce ATP (Shigenaga et al., 1994). During this process, a portion of consumed oxygen is converted into free superoxide ( $O_2^-$ ). The copper/zinc superoxide dismutase (Cu/Zn SOD) converts  $O_2^-$  into hydrogen peroxide ( $H_2O_2$ ) then  $H_2O_2$  is converted into water by peroxidases and catalases, thus the free radicals that may cause mitochondrial or cellular damages are eliminated by this tightly regulated process (Green et al., 2004; Shigenaga et al., 1994; Wallace, 2005). In case of a defect of the conversion machinery by extracellular stimuli, genetic disorders, or enzymatic defects, ROS are accumulated in mitochondria (Sies, 1993). Mitochondria and other cellular organelles are exposed to free radicals causing oxidation of proteins, DNA, and lipids, thus altering their functions (Liu et al., 2002; Shigenaga et al., 1994). Furthermore, the interaction of  $O_2^-$  with nitric oxide (NO), which that is present in the cytosol and produced in the mitochondria as well, produces the peroxynitrite ( $ONOO^-$ ) radicals, which are also highly damaging reactive species. (Carreras et al., 2004; Green et al., 2004).

Neurodegenerative diseases, such as Huntington's disease (HD), amyotrophic lateral sclerosis (ALS), Alzheimer's disease (AD), and Parkinson's disease (PD) are characterized by a progressive loss of the neuronal system. Mitochondrial dysfunction is a common factor in these diseases. Increased ROS production and impeded mitochondrial dynamics are some of the characteristics of neuronal disorders, in particular AD. Highly fragmented mitochondria in AD patients prevent mitochondrial restoration, which mainly accrues during mitochondrial fusion (Calkins et al., 2011), thus, leads to increased oxidative damage in neurons, mitochondrial dysfunction, and impairment of energy homeostasis (Swerdlow, 2018). Furthermore, it has been shown that the mitochondrial distribution in neuronal cells (axonal and synaptic parts) is crucial for proper neuronal function, which is disturbed in many neurodegenerative diseases (Calkins et al., 2011; Stokin et al., 2005; Trushina et al., 2012). Inhibition of mitochondrial CI mimics the pathological phenotype of PD. Therefore mitochondrial CI inhibitors, such as rotenone, are used in laboratory animal models of PD (Betarbet et al., 2000). Additionally, in PD patients, the CI activity is disordered and accompanied by increased oxidative stress (Schapira et al., 1990).

Furthermore, mitochondrial dysfunctions is found to participate in several cardiac diseases, such as ischemia, atherosclerosis, heart failure. Increased ROS production, and disruption of cellular energy production are the common features of different cardiac diseases. Uncontrolled ROS production leads to the damage of vascular endothelial cells, thus facilitate enhanced immune reaction against the vascular wall and initiates atherosclerotic plaque formation (Chrissobolis et al., 2011). Furthermore, impaired lipid metabolism, increased the vulnerability of unstable plaque formation (Libby et al., 2016; Madamanchi & Runge, 2007)

mtDNA mutation is another factor of mitochondria dysfunction in both cardiovascular and neurodegenerative diseases (Sazonova et al., 2017; Heidari et al., 2020; Vecoli et al., 2018). Accumulation of ROS is the most important factor that induces mtDNA mutagenesis. Increased frequency of mutations in mtDNA results in inefficient ETC complexes, thereby reducing mitochondrial respiration. ROS production also influences mitochondrial DNA polymerase  $\gamma$  (POLG) function by reducing its replication fidelity of mtDNA, which is another source of mtDNA mutation. Reports demonstrated that the transfer of mtDNA of AD patients into cell lines with deficient mtDNA showed a deficiency in ETC enzymes, which is a hallmark of mitochondrial dysfunction, the authors speculated that a part of mitochondrial dysfunction in AD is due to mtDNA mutations (Wang et al., 2005). Similar assay, introducing an mtDNA of PD patients in to human cells with depleted mtDNA, resulted in a variety of pathological features of PD, such as impaired CI activity, increased ROS production, and cell sensitivity to stress (Gu et al., 1998; Swerdlow et al., 1996). The authors hypothesized that mtDNA impairment is a part of PD-inducing factors (Giannoccaro et al., 2017).

## Cross-talk between the UPS and mitochondria

UPS, as discussed above, is involved in several cellular processes, such as cell cycle, apoptosis, and protein turnover (Voges et al., 1999). Proteasomes are present in the cytosol, nucleus, and they interact with ER as well (Enenkel, 2014). Moreover, the mitochondria are also considered as a compartment of various UPS components (Cilenti et al., 2014; Karbowski et al., 2007; Nakamura et al., 2006; Yonashiro et al., 2006). The crosstalk between mitochondria and the UPS has been revealed in different mitochondrial processes, such as dynamics, activity, and homeostasis (Bragoszewski et al., 2013; Tatsuta, 2009). Moreover, impaired UPS function influence various mitochondrial functions (Altmann & Westermann, 2005). The ubiquitination of the key mitochondrial fission and fusion proteins, located at the OMM, facilitates the recognition and turnover of proteins by the UPS. Thereby, the mitochondrial dynamics and homeostasis are also UPS-dependent. The OMM is orchestrated by several UPS components, such as E3 ligases, for ubiquitination, and DUBs for deubiquitination (Karbowski et al., 2007; Nakamura & Hirose, 2008). There are two well-known mitochondrial ubiquitin ligase enzymes, the E3 Ub ligase known as MITOchondrial ubiquitin Ligase (MITOL), which is anchored to OMM and mediates the ubiquitination of a variety of mitochondrial-linked protein substrates. The substrates of MITOL include the key proteins for the mitochondrial fission and fusion machinery; Drp1, Fis1, MiD49, Mfn2, and Mcl1 proteins (Nakamura et al., 2006; Park et al., 2010; Sugiura et al., 2013; Xu et al., 2016; Yonashiro et al., 2006). Furthermore, MITOL ensures the ubiquitination of damaged and mutated mitochondrial-associated proteins (Karbowski et al., 2007; Yonashiro et al., 2006, 2009). The other E3 Ub ligase is named Mitochondrial Ubiquitin Ligase Activator of NF- $\kappa$ B (MULAN). Similar to MITOL, MULAN is incorporated in the OMM and modulates the mitochondrial dynamics by reducing the level of Mfn2 (Cilenti et al., 2014). Importantly, the UPS targets mitochondrial proteins from different biological processes; such as the TCAC, and oxidative phosphorylation (Jeon et al., 2007; Peng et al., 2003; Sickmann et al., 2003).

Several hypotheses were proposed regarding the mechanism of internal mitochondrial protein turnover, one of hypothesizes proposes the existence of a mechanism that retro-translocates the IMM and matrix proteins to the cytosol and the OMM for degradation. This type of degradation is named the mitochondria-associated degradation (MAD) system (Chatenay-Lapointe & Shadel, 2010; Heo et al., 2010). In support of this hypothesis, one report has been demonstrated that the

inhibition of heat shock protein 90 (HSP90) in colon cancer cells (COLO 205) leads to cell death mediated by mitochondrial dysfunction (Magineantu et al., 2007). The impaired mitochondria were characterized by the accumulation of proteins located to the IMM and the mitochondrial matrix due to the delay of degradation and increased half-life of the proteins. The oligomycin sensitivity-conferring protein (OSCP), which is a component of complex V, and resides at the IMM, is also one of these proteins. These findings suggested that the degradation of the OSCP protein requires its retro-translocation from the IMM to the OMM to be accessible for UPS, and that is an HSP90 dependent process (Magineantu et al., 2007). Moreover, using proteasome inhibitors led to the accumulation of mitochondrial encoded protein COX1 (Cytochrome *c* oxidase I), which also requires retro-translocation for access by the proteasome, similarly to UCP2 (uncoupling protein 2), and UCP3 (Azzu et al., 2010; Azzu & Brand, 2010). It is evident that the IMM and mitochondrial matrix proteins are retro-translocated to the OMM for degradation purposes, but the mechanism of interaction between the UPS and the OMM remains unclear.

## AIMS

Our main goal in the present study is to reveal new cellular functions of PA200, an alternative activator of the proteasome.

First, we planned to determine the effects of PA200 on cell viability, necrosis, and apoptosis under normal conditions and stressed mitochondria using different mitochondrial inhibitors (rotenone, oligomycin, antimycin A). Furthermore, since PA200 is a chromatin component and translocated to the nucleus upon irradiation exposure, we aimed to investigate the possible role of PA200 in the transcriptional machinery under normal conditions and upon mitochondrial stress using ChIP and ChIP-seq approaches supported by RT-qPCR analysis. Second, we aimed to reveal new promising functions of PA200 by investigating the global transcriptomic pattern upon depletion of PA200 using RNA-seq approach and functional gene category analysis supported by functional validations. Deletion of the PA200 ortholog in yeast (Blm10) leads to mitochondrial dysfunction, thus we speculated that this function is conserved in mammals; we aimed to investigate mitochondrial activity, biogenesis, and dynamics.

The obtained data may provide more information on the interplay between the proteasome activator, PA200, cell survival, and mitochondrial integrity, and might contribute to develop therapies for aging-related diseases, such as neurodegenerative diseases.

# MATERIALS AND METHODS

## Chemical and reagents

All materials were purchased from Sigma-Aldrich unless specified otherwise. The chemicals and the reagents were used in this study are the following; Dulbecco's Modified Eagle's Medium-high glucose (DMEM), Trypsin/EDTA (T/E), phosphate buffer saline (PBS), heat-inactivated fetal bovine serum (FBS, Gibco™, Thermo Fisher), L-glutamine (LG), penicillin/streptomycin (PS), puromycin (Gibco™, Thermo Fisher), RNA extraction Kit (Zymo Research), Trizol, High-Capacity cDNA reverse transcription Kit (Applied Biosystems), SYBR Premix Ex Taq II (Clontech), sulforhodamine B (SRB, 80100), lactate dehydrogenase (LDH) cytotoxicity assay Kit (786-210, G-Biosciences), propidium-iodide (PI), dimethyl sulfoxide (DMSO), rotenone, oligomycin, antimycin A, carbonyl cyanide-4 (trifluoromethoxy) phenylhydrazone (FCCP), formaldehyde, glycine, bovine serum albumin (BSA) (Roche, Germany), PCR Clean-up Kit (Qiagen), Radioimmunoprecipitation assay (RIPA) buffer (50 mM Tris-HCl, 150 mM NaCl, 0.5 % Na-deoxycholate, 2 mM EDTA, 1 % NP-40, 50mM NaF), Bradford reagent (500-0205, Bio-Rad laboratory), nitrocellulose membranes (0.45 µm NC Amersham. Germany), Hydrophilic polyvinylidene fluoride (PVDF) membrane (0.45 µm NC Amersham. Germany), western blotting luminol reagent (sc-2048, Santa Cruz Biotechnology), plasmids pGIPZ-GFP (Dr. Marion Schmidt, shRNA Facility of the Albert Einstein College of Medicine, Bronx, NY, USA), packaging and enveloping vectors; HDM-Hgpm2, RC-CMV/Rev, HDM-tat1b, and HDM-VSV-G (Dr. Orsi Giricz, Albert Einstein College of Medicine, Bronx, NY, USA), lipofectamine 3000 (ThermoFisher), gelatin, Mitotracker Red CMXRos (ThermoFisher), Hoechst 33342 (62249, Thermo scientific), FluoroBrit DMEM medium (A18967-01, Gibco), agarose, tetramethylrhodamine ethyl ester (TMRE) (ThermoFisher), 41µm nylon Net Filter (Merck Millipore), seahorse bioscience XF96 calibrant solution (pH 7.4) (Seahorse Bioscience), XF assay medium (Seahorse Bioscience), D-Glucose, 2-deoxy-D-glucose (2-DG), oxyblot protein oxidation detection kit (S7150, Millipore), Dithiothreitol (DTT), sodium dodecyl sulfate (SDS), reactive oxygen species (ROS) detection assay Kit (ab 186029, Abcam, UK), Ribonuclease I, nonfat-dried milk bovine, Trichloroacetic acid (TCA), Human Phospho-Kinase Array Kit.

## Antibodies

*Table 1. List of antibodies used in this study*

Antibody	Source	Catalog Number	Host	Dilution
Drp1	BD Biosciences	#611112	Mouse	1:1000
Mfn1	Abnova	#H00055669-M04	Mouse	1:1000
Mfn2	Sigma Aldrich	#WH0009927M3	Mouse	1:800
Opa1	Novus Biologicals	#NB110-55290	Rabbit	1:1000
PA200	Novus Biologicals	# NBP2-22236	Rabbit	1:2000
Fis1	Invitrogen	#PA1-41082	Rabbit	1:1000
Mff	Proteintech	#17090-1-AP	Rabbit	1:1000
β-actin	Santa Cruz Biotechnology	#sc-1616	Goat	1:5000
Hsp60	Invitrogen	# MA3-012	Mouse	1:1000
Total OXPHOS	Abcam	# ab110413	Mouse	1:250
PCNA	CST	# 13110	Rabbit	1 :1000
Anti-Mouse, HRP conjugate	Sigma-Aldrich	# A9044	Rabbit	1:3000
Anti-Rabbit, HRP conjugate	Sigma-Aldrich	# A0545	Goat	1:3000
SAPK/JNK	CST	# 9252	Rabbit	1:1000
P-SAPK/JNK (T183/Y185)	CST	# 9251	Rabbit	1:1000
c-Jun	Santa Cruz Biotechnology	# sc-74543	Mouse	1:250
P-c-Jun (S63)	Santa Cruz Biotechnology	# sc822	Mouse	1:250
Cleaved –PARP1	CST	#5625	Rabbit	1:1000
P- H2AX (S139)	TREVIGEN	4418-APC-100	Rabbit	1:1000

## Cell culture

Human neuroblastoma (SH-SY5Y) and Human embryonic kidney 293 cells (HEK293T) cells lines (European Tissue Culture) were maintained in DMEM-high glucose supplemented with 10 % heat-inactivated fetal bovine serum (FBS), 2 mM L-glutamine, 100 units/mL penicillin, and 100 µg/mL streptomycin in 5% CO<sub>2</sub> humidified incubator at 37 °C.

Lentiviral technology was used to downregulate the expression of *PSME4/PA200* in the SH-SY5Y neuroblastoma cell line.

## Downregulation of *PSME4/PA200*

Lentiviral technology was used to generate stable *PSME4/PA200* depleted cells using the SH-SY5Y neuroblastoma cell line. First, the virus soup was produced in HEK293T cells as the following, HEK293 cells were seeded in 24-well plates in DMEM high glucose to reach 80% confluency. The HEK 293T cells were co-transfected with the packaging-enveloping vectors (HDM-Hgpm2, RC-CMV/Rev, HDM-tat1b (25 ng/µl each), HDM-VSV-G (50 ng/µl)) and the expression plasmids pGIPZ-GFP containing the shRNA target sequences (100 ng/µl). pGIPZ-GFP plasmids containing Non-silencing shRNA sequences were used as a control. shRNA sequences are provided in Table 2. The packaging-enveloping vectors and the expression plasmids were co-transfected at a 1:1 ratio using Lipofectamine 3000 according to the manufacturer's protocol. The culture medium was collected at two time points after transfection, the first was at 48h and the same volume of cutler medium was added, and the second at 96 h, then the medium was filtered through 0.45-µm pore filters and immediately used for transduction. The transduction of human SH-SY5Y neuroblastoma cells was assessed as the following protocol, SH-SY5Y cells were seeded in 24 well plates at 60% confluency in DMEM high glucose. On the day of transduction (80% confluency), cells were incubated with virus-containing antibiotic-free media supplemented with 8 µg/ml polybrene, in a 5% CO<sub>2</sub> humidified incubator at 37°C. The GFP expression was monitored every day under a fluorescent microscope. After 72h of viral transduction, the culture medium was supplemented with 1.25 µg/ml puromycin for selection. The puromycin selected and amplified cells were further analyzed by RT-qPCR and Western blot to verify the depletion of *PSME4/PA200*.

**Table 2. List of shRNA sequences used for PA200 silencing**

Gene ID	Gene symbol	Species	Vector	Marker	Sense strand sequence	Start	End	Target
23198	PSME4	Human	pGIPZ	GFP	CCCAGCGATGTGTTGC AGA	4180	4198	CDS
23198	PSME4	Human	pGIPZ	GFP	AGGTCTGTCTTCTACG TTT	1808	1826	CDS
None	GIPZ empty vector		pGIPZ	GFP	Empty pGIPZ vector (no shRNA)			

### **Antibiotic titration and selection of shPA200 cells**

To select the successfully transduced cells (only cells that constitutively express the shRNA sequence), first, the titration of puromycin was assessed in the SH-SY5Y cells. Cells were seeded in 6 well plates in DMEM high glucose medium to reach 90% confluency. Puromycin was diluted in complete medium at the final concentrations; 0, 0.5, 1, 1.25, 2.5, or 5 µg/ml. Cells were incubated with a selection medium for 10 days and replaced every 2 days, the lowest concentration of puromycin that begins to give massive cell death in 7 days and kills all the cells within 10 days was determined as 1.25µg/ml. The transduced cells were maintained in 1.25 µg/ml puromycin in DMEM high glucose.

## **Cell lysis and protein measurement**

The total cell lysates from control or shPA200 cells treated with appropriate drugs were extracted using RIPA buffer (50mM Tris-HCl, 150mM NaCl, 0.5 % Na-deoxycholate, 2 mM EDTA, 1% NP-40, 50mM NaF) supplemented with protease inhibitors cocktail and EDTA-free protease inhibitors. Benzamedin and PMSF were used at the final concentration of 1mM and 1xEDTA-free protease inhibitors. Cells were scraped on ice for 5min and then the homogenate was centrifuged for 10 min at 4°C /12.000 rpm. The supernatant was transferred carefully into a clean Eppendorf tube. The protein concentration was determined using the Bradford protein assay protocol. Briefly, before the measurement, each protein sample was diluted 5 times to get more precise measurements and to avoid saturation. 5µl from each diluted sample was added to 125µl Bradford reagent in 96-well clear-bottom plates. In parallel, the standard curve of BSA protein was made by making a serial dilution of BSA in ddH<sub>2</sub>O (2, 1, 0.5, 0.25, 0.125, and 0.0625 µg/µl). Then the plate was incubated with shaking for 5 min at 37°C, 500 rpm in dark. The air bubbles were removed and the absorbance was measured at 595 nm using a microplate reader. The BSA standard curve equation was used to determine the concentration of each sample. The protein samples were denatured and reduced using 5 x SDS loading buffer 1:5 (v/v), the reducing reagent DTT was used at the final concentration of 50 mM. Before the loading, the samples were boiled for 5 min at 95°C.

## **Subcellular fractionation**

The subcellular fractionation of control and shPA200 cells was performed using cell fractionation kit according to the manufacturer's protocol. Cells were fractionated on three fractions, cytosolic, mitochondrial, and nucleus fraction. The fractionation was based on centrifugation and detergent-buffers formulations provided in the kit. We used 20 µg of protein from each mitochondrial fraction of control and shPA200 cells for western blot analysis.

## **RNA extraction**

The cells were seeded in 6 well plates (8 x10<sup>5</sup> cell/well) in DMEM-high glucose at 37°C in a 5 % CO<sub>2</sub> incubator. Cells were subjected to mitochondrial inhibitors with appropriate concentrations for 24h. Total RNA was extracted using RNA extraction kit according to the manufacture's protocol, briefly, after washing the cells with 1 x PBS, cells were lysed using 300µl TRIzol reagent and homogenized by pipetting up and down for 5 min at 4°C. The homogenized samples were

transferred into the Zimo Speen column. After centrifugation and DNAase I digestion, the RNA was washed several times with washing buffers (provided in the kit) and eluted in clean RNAase-free Eppendorf tubes. The concentration and purity of RNA were determined using NanoDrop™ Spectrophotometers.

### **Reverse transcription and cDNA synthesis**

The cDNA preparation was assessed by a High capacity cDNA reverse transcription kit. The reverse transcription was performed by the following steps; first, the 2 x reverse transcription master mix for one reaction was prepared by mixing 4.2 µl nuclease-free water, 2µl 10 x RT-Buffer, 0.8 µl 25 x dNTP Mix (100 mM), 2µl 10 x RT Random Primers, and 1 µl Multi-Scribe™ reverse transcriptase at 4°C. 1 µg from the total mRNA was diluted with nuclease-free water to 10µl final volume. 10 µl from the 2 x master mix was mixed with 10µl (1µg mRNA) at 4°C. The tubes were centrifuged to spin down the content and to eliminate any air bubbles. The thermal cycler was programmed as the following; Step 1; 25°C (10 min), Step 2; 37°C (120 min), Step 3; 85°C (5 min) and finally Step 4; 4°C (∞). The quality of cDNA was checked by loading a 1 µl sample on a 1% agarose gel.

### **Quantitative Real-Time PCR**

Real-time qPCR (RT-qPCR) was performed using SYBR Premix Ex Taq II from Takara (Clontech) according to the manufacturer's protocol. Briefly, the cDNA was diluted at 1:20 (v/v) in nuclease-free water. For one RT-qPCR reaction, 5 µl SYBR premix, 0.4 µl (10µM ) reverse primers, 0.4 µl (10µM ) forward primers, 2.2 µl Nuclease-free water, and 2 µl diluted cDNA (1:20) were added to each port of 384 well PCR plate at 4°C. The PCR plate was then centrifuged for 20 sec at 2000 rpm (24°C) to spin down the content and to eliminate any air bubbles. The Light cycler 480 thermocycler (Roche) was set to the following cycling conditions ; Stage 1: Initial denaturation 95°C (30 sec) 1 cycle, Stage 2: PCR 95°C (5 sec), 60°C (30 sec) 40 cycles, Stage 3: Melting Curve Analysis 95°C (0 sec), 65°C (15 sec), 95°C (0 sec), Cooling 50°C (30 sec) 1 cycle. Threshold values ( $C_p$ -values) of all replicate analyses were normalized to GAPDH and/or ACTB.  $2^{-\Delta\Delta C_t}$  values were used to calculate the fold change in the expression levels. The primer pairs used in the RT-qPCR experiments are summarized in Table 3. Data were statistically analyzed according to (Livak & Schmittgen, 2001).

**Table 3. Primer pairs used for RT-qPCR analysis**

Gene symbol	Species	Forward sequence (5'-3')	Reverse sequence (5'-3')
PSME4	human	ATGGAGAGTGCCTGAACTATTG	GTAGGTCAGCACACTTCCTATTC
cJUN	human	CCCCAAGATCCTGAAACAGA	CCGTTGCTGGACTGGATTAT
cFOS	human	CCGGGGATAGCCTCTCTTAC	GTGGGAATGAAGTTGGCACT
MAPK8	human	TGTGGAATCAAGCACCTTCA	GTTTTCTTGTAGCCCATGC
MAPK9	human	GGGAACACCATCAGCAGAGT	GTATGGGTGACGCAGAGCTT
MAPK10	human	TGGAAGTGGGAGACTCAACC	TGGTTCTGAAAGGGTCTGCT
CASP5	human	ACGGATCAAAGTCGACCAG	GATCAGGGCCTTGTCTTCAA
CASP4	human	TCTCACCTGTTGGAATGCAC	TGACCCGAACCTTGTCTTCA
ATP5E	human	CCTACTGGAGACAGGCTGGA	TTTTACGTTGCTGCCAGAAG
ATP6VOE 1	human	TTGTGATGAGCGTGTCTCTGG	CTTCTCCTCAAGGCCAATG
PPP1R12B	human	ACCAGTTCCCACCTGCTATG	ATTGATGCCTGTGCCTCTTC
API5	human	CTCACCATGCCGACAGTAGA	CAGCCAATTCTGGAAAATGC
CDC6	human	AGTTTGTTCAGGGGCTTGTG	CGAGACAGCTTCCTTTTTGG
GAPDH	human	GAGTCAACGGATTTGGTCGT	GATCTCGCTCCTGGAAGATG
OPA1	human	CACTTCCTGGGTCATTCTCTG	TGCTTCGTGAAACCAGATGT
FIS1	human	AGCTGGTGTCTGTGGAGGAC	ACGATGCCTTTACGGATGTC
MIEF2	human	GCAGAGTTCTCCCAGAAACG	GTCTGCCTTGGTGTTCATCCT
MIEF1	human	GCAAAGGCAAGAAGGATGAC	CTTCATGTCCCTGTTTCAGCA
MFF	human	AAACGCTGACCTGGAACAAG	TTTTCAGTGCCAGGGGTTTA
MIEF1	human	GCAAAGGCAAGAAGGATGAC	CTTCATGTCCCTGTTTCAGCA
MIEF2	human	GCAGAGTTCTCCCAGAAACG	GTCTGCCTTGGTGTTCATCCT
ACTB	human	GACCCAGATCATGTTTGAGACC	CATCACGATGCCAGTGGTAC

**Table 3. Continued**

MFN1	human	CGGAACTTGATCGAATAGCC	AGAGCTCTTCCCCTGCTTG
MFN2	human	ATGCATCCCCACTTAAGCAC	AGCACCTCACTGATGCCTCT
DNM1L	human	AGATCTCATCCCGCTGGTC	CAGATCCTCGAGGCAAGAAG

### **Chromatin Immunoprecipitation (ChIP)**

ChIP assay was assessed in SH-SY5Y cells. Cells were grown in T-75 flasks, in DMEM high glucose medium, to reach by the next day 75 % confluency, the cells then were treated either with vehicle (DMSO) or mitochondrial inhibitors at the final concentrations of 10 $\mu$ M rotenone, 3  $\mu$ M oligomycin and 100 nM antimycin A, for 3h in 5 % CO<sub>2</sub> humidified incubator at 37 °C. After treatment, the cells were washed twice with 1 x PBS, trypsinized for 2 min at 37 °C, and collected in complete medium in 15 ml falcon tubes. Formaldehyde, at a final concentration of 1%, in culture medium was used to cross-link the cells for 10 min at 24 °C. 125 mM glycine was applied for 10 min at 24 °C to quench the cross-linking. Cells were spun for 2 min / 400  $\times$  g at 4 °C, washed two times in cold PBS, and suspended in lysis buffer (1 % Triton, 0.1 % SDS, 150 mM NaCl, 2 mM EDTA, 1 mM EGTA, 20 mM Tris (pH 8.0)). The samples were then sonicated twice, 5 cycles for 30 s on/off with maximum level. The cell debris was pelleted by centrifugation for 2 minutes at 10,000  $\times$  g, and the supernatant was used for subsequent ChIP. Antibodies against PA200 proteasome activator, and H3K27ac were used for immunoprecipitation (IP). 200  $\mu$ l of supernatant from each sample was diluted in IP wash buffer 1 (1 % Triton, 0.1 % SDS, 150 mM NaCl, 2 mM EDTA, 1 mM EGTA, 20 mM Tris (pH 8.0), 2  $\mu$ g/ $\mu$ l BSA, and complete protease inhibitor) and incubated with the antibody overnight with rotating at 4 °C. The immunocomplex was then incubated with magnetic protein A conjugated beads for 6h at 4°C, with gentle rotation. The beads and immune complex conjugate were washed twice with IP wash buffer 1, once with IP wash buffer 2 (1 % Triton, 0.1 % SDS, 500 mM NaCl, 2 mM EDTA, 1 mM EGTA, 20 mM Tris [pH 8.0]), once with IP wash buffer 3 (0.25 M LiCl, 1 % NP-40, 1 % deoxycholic acid, 1 mM EDTA, 0.5 mM EGTA, 10 mM Tris [pH 8.0]), and finally twice with Tris-EDTA buffer, all at 4 °C. The elution of the protein-DNA complex was performed by adding 400  $\mu$ l of elution buffer (1 % SDS and 0.1 M NaHCO<sub>3</sub>) and decross-linked by adding NaCl to a final concentration of 0.2 M, followed by

shaking overnight at 65 °C. DNA was purified using the PCR Clean-up Kit, according to the manufacturer's protocol, and analyzed by ChIP-seq.

### **ChIP-Seq analysis**

ChIP-Seq analysis was performed in Galaxy version 18.01.rc1 (Afgan et al., 2018) using data released by NextSeq 500 System from Illumina (Center for Clinical Genomics and Personalized Medicine, Core Facility, University of Debrecen) for anti-PA200 pull-downs and publicly available data from the GEO database (SRR1631233, Bioproject PRJNA264969) for anti-H3K27ac pull-downs in control (DMSO treated) SH-SY5Y. FASTQ format files were unified to Sanger FASTQ encoding with FASTQ Groomer (Blankenberg et al., 2010). Reads were aligned to the Human Genome (v 19) using Map with Bowtie for Illumina (Langmead et al., 2009). ChIP-seq peaks were called in MACS (Zhang et al., 2008) with a p-value cutoff for peak detection set at  $10^{-3}$ .

PA200 distribution around the transcription start site (TSS) was visualized using compute Matrix/plot Profile (deepTools (Ramírez et al., 2016)) with score file: PA200 reads in bigWig format and regions to the plot: UCSC Main on Human: gtexGene in BED format. Gene promoters, enriched in PA200 and H3K27ac, were identified by returning intersects of PA200/H3K27ac peaks (in bed) and genomic regions  $\pm 2000$  bp centered on TSSs (overlapping intervals of both datasets for at least 1 bp). To compare PA200 occurrence in the genome between control and mitochondrial inhibitor-treated cells, read depth (bedtools MultiCovBed, mapped reads as BAM to count) was calculated for a set of genomic regions (merged peak intervals as bed for all considered samples). Venn diagrams were created in InteractiVenn (<http://www.interactivenn.net/>) from generated gene lists (Schmidt et al., 2005). Enriched gene ontology terms (GO) were derived using PANTHER Classification System (<http://pantherdb.org/tools/compareToRefList.jsp>; test type – Fisher's Exact; Reference List – Homo sapiens (all genes in the database) with no correction).

### **Mitochondrial live staining in high content screening (HCS) system**

PA200 depleted and control cells were seeded at the density of  $1.5 \times 10^4$  cell/well in cell carrier-96 ultra microplates in DMEM high glucose, to reach 70% confluence. After determining the type and concentration of mitochondrial inhibitor necessary to acquire high mitochondrial fragmentation among the following drugs and concentrations; 5  $\mu$ M and 10 $\mu$ M rotenone, 3  $\mu$ M and 10 $\mu$ M oligomycin, and 100 nM antimycin A. Cells then were treated for 24h with vehicle and 3

$\mu\text{M}$  oligomycin. Cells were rinsed with serum-free medium and fluoroBrit DMEM medium, respectively. Cells were incubated at  $37^{\circ}\text{C}$  in a 5%  $\text{CO}_2$  incubator with 50 nM Mitotracker Red CMXRos and 10  $\mu\text{M}$  Hoechst 33342 in serum-free media for 30 minutes. Cells were washed twice by fluoroBrit DMEM medium and live-cell imaging was assessed using an Opera Phenix HCS System (Perkin Elmer). The temperature ( $37^{\circ}\text{C}$ ) and  $\text{CO}_2$  (5%) were adjusted 25 min before starting the measurements.

### **Mitochondrial morphology analysis**

Live microscopy image acquisitions were assessed in Opera Phenix HCS System. The instrument was set up as follows; water objective (63 x, NA=1.15), the filters were adjusted according to the excitation /emission of EGFP, Hoechst 33342, and Mitotracker Red CMXRos in sequential mode to avoid the spectra overlap. After the selection of the optimal z frame position, the detection was done with a 16-bit camera with non-saturating conditions. Images were analyzed using Harmony 4.8 software and different subcellular fluorescence staining was used for cell segmentation (EGFP determines the cytoplasm, Hoechst determines the nuclei, and Mitotracker red determines the mitochondria compartments). Mitochondria were spotted using the Findspot building block and classified as follows: fragmented, short tubular, long tubular, and compact tubular based on measured properties using the PhenoLOGIC machine learning. The percentage of each class presented in total mitochondria was calculated by the following formula: (mitochondria class area / total mitochondria area) x 100.

### **Measurements of mitochondrial membrane potential ( $\Delta\Psi\text{m}$ )**

To measure the mitochondrial  $\Delta\Psi\text{m}$  in control and PA200 depleted cells, cells were seeded in 6 well plates in DMEM high glucose to reach 70% confluency. Cells were used in normal conditions or treated either with vehicle or 3  $\mu\text{M}$  oligomycin for 24h. After washing twice with serum-free medium, cells were stained with 100nM TMRE for 10 min at  $37^{\circ}\text{C}$  in 5% $\text{CO}_2$  incubators. Cells were washed with PBS and harvested with Trypsin /EDTA at 300 x g for 5min, the pelleted cells were then suspended in 200  $\mu\text{l}$  of 0.2% BSA (w/v) in PBS and 50 $\mu\text{M}$  EDTA. Before proceeding with fluorescence-activated single cell sorting (FACS), the cells were filtered through a 41 $\mu\text{m}$  nylon net filter in FACS tubes. FACS Aria III flow cytometer (BD Biosciences, Franklin Lakes,

NJ, USA) was used. Data analysis was acquired using FlowJo software version 10 (FlowJo LLC, Ashland, OR, USA).

### **Measurement of reactive oxygen species (ROS)**

Cellular ROS was measured using ROS Detection Assay Kit, as instructed by the manufactures. Cells were seeded 24 h in complete medium DMEM at 37°C, 5% CO<sub>2</sub> to reach 70 % confluence and then used in normal conditions or treated either with DMSO or 3 μM oligomycin for 24h. Cells were washed two times with PBS and incubated with ROS Deep Red dye for 30 min at 37 °C in a 5% CO<sub>2</sub> incubator in the dark. For the FACS measurement, cells were harvested by Trypsin-EDTA, suspended in 0.2 % BSA-50μM EDTA in 1x PBS, and filtered through a 41 μm nylon net filter. Data acquisition was performed using a FACS Aria III flow cytometer. Data were analyzed with FlowJo software version 10. Images of ROS-mediated deep red fluorescence were taken using a FLoid™ Cell Imaging Station fluorescence microscopy (Thermo Fisher).

### **Sulforhodamine B (SRB) assay**

Cellular viability was determined using SRB assay, which based on the measurement of total cellular protein content, the protocol used was described by Vichai and Kirtikara (Vichai & Kirtikara, 2006). Cells were seeded in 96 well plates at the confluence of 70% in DMEM high glucose. The next day cells were treated for 24h with a vehicle and mitochondrial inhibitors (10μM rotenone, 3μM oligomycin, or 100 nM antimycin A) in a complete medium. After 24 h treatment, the cells were fixed as the following; the culture medium was removed and replaced with 100μl 10% ice-cold TCA, then the plate was incubated for 1h at 4°C. To remove the remaining TCA, the plates were washed four times with slow-running tap water in plastic tubing connected directly to a faucet. The excess water was removed using paper towels. To completely dry out the plates, a blow dryer was used. 100 μl of 0.057% (wt/vol) SRB solution in 1% acetic acid was added to each well and incubated for 30 min at 24 °C. Then, the plates were washed quickly several times with 1% acetic acid and dried using a blow dryer. The protein-bound dye was solubilized with 200μl 10 mM Tris base solution (pH 10.5) with shaking for 5 min at 24 °C. The optical density OD of the solubilized dye was measured at 564 nm using a microplate reader. The data were calculated by the following formula; % cell viability = (Absorbance of sample/Absorbance of negative control or untreated) × 100.

### **Lactate dehydrogenase (LDH) assay**

Cellular cytotoxicity assay was assessed using Cytoscan™-LDH Cytotoxicity Assay kit, according to manufacturer's protocol with some modifications. Briefly, cells were seeded on triplicate at 70% confluency in 96 well plates in 100 µl DMEM high glucose medium. The next day, cells were treated with mitochondrial inhibitors at the final concentrations of 10µM rotenone, 3µM oligomycin, 100 nM antimycin A, and 1% (v/v) DMSO was used as a vehicle (negative control) in 100 µl complete medium for 24h. The positive control wells were filled with fresh complete medium. After 23 h treatment, 10 µl of 10x lysis buffer was added to triplicate cell-containing wells (positive control wells) and mixed gently, and then the plates were incubated for 45 min in a humidified chamber at 37°C, 5% CO<sub>2</sub>. Those cells were referred to as maximum LDH activity controls. 50µl medium from each sample was transferred into a new flat-bottom 96 well plates and gently mixed with a 50 µl Reaction Mixture. The plates were incubated in dark at 24 °C for 30 minutes. The maximum absorbance of the reaction product (formazan) was measured at 490 nm using a microplate reader. The data were calculated as following; after subtraction of OD of the complete medium, the % LDH release = (mean OD of sample /mean OD of positive control) x 100.

### **Cell cycle assay**

Cell cycle analysis was assessed based on DNA content quantitation, using flow cytometry, as described in Abcam protocol (<https://www.med.cam.ac.uk/wp-content/uploads/2012/10/pi.pdf>) Cells were seeded in 6 well plates in DMEM high glucose at the density of 8 x 10<sup>5</sup> cells/well. After 24h treatment with mitochondrial inhibitors (10µM rotenone, 3µM oligomycin, and 1% (v/v) DMSO), the cells were harvested with Trypsin/EDTA in complete medium at 300 x g for 5 min and washed with 1 x PBS. 800 µl ice-cold 70% ethanol was added to each cell pellet, vortexed for 5 sec, and incubated on ice for 30 min. The fixed cells were spin at 850 x g for 5 min and washed with 1 x PBS. Cell pellets were resuspended in 50µl of 100µg/ml RNAase A and incubated in a water bath for 15 min at 37°C. 200µl of 10µg/ml PI in PBS was added to each tube and mixed by pipetting. Before assessing the FACS, cells were filtered through a 41 µm Nylon Net Filter in FACS tubes. Data acquisition was performed using a FACS Aria III flow cytometer. Data were analyzed with FlowJo software version 10.

## **Human phospho-kinase array analysis**

Analyzing the phosphorylation profiles of 43 kinases in shPA200 and control cells was assessed using Human Phospho-Kinase Array Kit according to the manufacturer's protocol. Briefly, cells were seeded in 10 cm dishes at 70% confluence in DMEM high glucose. Cells were treated with either vehicle or 10 $\mu$ M rotenone in complete medium for 24h and then washed with 1 x PBS, lysed with lysis buffer (provided in the kit), and incubated on ice for 30 min. The cell lysate was centrifuged for 5 min at 10.000 x *g* / 4°C. The phosphokinase-array was calibrated with lysis buffer and blocked for 1 h at room temperature, 350  $\mu$ g protein was applied for each array set (treated and non-treated sample) in a final volume of 2 ml lysis buffer, the plate was incubated overnight on a rocking platform shaker at 4°C. After three washes with washing buffer, the detection antibody cocktail was applied for 2h at room temperature on a rocking platform. After the washing step, the Streptavidin-HRP was incubated for 30 min at 24 °C. After three washes, 1ml of prepared Chemi-reagent mix was added to each set of membranes. The images were taken using a ChemiDoc Imager and the pixel intensity was quantified using Image Lab software.

## **SDS-PAGE and Western blot**

The cell lysates for western blot analysis were prepared as previously described (see cell lysate and protein measurement). Control and shPA200 cells were treated with different mitochondrial inhibitors for appropriate time points in DMEM high glucose in a humidified incubator with 5% CO<sub>2</sub> at 37°C. After washing two times with 1 x PBS, the cells were lysed with RIPA buffer supplemented with protease inhibitors, and the protein was measured using the Bradford method (see cell lysate and protein measurement). 30 $\mu$ g from each sample was mixed with 5 x SDS loading buffer and DTT to final concentrations of 1x SDS loading buffer and 50mM DTT respectively. The mixed samples were boiled for 5 min at 95°C. 30 $\mu$ g of protein with equal volumes from each sample was loaded into a polyacrylamide gel (8 to 15%). Proteins were separated first in low voltage (60V for 10min) and then at 120V. The blots were then transferred onto either nitrocellulose membrane or reactivated PVDF membrane for 1h at 4°C. Membranes were blocked either with 5 % nonfat dried milk in TBS-T or 5 % BSA in TBS-T for anti- phosphoprotein antibodies. The blocking buffer was applied for 1h at 24 °C. The primary antibodies were incubated overnight at 4°C on a rocking platform, the list of primary antibodies is provided in (Table 1). After washing step (3x) with TBS-T, anti-rabbit/anti-mouse HRP-conjugated antibodies were applied for

1h at 24 °C. The immunoreaction was detected by an enhanced chemiluminescence detection system (ECL) and the images were taken using a ChemiDoc Imager. The pixel intensity was quantified and normalized to internal control ( $\beta$ -actin or HSP60) using Image Lab software.

### **Glycolysis and mitochondrial bioenergetics measurements**

To monitor glycolysis and mitochondrial bioenergetics of control and shPA200 cells, seahorse XF96 extracellular flux analyzer were used. Cells were seeded at the density of  $3.5 \times 10^4$  cells /well on XF96 cell culture microplate in DMEM high glucose medium in a 5% CO<sub>2</sub> humidified incubator at 37°C. To monitor the extracellular acidification rate (ECAR), the complete medium was replaced with 180 $\mu$ l XF assay medium glucose-free, and then the plate was incubated for 1h in a CO<sub>2</sub>-free incubator at 37°C. After calibration of the sensors with calibrant solution (pH 7.4) overnight in a CO<sub>2</sub>-free incubator at 37°C, the drugs were added to the cartridge ports as the following: port A: 100 mM glucose (Glu), port B: 10  $\mu$ M oligomycin (Olig), and port C: 500 mM 2-deoxy-D-glucose (2-DG). The final concentration of drugs injected to each well is 10 mM glucose (Glu), 1  $\mu$ M oligomycin (Olig), and 50 mM 2-deoxy-D-glucose (2-DG). The ECAR baseline was determined for 30min. The glycolysis and the glycolytic capacity were monitored after glucose and oligomycin injection, respectively.

To monitor the oxygen consumption rate (OCR), the complete medium was replaced with a 180 $\mu$ l XF assay medium supplemented with 4.5 g/l glucose, and then the plate was incubated for 1h in a CO<sub>2</sub>-free incubator at 37°C. After calibration of the sensors in XF96 calibrant solution (pH 7.4) overnight in a CO<sub>2</sub>-free incubator at 37 °C, the drugs were added to the cartridge ports as the following: port A: 15  $\mu$ M oligomycin (Olig), port B: 10  $\mu$ M FCCP , and port C: 10  $\mu$ M antimycin-A/rotenone. The final concentrations injected to each well are; 1, 5  $\mu$ M oligomycin, 1  $\mu$ M FCCP, and 1  $\mu$ M antimycin-A/rotenone. After 20 min of instrument calibration, the baseline of OCR was determined for 30 min, and then the ATP production and proton leak were determined following the oligomycin injection. The maximum respiration and spear respiratory capacity were determined after FCCP injection. Bradford assay was used to measure protein concentration for normalization. Data analysis was performed by using Wave 2.3 Agilent Seahorse Desktop software.

## **Protein carbonyl assay**

The detection and quantification of proteins modified by oxygen free radicals were assessed using OxyBlot™ Protein Oxidation Detection Kit. Briefly, PA200-deficient and the corresponding control cells were seeded in 6 well plates in DMEM high glucose in a humidified incubator at 37°C/5 % CO<sub>2</sub>. The following day, the cells were treated with DMSO and 3 μM oligomycin for 24 h. Cells were lysed by RIPA buffer supplemented with a protease inhibitor cocktail (see cell lysate and protein measurement) and 50mM DTT for 5 min at 4°C. The cell homogenate was centrifuged at 300 x g for 5 min at 4°C and the protein concentration was measured using the Bradford method. Two aliquots of each sample, containing 20 μg protein / each, were treated as the following, first, the proteins of both aliquots were denatured with 12% SDS (v/v) (6% SDS final) for 5 min at 24 °C. The samples were derivatized with the derivatization solution (1x DNPH). The non-derivatized samples were used as a negative control. The protein samples were separated by SDS-PAGE. Non-specific sites were blocked by blocking/dilution buffer 1% BSA in PBS-T (PBS-T: PBS containing 0.05% Tween-20, pH 7.2-7.5) for 1 hour with gentle shaking at 24°C. The primary antibody was diluted 1:150 in blocking/dilution buffer and applied overnight at 4°C. The secondary antibody was applied for 1h at 24°C. Images were taken using ChemiDoc Imager. The image adjustment and band quantification were assessed using Image Lab software.

## **RNA sequencing (RNA-seq) and RNA-Seq data analysis**

PA200 depleted cells and control cells were seeded in T-75 flasks in DMEM high glucose medium to reach 90% confluency. The total RNA was extracted in normal condition according to the protocol described above (see RNA extraction). Three independent flasks from each clone (control and shPA200) were used. The samples for RNA sequencing were performed on Illumina sequencing platform (Center for Clinical Genomics and Personalized Medicine, Core Facility, University of Debrecen, Hungary). The obtained data were analyzed with Dr. Agnieszka Robaszekiewicz (Department of General Biophysics, University of Lodz). Total RNA sample quality was checked on Agilent BioAnalyzer using Eukaryotic Total RNA Nano Kit according to the manufacturer's protocol. Samples with RNA integrity number (RIN) value >7 were accepted for the library preparation process. RNA-Seq libraries were prepared from total RNA using Ultra II RNA Sample Prep kit (New England BioLabs) according to the manufacturer's protocol. Briefly, poly-A RNAs were captured by oligo-dT conjugated magnetic beads then the mRNAs were eluted

and fragmented at 94°C degrees. First-strand cDNA was generated by random priming reverse transcription and after second strand synthesis; step double-stranded cDNA was generated. After repairing ends, A-tailing and adapter ligation steps, adapter-ligated fragments were amplified in enrichment PCR, and finally, sequencing libraries were generated. Sequencing runs were executed on Illumina NextSeq500 instrument using single-end 75 cycles sequencing.

Raw sequencing data (fastq) was aligned to human reference genome version GRCh38 using HISAT2 algorithm and BAM files were generated. Downstream analysis was performed using StrandNGS software ([www.strand-ngs.com](http://www.strand-ngs.com)). BAM files were imported into the software DESeq1 algorithm was used for normalization. To identify differentially expressed genes (DEGs) between conditions, moderated t-test with Benjamini-Hochberg false discovery rate (FDR) for multiple testing corrections was used.

### **Functional analysis of RNA-Seq data**

The threshold for significantly up- and down-regulated genes was set at 1.3 of the fold change in gene transcription between shPA200 versus shCTRL. The genes above and below the threshold values were considered as DEGs. The heat map of the Log<sub>2</sub> fold change (Log<sub>2</sub>FC) of gene transcription in shPA200 versus shCTRL was generated in the Heatmapper using average linkage for clustering and Euclidean distance measurement among DEGs. The statistical over-representation test for gene ontologies of biological processes was carried out in Panther, using Fisher's exact test with no correction. Gene-regulatory signaling networks were generated in Network Analyst. The number of nodes and edges was reduced using a minimum network tool, and their colocation was set up using reduce overlap layout. Nodes representing particular processes (metabolism, MAPK cascade, PI3K-Akt signaling pathway, and the regulation of programmed cell death) were assigned to biological processes (Database:GO: BP) in Functional Explorer and highlighted in blue.

### **Statistical analysis**

Data from each experiment were summarized with the mean and standard deviation (SD) of  $n \geq 3$  experiments. Statistical analysis was performed with one-way, two-way ANOVA, or unpaired Student's *t*-test where is applicable using GraphPad Prism v8.2.1. Statistical significance was determined as \*  $p < 0.05$ , \*\*  $p < 0.01$ , \*\*\*  $p < 0.001$ , \*\*\*\*  $p < 0.0001$ .

## RESULTS

### Stable depletion of PSME4/PA200 in SH-SY5Y human neuroblastoma cells

The proteasome activator PA200 (Blm10 ortholog in yeast) is involved in several cellular processes, such as DNA repair (Schmidt et al., 2005; Ustrell et al., 2002), normal spermatogenesis, and male fertility (Khor et al., 2006), the proteasome core 20S assembly (Fehlker et al., 2003), and the maintenance of genome stability (Blickwedehl et al., 2008). Furthermore, reports demonstrated that Blm10 is involved in the maintenance of mitochondrial function (Sadre-Bazzaz et al., 2010; Tar et al., 2014). A recent study demonstrates for the first time the role of PA200 in diseases, which shows that the PA200 is upregulated in myofibroblasts of fibrotic lungs (Welk et al., 2019). In our current work, we established a model in which we can study the potential role of PA200 in transcriptomic regulations and the maintenance of mitochondrial integrity.

Lentiviral technology was used to generate stable PA200 knockdowns in SH-SY5Y neuroblastoma cells. The efficiency of depletion was confirmed by RT-qPCR and western blot (Fig. 10A and B). In two out of five clones, PA200 expression was successfully down-regulated (*PMSE4* clone # 4 referred to as shPA200\_A and *PMSE4* clone # 5 referred as shPA200\_B) (Fig. 10A). Control cells containing pGIPZ-GFP plasmids without the silencing shRNA sequence. PA200 depleted and the control cells were treated with selective mitochondrial inhibitors. The mitochondrial inhibitors specifically inhibit different elements of ETC: (rotenone inhibits CI, oligomycin blocks ATP synthase, and antimycin A inhibits CIII). The mRNA level of the *PSME4* gene was analyzed in shPA200 upon 24h treatment with mitochondrial inhibitors to confirm that the gene depletion was not affected by specific treatments (Fig. 10C). There was no significant change in the mRNA expression level of *PSME4* in control cells upon 24h treatment with mitochondrial inhibitors (Fig. 10D).

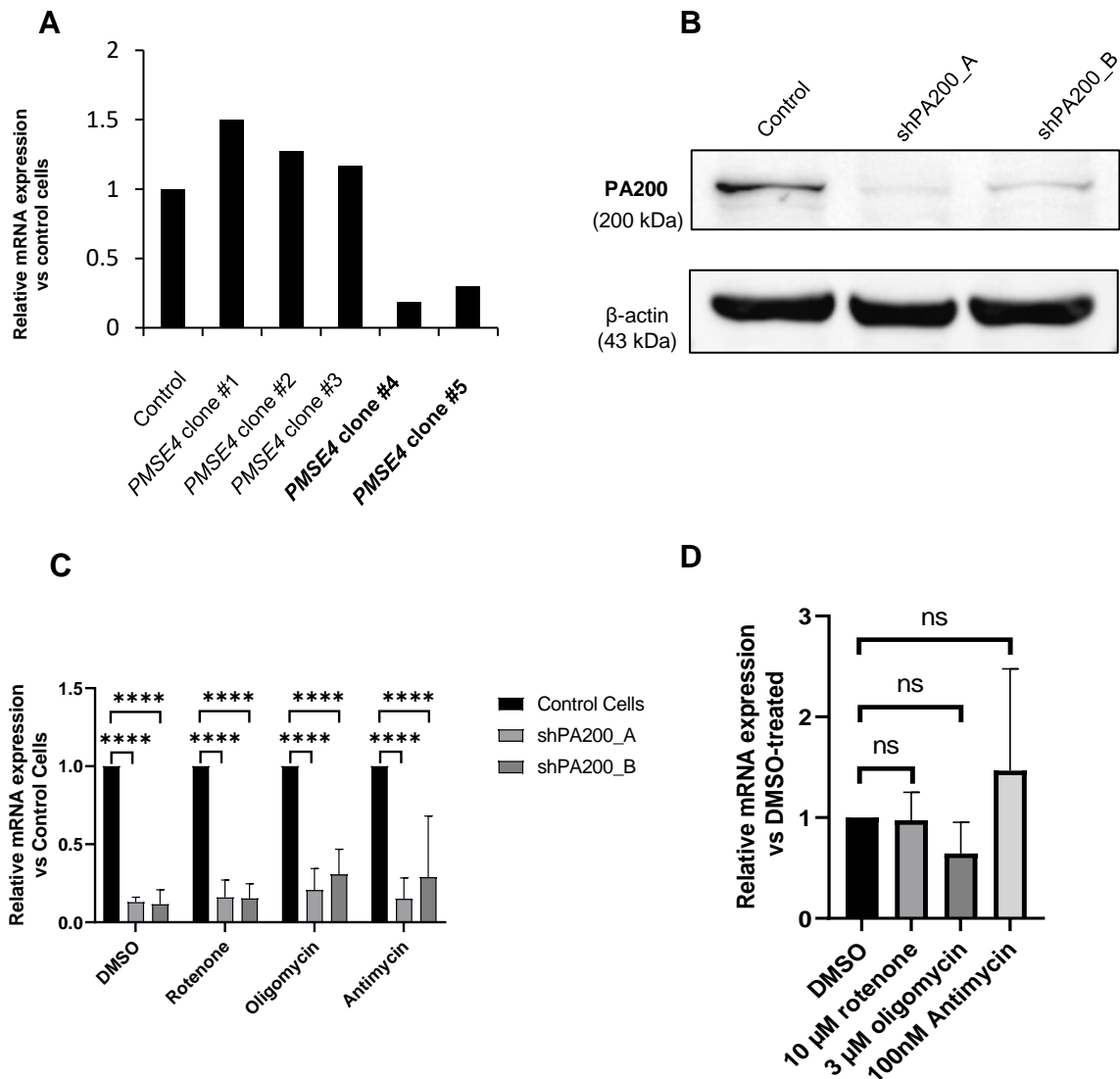


**Figure 10. Downregulation of PSME4/PA200 in SH-SY5Y cell line.** The stable silencing of PA200 expression was achieved using lentiviral technology. (A) RT-qPCR analysis of mRNA expression level of PSME4 in different clones (clone # 1-5), PSME4 clone #4, and PSME4 clone #5 showed silencing of PA200, which later referred to as shPA200\_A and shPA200\_B, respectively. The A panel is generated from one biological replicate. (B) PA200 protein level in control and shPA200 cells (shPA200\_A, shPA200\_B) was analyzed using SDS-PAGE western blotting. Images were taken and adjusted using a ChemiDoc Imager and Image Lab software, respectively. (C) RT-qPCR analysis of mRNA expression level of PSME4 clone #4, and PSME4 clone #5 showed silencing of PA200 in the presence or absence of mitochondrial inhibitors. (D) The relative mRNA expression level of PSME4 in control cells treated with mitochondrial inhibitors. Statistical analysis was performed by ANOVA using GraphPad Prism v8.2.1.  $n=4$ , (\*\*\*\* indicates  $p < 0.0001$ , ns, indicates non-significant).

## Depletion of PA200 in neuroblastoma cells increases the expression of necrotic and apoptotic markers upon rotenone treatment

We investigated the effect of PA200 on cell viability using SRB assay. PA200-deficient cells and the corresponding control cells were subjected to selective mitochondrial inhibitor treatments for 24h (Fig. 11). Treatment with either 100 nM antimycin A or 3 $\mu$ M oligomycin did not result in significant changes in cell viability between control and shPA200 cells. 10 $\mu$ M rotenone treatment, however, significantly reduced cell viability of PA200 depleted cells compared to control cells (Fig. 11A). The impact of rotenone on cell viability in shPA200 cells was confirmed by investigating necrotic and apoptotic markers. LDH release assay was used to monitor necrosis upon 24h treatment with mitochondrial inhibitors (Fig. 11B). As expected, 24h treatment with rotenone significantly increased LDH release in shPA200 cells compared to rotenone-treated control cells (Fig. 11B). Oligomycin treatment did cause a significant change in LDH release in shPA200 compared to control cells.

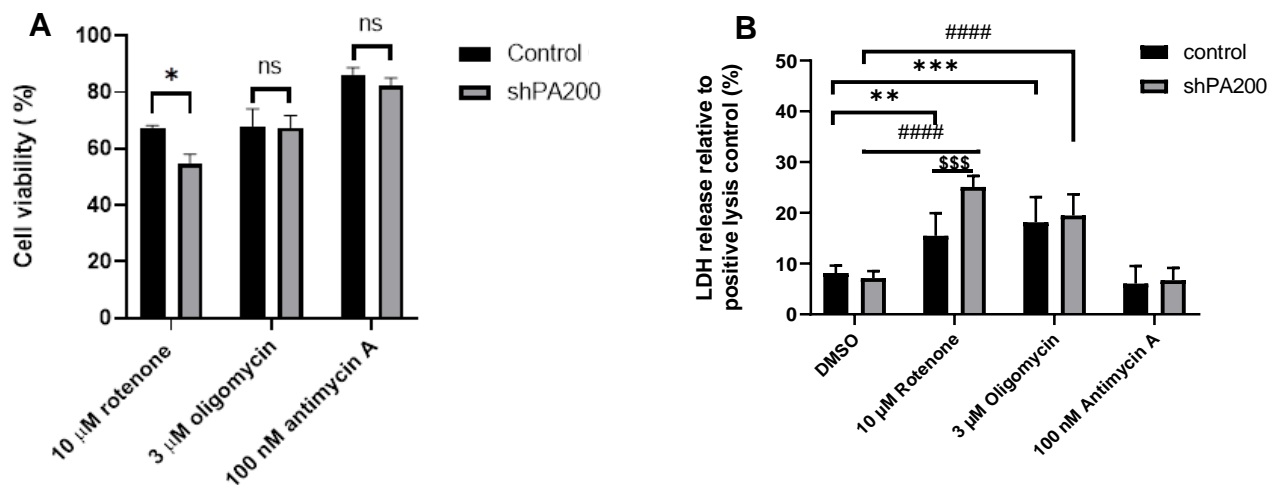


**Figure 11. Loss of PA200 reduces cell viability upon rotenone treatment.** Control and PA200-depleted cells were treated for 24h with appropriate mitochondrial inhibitors. (A) Cell viability was assessed using SRB assay (B) Percentage of LDH release in control and PA200 depleted cells upon selective mitochondrial stress. Results are presented as the mean  $\pm$  SD of six independent experiments. Statistical analysis was performed by ANOVA using Graph Pad Prism v8.2.1. (\* $P < 0.05$ , \*\* $P < 0.01$ , \*\*\* $P < 0.001$ , ####  $P < 0.0001$ , and \$\$\$  $P < 0.001$ , ns, indicates non-significant).

Western blot analysis of apoptotic markers in control and PA200-depleted cells shows a significant increase in both H2AX phosphorylation at serin139 and cleaved-PARP1 in rotenone-treated shPA200 compared to rotenone-treated control cells (Fig. 12A-B). H2AX phosphorylation and PARP1 cleavage are considered as a hallmark of DNA damage and apoptotic cell death, respectively (Chaitanya et al., 2010; Sharma et al., 2012). Moreover, live images were taken after 24h treatment with mitochondrial inhibitors. Microscopy images did not indicate a major difference in cell morphology between shPA200 and control cells following oligomycin or antimycin A treatment (no signs of cell death), however, treatment with 10 $\mu$ M rotenone lead to a massive formation of apoptotic bodies in shPA200 compared to rotenone treated control cells (Fig. 12C, arrows).

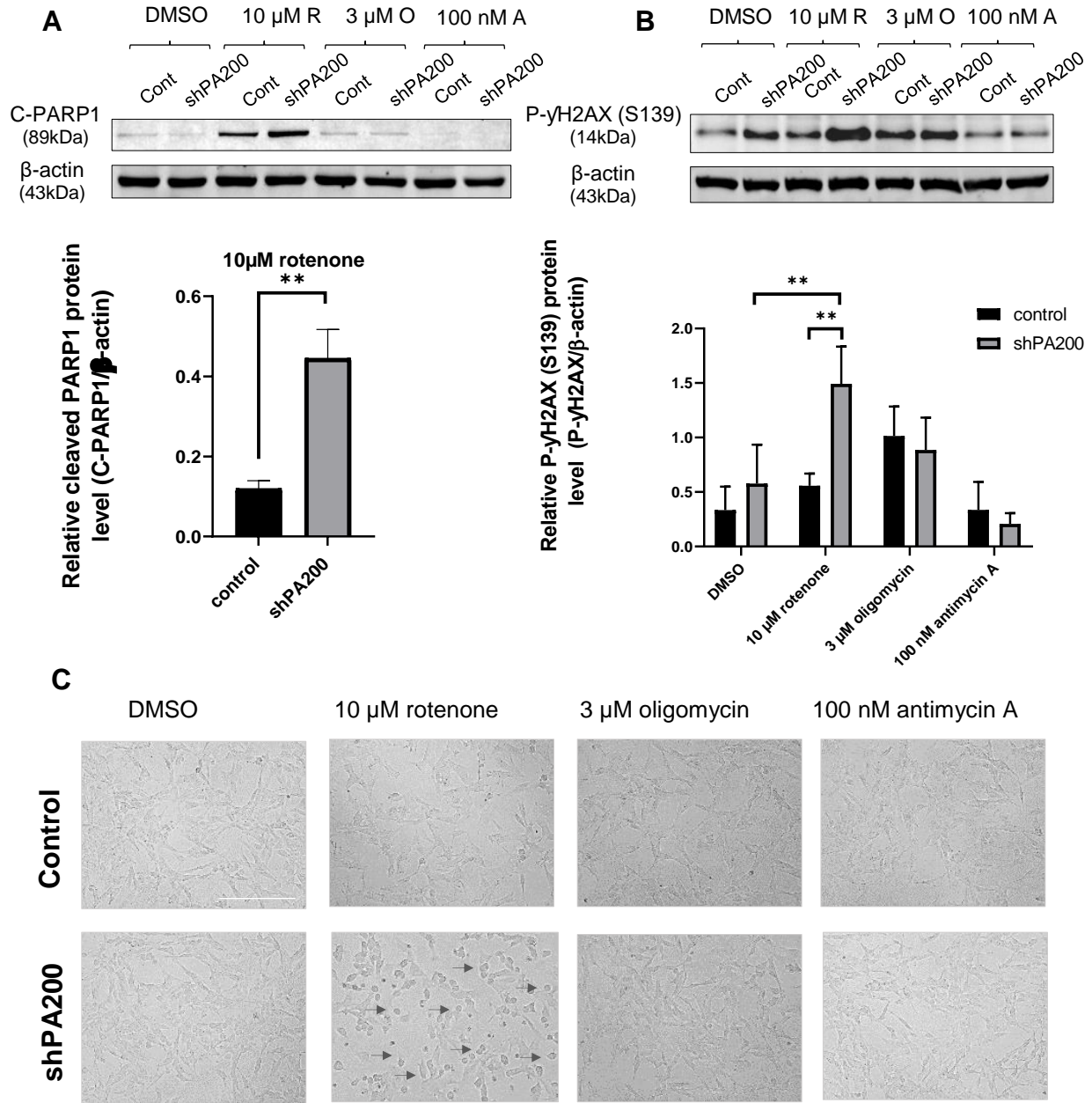


**Figure 12. Rotenone-treated PA200 depleted cells exhibit an increase in DNA damage and apoptosis markers.** 30 $\mu$ g protein from total cell lysates of control and PA200-depleted cells treated for 24h with mitochondrial inhibitors (10 $\mu$ M rotenone (R), 3  $\mu$ M oligomycin (O), 100nM Antimycin A (A)) were analyzed by western blot. (A-B) SDS-PAGE and western blot analysis of apoptosis using cleaved-PARP1 and phospho-H2AX antibodies.  $\beta$ -actin was used as a loading control. Results are presented as the mean  $\pm$  SD of  $n \geq 3$  independent experiments. Statistical analysis was performed using Two-way ANOVA and unpaired t-test using GraphPad Prism v8.2.1. (\*\* $P < 0.01$ ). (C) Light microscopy images of control and shPA200 cells treated for 24h with mitochondrial inhibitors. Arrows indicate apoptotic bodies. Scale bar=100  $\mu$ m.

## **PA200 is over recruited to promoter regions of genes involved in cell cycle, metabolism, and protein modification processes**

It has been demonstrated that PA200/Blm10 is involved in the DNA repair process upon IR exposure through degradation of acetylated core histones (Qian et al., 2013). Structural analysis of PA200/Blm10 revealed the presence of a BRD-like region that binds to acetylated histones. However, compared to well-known human BRD families, PA200/Blm10 BRD-like domain does not share any sequence homology with any known BRDs (Guan et al., 2020; Qian et al., 2013). In addition to its role in peptide degradation, studies demonstrated that the deletion of PA200 orthologue in yeast (Blm10) shows overall changes in gene expression encoded for proteins required for chromosome organization and cell cycle progression (Doherty et al., 2012). Based on differential sensitization of PA200-deficient and control cells to mitochondrial inhibitors, and the impact of Blm10 deletion on gene expression, we hypothesized that the depletion of PA200 in SH-SY5Y cells is associated with overall changes in gene expression through the direct or indirect binding of PA200 to promoters of relevant genes.

To verify our hypothesis, we assessed ChIP followed by ChIP-seq analysis. Bioinformatics data analysis shows anti-PA200 enriched regions in the genome of the SH-SY5Y neuroblastoma cell line (Supplementary Table 1). Furthermore, we monitored the distribution of chromatin-bound PA200 and found that protein peaks were centered in the vicinity of TSSs (Fig. 13A). To investigate whether anti-PA200 enriched promoters were actively transcribed or repressed, we collated H3K27ac peaks with PA200 peaks in the Genome Browser (Fig. 13B). The collected peaks revealed that PA200 was associated with both, transcriptionally active regions and non-transcriptionally active gene promoters (Fig. 13B and C). Gene ontology annotation has showed that promoters enriched in the anti-PA200 ChIP contribute to cellular physiology regulation including proliferation, protein modifications, and metabolism (Fig. 13D, Table 4).

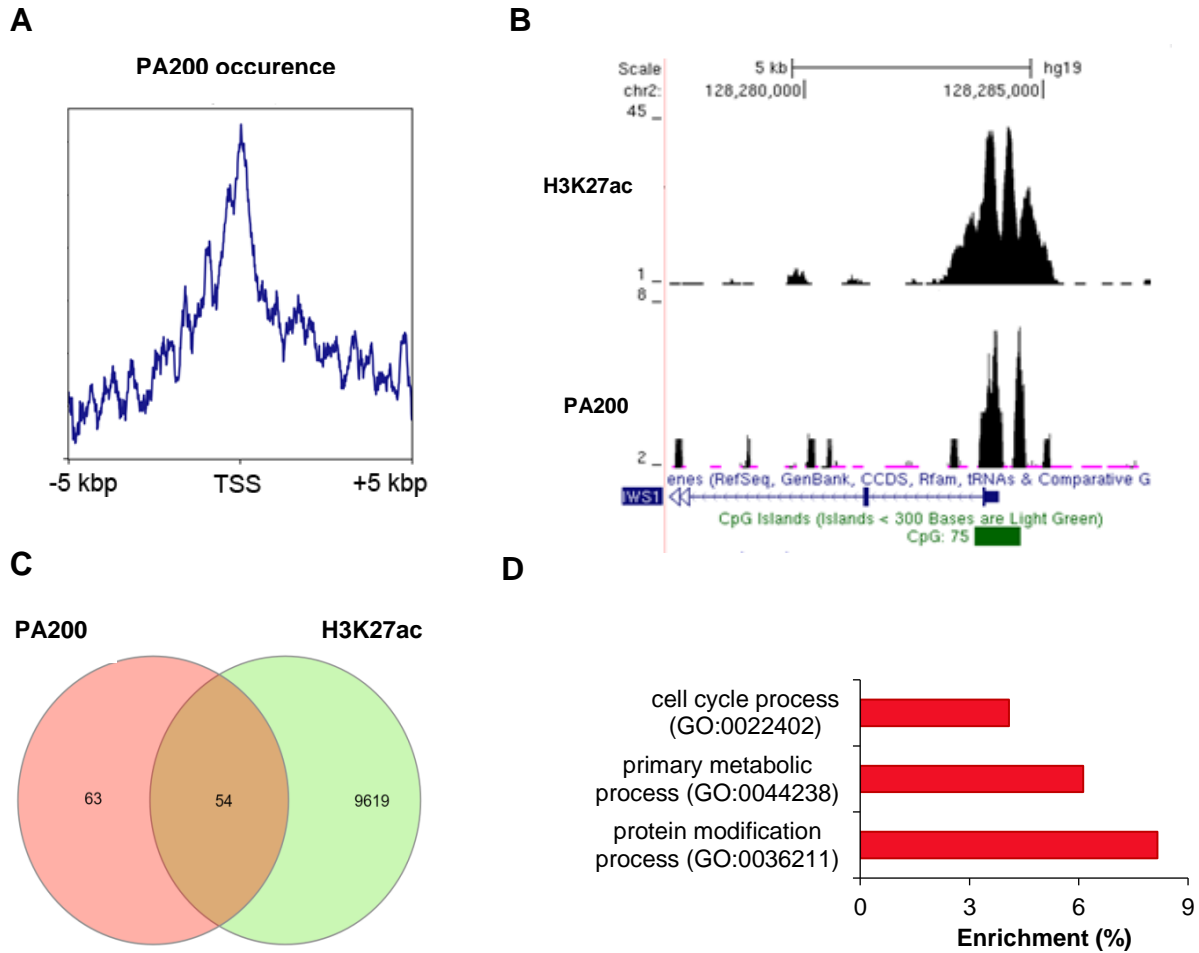


**Figure 13. The occurrence of PA200 in transcriptionally active and non-active promoters in SH-SY5Y cells.** (A) ChIPseq reads analysis with deep Tools revealed that PA200 presents around gene transcription start sites (TSS). (B) Some PA200-positive promoters were simultaneously characterized by histone acetylation (H3K27ac) that marks actively transcribed genes. (C) Venn diagram displays PA200-enriched active (H3K27ac) and inactive (-H3K27ac) gene promoters. (D) The biological function of genes whose promoter is enriched in the anti-PA200 ChIP.

## PA200 binds to and is distributed on promoters depending on the mitochondrial status

Blm10 is required for the maintenance of mitochondrial integrity (Sadre-Bazzaz et al., 2010; Tar et al., 2014). Here, we investigated the effects of mitochondrial inhibition on PA200 chromatin-binding and distribution. Three hours treatment with either rotenone, antimycin A, or oligomycin causes an eviction of PA200 from chromatin compared to vehicle-treated SH-SY5Y cells. These data suggest that PA200 binding to the genome is influenced by mitochondrial activity by shifting from a promoter region to another in a mitochondrial inhibitor-dependent manner (Fig. 14A-B).

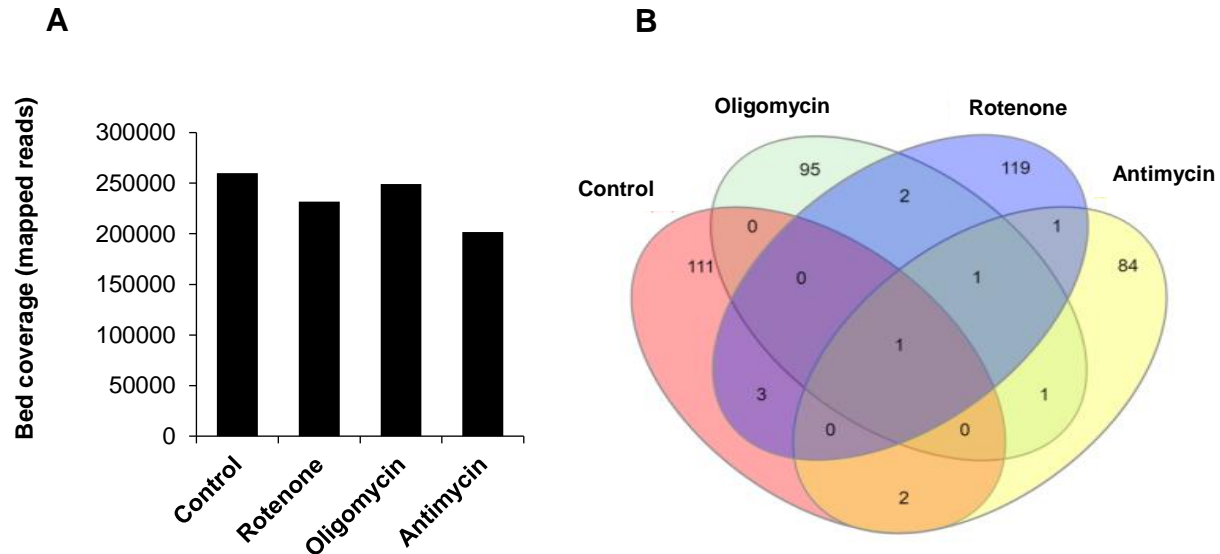


**Figure 14. Mitochondrial inhibitors influence PA200-promoters binding in SH-SY5Y cells.** (A) PA200 association with chromatin after cell treatment with 10  $\mu$ M rotenone, 3  $\mu$ M oligomycin, and 100 nM antimycin A was monitored and quantified by bed coverage. (B) Alterations in the occupancy of gene promoters by PA200 in untreated cells and cells challenged with mitochondria-impairing agents were compared by Venn diagram.

**Table 4. The function of genes whose promoters are enriched in the anti-PA200 ChIP**

Gene functions	<i>P</i> -value
peptidyl-lysine trimethylation (GO:0018023)	1.85E-02
ribonucleoside triphosphate metabolic process (GO:0009199)	2.30E-02
regulation of exit from mitosis (GO:0007096)	2.30E-02
protein transport to vacuole involved in ubiquitin-dependent protein catabolic process via the multivesicular body sorting pathway (GO:0043328)	2.30E-02
ribonucleoside triphosphate biosynthetic process (GO:0009201)	2.30E-02
mitotic cell cycle phase transition (GO:0044772)	2.76E-02
peptidyl-lysine methylation (GO:0018022)	3.21E-02
positive regulation of neuron differentiation (GO:0045666)	3.21E-02
ribonucleotide biosynthetic process (GO:0009260)	3.21E-02
ribonucleotide metabolic process (GO:0009259)	3.66E-02
protein methylation (GO:0006479)	4.55E-02
protein alkylation (GO:0008213)	4.55E-02
protein catabolic process in the vacuole (GO:0007039)	4.99E-02
negative regulation of mitotic cell cycle (GO:0045930)	5.98E-03
cell cycle phase transition (GO:0044770)	1.36E-03
regulation of mitotic cell cycle phase transition (GO:1901990)	2.10E-02
regulation of mitotic cell cycle (GO:0007346)	2.10E-02
negative regulation of cell cycle (GO:0045786)	2.44E-02
organonitrogen compound biosynthetic process (GO:1901566)	4.10E-02
cell cycle process (GO:0022402)	1.56E-02
protein modification by small protein conjugation or removal (GO:0070647)	1.24E-02
lipid metabolic process (GO:0006629)	3.64E-02
primary metabolic process (GO:0044238)	1.68E-02
cellular protein modification process (GO:0006464)	1.24E-02
protein modification process (GO:0036211)	1.26E-02

## Expression profile of genes whose promoters are enriched in the anti-PA200 ChIP

Next, we investigated the expression pattern of genes whose promoters show over recruitment of PA200 and regulate cell cycle progression, mitochondrial function, and apoptosis by RT-qPCR analysis. Cells were treated with vehicle (DMSO) or with selective mitochondrial inhibitors for 3h to conserve the experimental conditions of the ChIP experiment (Fig. 15). Gene expression patterns of selected genes showed differential expression in both clones upon 3h treatment with mitochondrial inhibitors compared to DMSO-treated cells (Fig. 15). For example, upon oligomycin and rotenone treatment, the promoter region of *CASP4* and *CASP5* were enriched in PA200, respectively (Supplementary Table 1). The RT-qPCR data analysis showed a significant down-regulation of both genes, *CASP4* and *CASP5*, in PA200 depleted cells compared to control cells upon oligomycin and rotenone treatments, respectively (Fig. 15). Furthermore, the expression of *API5*, *ATP5E*, and *ATP6VOE1* genes was significantly down-regulated in shPA200 cells upon oligomycin treatment compared to vehicle-treated shPA200 cells, however, control cells did not indicate any change in the expression of indicated genes upon oligomycin treatment. Together, this data suggests that PA200 enrichment to specific promoters might influence transcriptional patterns.

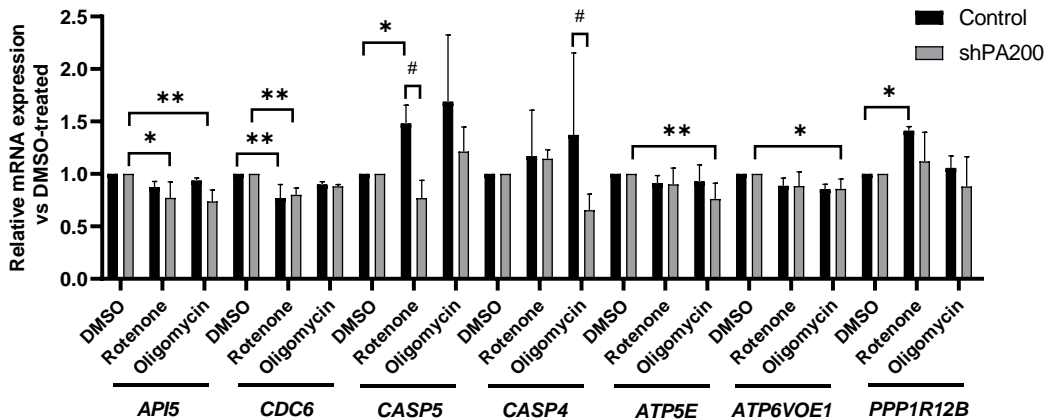


**Figure 15. Expression profile of genes enriched in PA200.** RT-qPCR analysis was used to investigate the mRNA expression level of PA200 target genes. The mRNA expression level of selected target genes was tested after 3h treatment with mitochondrial inhibitors at the indicated concentrations. The mRNA expression of selective mitochondrial inhibitor-treated (10  $\mu$ M rotenone and 3  $\mu$ M oligomycin) control and shPA200 cells was normalized to DMSO-treated cells. Data are presented as the mean  $\pm$  SD of three independent experiments. Statistical analysis was performed by ANOVA using GraphPad Prism v8.2.1. (\* $P < 0.05$ , #  $P < 0.05$ , \*\* $P < 0.01$ , \*\*\* $P < 0.001$ , and \*\*\*\* $P < 0.0001$ ).

## **PA200 affects cell cycle in a mitochondrial inhibitor dependent manner**

ChIP-seq data analysis revealed that gene promoters that were significantly enriched in PA200 contribute to the regulation of crucial intracellular processes including cellular proliferation. We investigated the role of PA200 in cell proliferation by monitoring cell cycle phases in shPA200 cells and their corresponding control using flow cytometer and western blot analysis (Fig. 16). FACS data analysis shows a slight increase in the S phase population in shPA200 compared to control cells with or without treatment (Fig. 16A). Oligomycin-treated control cells did not show any significant changes in any cell cycle phases compared to vehicle-treated control cells, however, oligomycin-treated shPA200 cells show a significant increase in S phase population compared to vehicle-treated shPA200 cells (Fig. 16B). We verified these findings by western blot analysis of the proliferating cell nuclear antigen (PCNA), PCNA protein has an essential role in cell cycle progression regulation (Juríková et al., 2016). Western blot data revealed a reduction in PCNA protein level in control cells treated with oligomycin, or rotenone compared to vehicle-treated cells. The PCNA protein level was maintained in shPA200 cells upon mitochondrial inhibitors treatment compared to vehicle-treated shPA200 cells (Fig. 16C).

Rotenone treatment has a similar impact on both cell lines (Fig. 16D), represented by a reduction of G0/G1 populations, and an arrest in G2/M phases. Rotenone treatment led to an increase in sub G1 population in shPA200 cells indicative of apoptosis (Fig. 16D). Together, these data suggest that PA200 has a crucial role in cell cycle progression regulation.

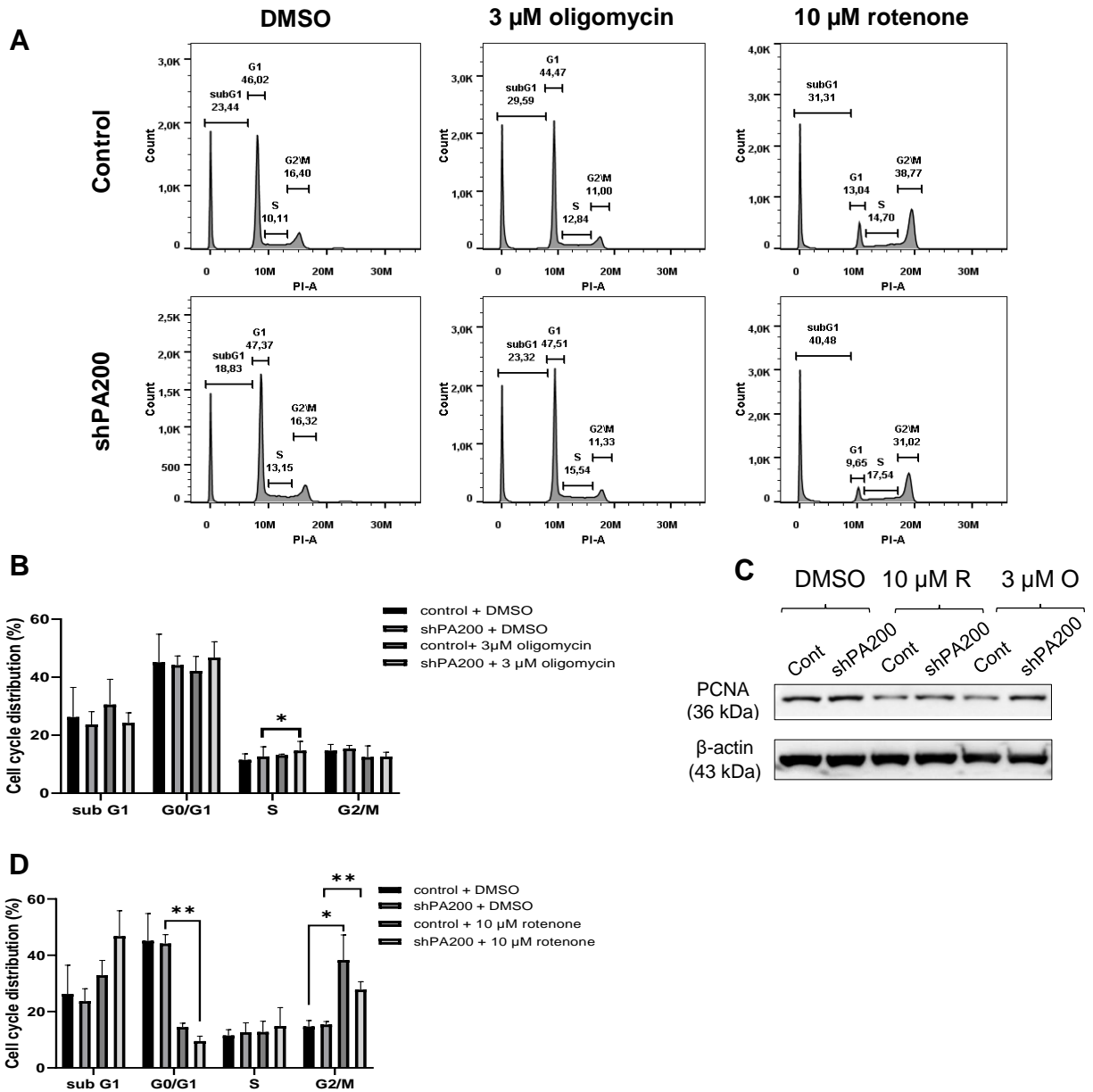
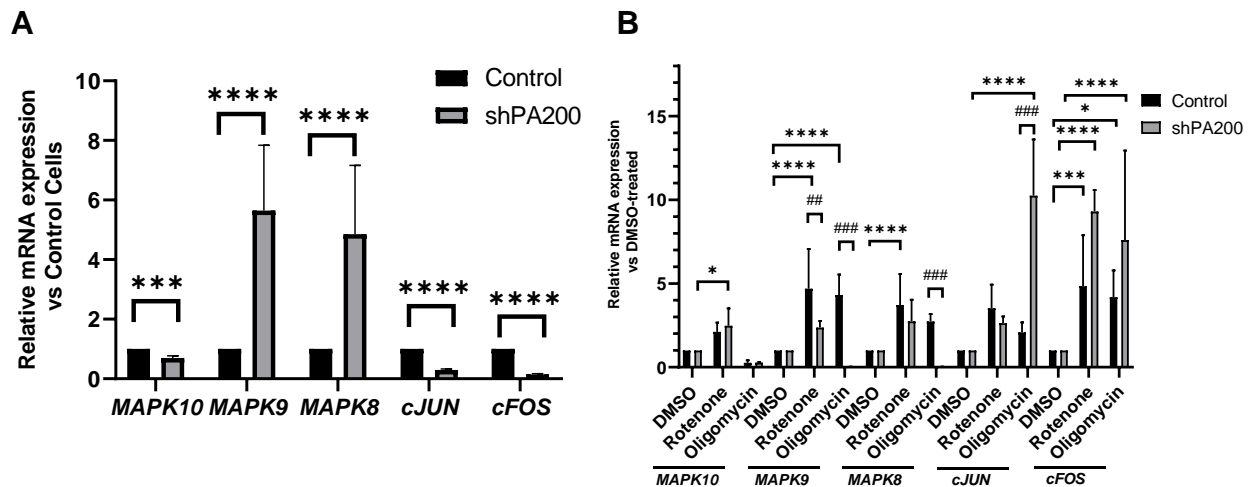


**Figure 16. Effects of PA200 depletion on cell cycle progression upon mitochondrial stress.** Cell cycle distribution was analyzed using flow cytometry. Quantification of DNA content was determined in control and shPA200 cells using PI staining. (A) Histogram depicting cell cycle distribution in shPA200 cells and control cells upon treatment with mitochondrial inhibitors for 24h. (B) Graphs represent a statistical analysis of cell cycle phase populations in control and shPA200 cells upon 24h treatment with oligomycin. (C) Western blot analysis of proliferative cell nuclear antigen protein (PCNA), total cell lysates of control, and shPA200 cells incubated with vehicle (DMSO), 10  $\mu$ M rotenone (R) or 3  $\mu$ M oligomycin (O) for 24 h.  $\beta$ -actin was used as an internal loading control. (D) Graphs represent a statistical analysis of cell cycle phase populations in control and shPA200 cells upon 24h treatment with rotenone. Results are displayed as mean  $\pm$  SD of 3 independent experiments, and statistically significant differences were calculated using the RM ANOVA test (\* $P < 0.05$ , \*\* $P < 0.01$ ).

## **PA200 regulates the expression of genes involved in cell proliferation and response to stress**

The rotenone treatment induces cell death in SH-SY5Y cells through the JNK pathway (Klintworth et al., 2007; Newhouse et al., 2004). We showed a significant increase in apoptotic markers in shPA200 cells upon rotenone treatment (Fig. 12). Additionally, the flow cytometry data demonstrated an increase in sub-G1 cell population in shPA200 upon rotenone treatment indicative of apoptosis. We investigated the expression pattern of genes involved in the JNK pathway, such as *MAPK8/JNK1*, *MAPK9/JNK2*, *MAPK10/JNK*, and *cJUN* (c-Jun) using RT-qPCR analysis (Fig. 17).

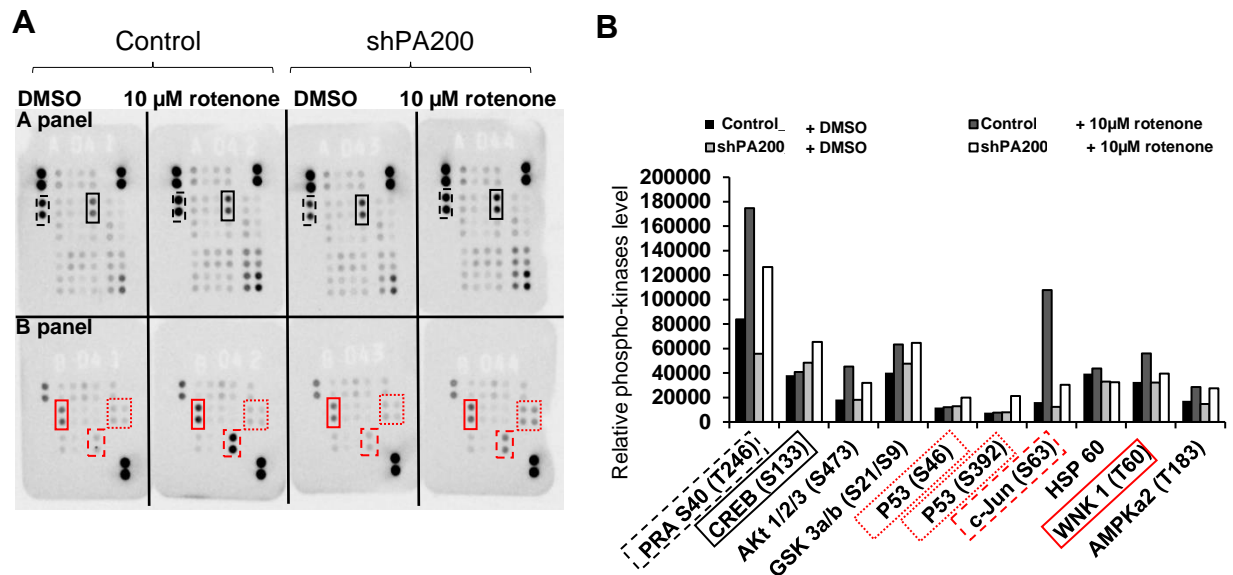
The fold changes in mRNA expression in control and PA200 depleted cells were compared in the presence and absence of mitochondrial inhibitors. RT-qPCR data show a strong upregulation in *MAPK8* and *MAPK9*, however, *MAPK10*, *cJUN* (c-Jun), and *cFOS* (proto-oncogene c-fos) were downregulated in shPA200 vehicle-treated cells compared to control vehicle-treated cells (Fig. 17A). The expression pattern of genes was dramatically changed in response to mitochondrial inhibitor treatment. Rotenone treatment led to a significant up-regulation of almost all of the examined genes compared to vehicle treatment in both clones (control and shPA200 cells) (Fig. 17B). Oligomycin-treated shPA200 cells show a strong downregulation in all MAPKs, while *cJUN* and *cFOS* expression was upregulated compared to vehicle-treated shPA200 cells (Fig. 17B). Control cells show an upregulation in all examined genes; except *MAPK10* upon oligomycin treatment compared to vehicle-treated cells (Fig. 17B). These differential changes in gene expression on shPA200 cells with or without treatment, compared to control cells suggest the important role of PA200 a regulator of cell survival through the JNK pathway in neuroblastoma cells.



**Figure 17. Loss of PA200 influences gene expression of JNK-pathway in the SH-SY5Y cell line.** The mRNA level of examined genes in control and shPA200 was analyzed using RT-qPCR analysis. Cells were incubated with vehicle (DMSO) or the mitochondrial inhibitors (10  $\mu$ M rotenone and 3  $\mu$ M oligomycin) for 24 h. (A) the mRNA levels of vehicle-treated shPA200 were normalized to vehicle-treated control cells. (B) The mRNA expression level in control and shPA200 cells upon selective mitochondrial inhibitor treatment were normalized to DMSO-treated control and DMSO-treated shPA200 cells, respectively. Data are presented as the mean  $\pm$  SD of four separate experiments. Statistical analysis was performed by two-way ANOVA and using GraphPad Prism v8.2.1. (\* $P < 0.05$ , \*\* $P < 0.01$ , \*\*\* $P < 0.001$ , and \*\*\*\* $P < 0.0001$ ).

### PA200 knockdown leads to reduced c-Jun and phospho-c-Jun following rotenone administration

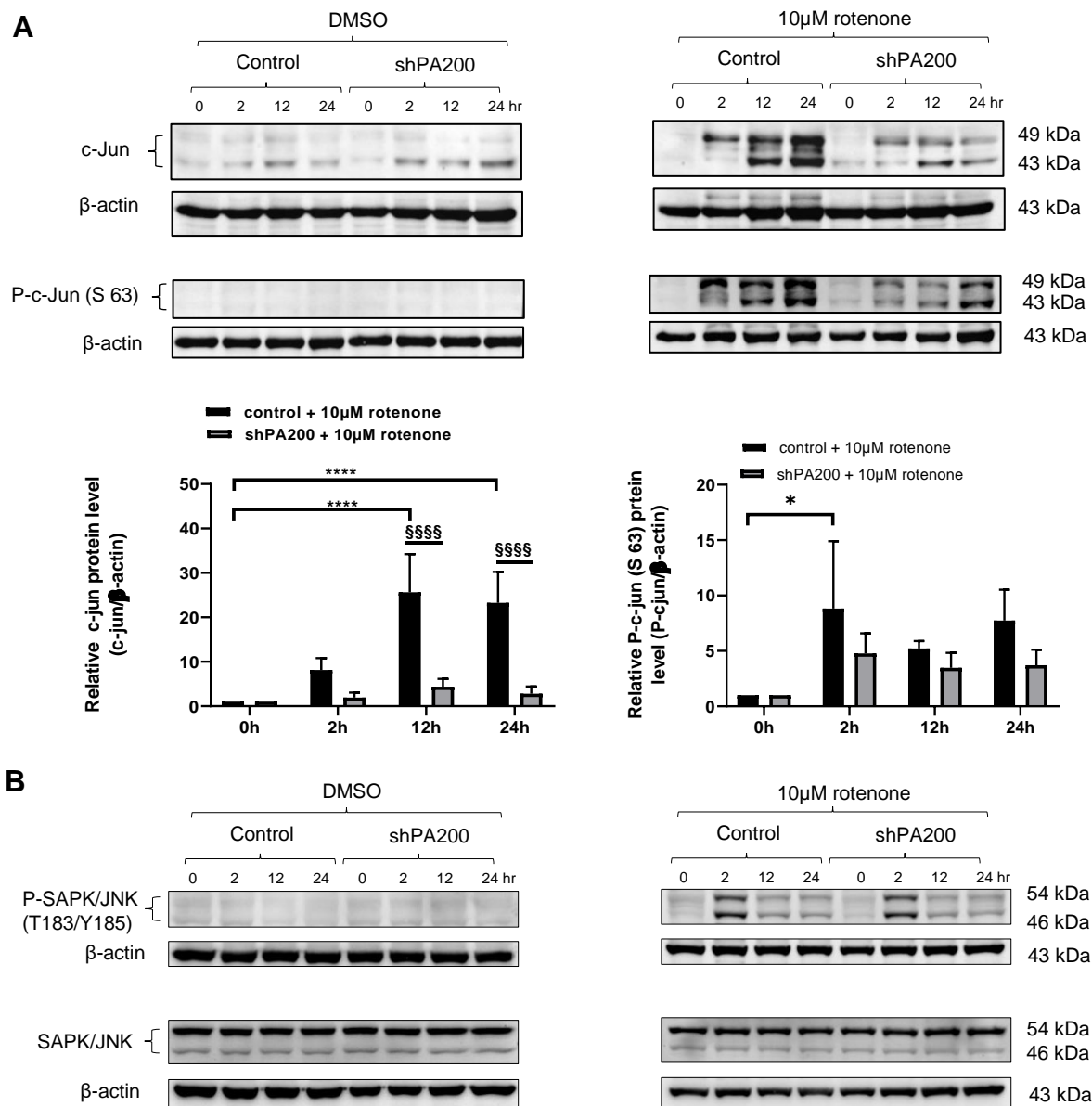
We investigated the impact of the differential expression pattern on signaling pathways in control and shA200 cells. Only rotenone treatment resulted in significant changes in cell viability and apoptosis in shPA200 cells compared to control cells. Therefore, we tested the phosphokinase profile in both clones upon 24h treatment with 10 $\mu$ M rotenone. 43 phosphosites of specific kinases and transcription factors were investigated using a humane phosphokinase array. The tested kinases showed quite similar levels of phosphorylation in both rotenone-treated shPA200 compared to rotenone-treated control cells (Fig. 18A-B), except the phospho-c-Jun at serine 63, which showed high phosphorylation in control compared to shPA200 rotenone-treated cells (Fig. 18A-B).



**Figure 18. PA200 deficient cells show reduced c-Jun phosphorylation after rotenone treatment.** (A) Control and shPA200 cells were incubated with vehicle (DMSO) or 10 μM rotenone for 24 h. Total cell lysates were used to analyze phosphorylation profiles of kinases using the human phospho-kinase array. (B) Representative bars of the pixel intensity of dots in the human phospho-kinase array. The black (A panel) and the red (B panel) frames indicate the phospho-kinases that influenced by the absence of PA200. The image was taken using a ChemiDoc Imager, and for data analysis, Image Lab 5.2.1 software was used.

Next, we confirmed the findings of the phosphokinase array by analyzing the total c-Jun and phospho- c-Jun protein levels from total cell lysates of control and shPA200 cells upon rotenone treatment at different time points by western blot analysis. The vehicle-treated clones did not show any phosphorylation of c-Jun during the time of the experiment (Fig. 19A). At two hours of treatment with rotenone, we observed an increase in c-Jun protein level and phospho-c-Jun at serine 63 in both PA200 depleted and control cells (Fig. 19A). The level of c-Jun phosphorylation was significantly less in shPA200 compared to control cells. In addition to its autoregulation, the expression of c-Jun is also regulated by JNKs (JNK1, JNK2, and JNK3) in neuroblastoma cells (Davis, 1998). With the same treatments, we analyzed the JNK expression and phosphorylation level using anti-total JNK antibody and anti-Phospho-JNK at the T183 and Y185. The total JNK protein level was constantly expressed in both cell lines, treated with vehicle or rotenone during the time of experiment (Fig. 19B). The vehicle treatment did not promote the JNK phosphorylation in both clones. The 2h treatment with rotenone induced a similar level of JNK phosphorylation in

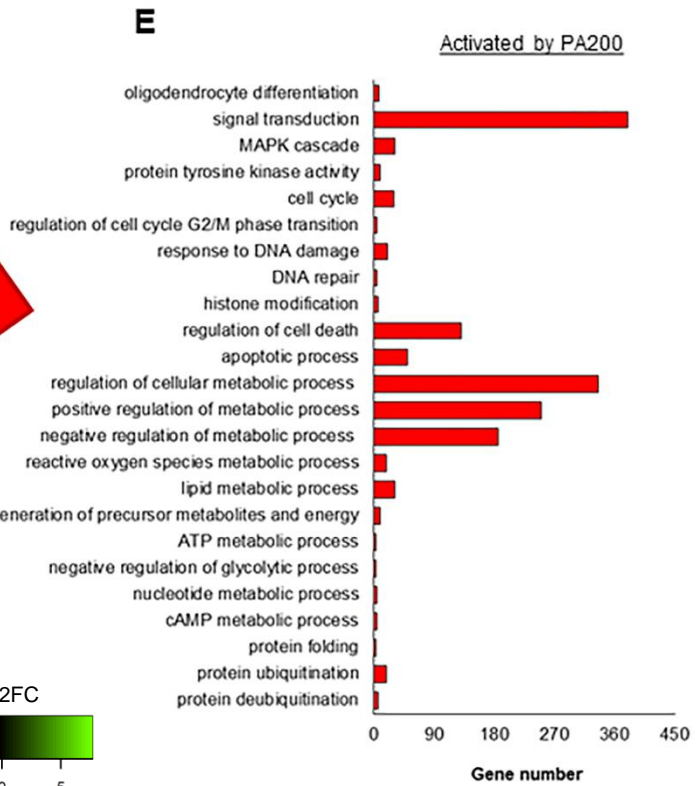
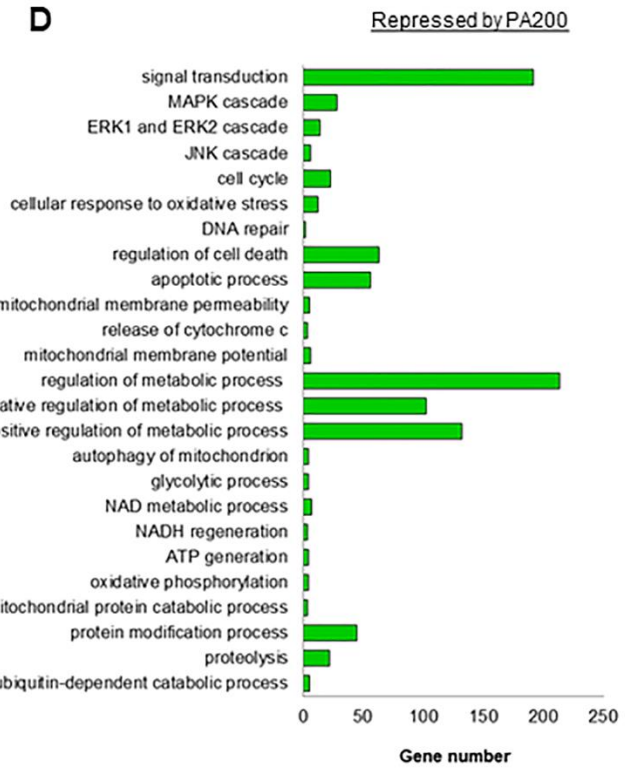
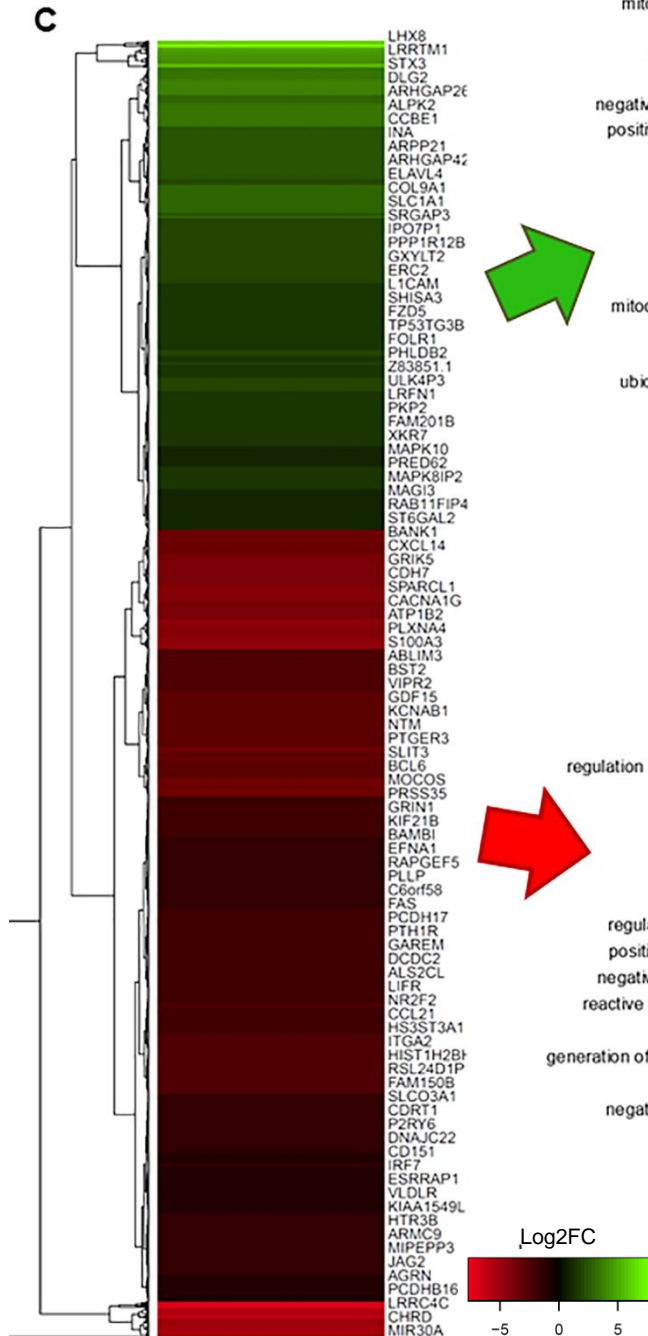
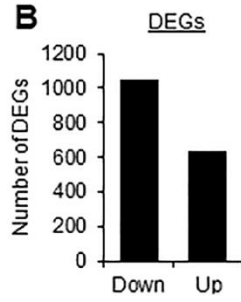
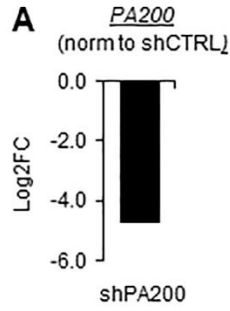
both control and shPA200 depleted cells, and it was considerably reduced in both clones at 12 and 24h time points (Fig. 19B). This data suggest that JNK pathways similarly respond to rotenone in both control and PA200 depleted cells. The reduced c-Jun phosphorylation in shPA200 cells upon rotenone treatment was not due to less activity of JNK, but the reduced protein level of c-Jun (c-Jun pool) as demonstrated in the gene expression level (Fig. 17), and western-blot analysis (Fig. 19A).



**Figure 19. PA200-depleted cells exhibit a reduction in c-Jun protein level upon rotenone treatment.** Control and shPA200 cells were incubated with vehicle (DMSO) or 10µM rotenone for the indicated time points. (A) Western blot analysis of c-Jun and p-c-Jun protein level in control and shPA200 cells upon rotenone treatment at different time points. Data are presented as mean values  $\pm$  SD of 3 independent experiments. Statistical analysis was performed by ANOVA using Graph Pad Prism v8.2.1. (\* $P < 0.05$ , and \*\*\*\* $P < 0.0001$ , §§§§  $P < 0.0001$ ). (B) Total JNK protein level and phosphorylated JNK were analyzed using SDS-PAGE and Western blot upon rotenone treatment at different time points. Western blot analysis was performed in 2 independent experiments.

## **PA200 influences cellular metabolism and mitochondrial activity at the transcriptional level**

As we mentioned above, the promoter of genes involved in several cellular processes, such as protein modifications, cell cycle, and cellular metabolism was enriched in PA200 in SH-SY5Y (Fig. 13 and Table 4). We confirmed the contribution of PA200 in cell cycle progression (Fig. 16) and its role in cellular death, especially upon selective mitochondrial inhibition. The role of PA200 in metabolic processes has not been studied yet. To test the possible contribution of PA200 to metabolism, we first investigated the role of PA200 in transcriptional control using the RNA seq approach in control and stably depleted cells of PA200. The mRNA-seq data analysis confirmed the stable silencing of PA200 in shPA200 cells (Fig. 20A). The differential gene expression (DGEs) analysis shows that the depletion of PA200 leads to an overall change in the gene expression of shPA200 cells compared to control cells (Fig. 20B, C). The functional annotation analysis of DEGs revealed that PA200 has a crucial role in cellular functions (Fig. 20D, E) including metabolism, apoptotic and cell death processes, neuron differentiation and proliferation, MAPK signaling pathway, histone modification, DNA repair, and autophagy. But the greatest representation of DEGs was assigned to cellular metabolism (Fig. 20D-G). Furthermore, the intervention of PA200 in metabolism appears in mitochondrial homeostasis, oxidative phosphorylation regulation, ATP production, and glycolysis (Fig. 20G).



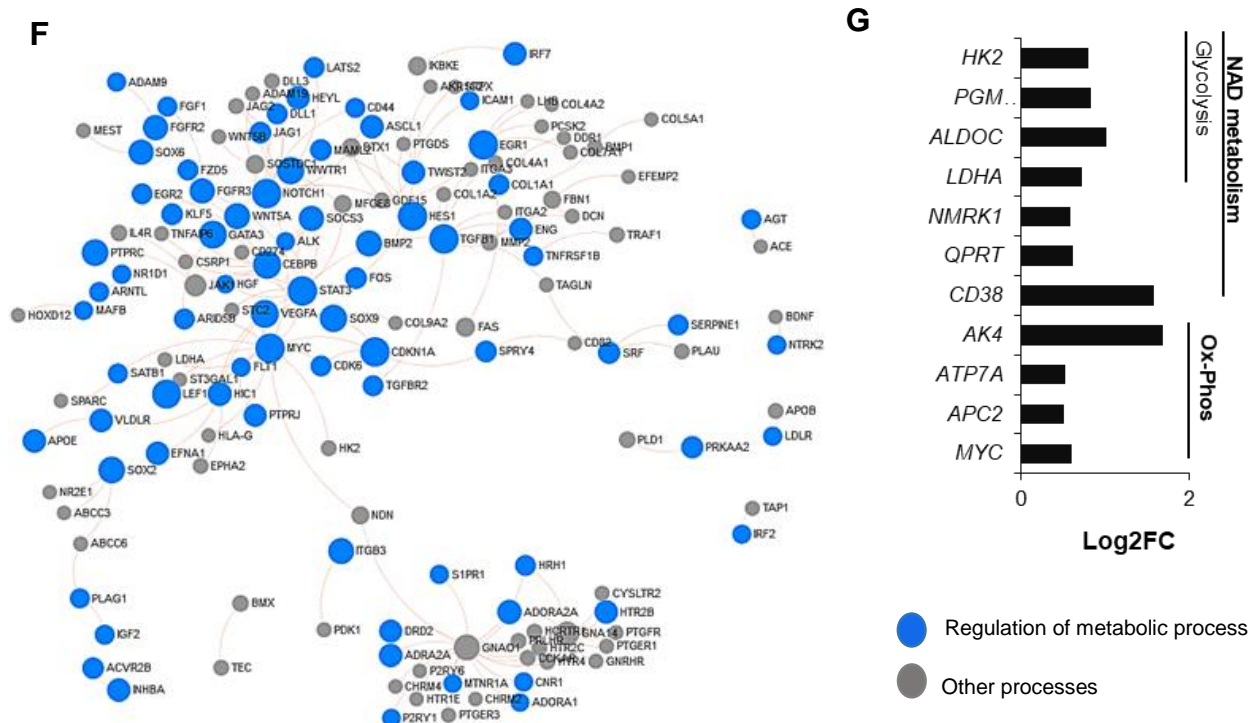


**Figure 20. Loss of PA200 influences gene expression as profiled by RNA-seq in SH-SY5Y neuroblastoma cells.** Transcriptomic analysis of PA200 depleted cells and their corresponding control in normal conditions using RNA sequencing. (A) Fold change of mRNA expression level of the PSME4 gene that expresses PA200 shows a successful depletion of PA200. (B) Numbers of the down and up-regulated genes in the PA200-depleted cells normalized to control cells (shCTRL) (C) Hierarchical clustering of log2FC of selected DEGs. The list on the right quotes every second gene. (D-E) pathway classification of the up (D) and down-regulated (E) DEGs following depletion of PA200. (F) Analyzing the signaling network of genes influenced by PA200 stably depletion represented by nodes. Gene regulatory networks indicating the genes related to metabolism by blue nodes and others gray nodes. (G) Loss of PA200 positively influences genes that contribute to mitochondrial respiration and NAD metabolism. DEGs are shown (shPA200 vs. shCTRL) derived from RNA-Seq data for regulation of oxidative phosphorylation (GO: 0002082), NAD metabolic process (GO: 0019674), and glycolytic process (GO: 0006096).

### **PA200-deficient cells exhibit mitochondrial dysfunction**

Stable depletion of PA200 influences several gene expressions including those involved in the regulation of metabolic processes, which strongly support the ChIP-seq data. Next, we investigated whether this overall change in the gene expression of shPA200, especially on cellular metabolism was also reflected in cellular functions. Notably, deletion of Blm10 in yeast reduced mitochondrial function and led to altered mitochondrial dynamics (Tar et al., 2014). Furthermore, the mRNA expression of Blm10 increased upon the switch from fermentation to oxidative metabolism (Lopez et al., 2011). Thus, we have first investigated the mitochondrial bioenergetics profile using Seahorse analysis in human cells. Cells were subjected to different mitochondrial inhibitors to investigate the different parameters of mitochondrial activity. First, oligomycin treatment blocks ATP synthase and provides information about ATP production in aerobic respiration (OXPHOS) and proton leak. FCCP uncouples mitochondrial respiration to measure maximal respiration and spare respiratory capacity. Finally, adding a combination of rotenone and antimycin A blocks the ETC and differentiates between mitochondrial and non-mitochondrial oxygen consumption. Seahorse data analysis of shPA200 cells showed a significant reduction in proton leak and spare respiratory capacity by 84.147% and 99.834%, respectively, compared to control. Maximal respiration was also dramatically, but not significantly reduced in shPA200 compared to control cells (Figure 21A, B). This data suggests that loss of PA200 negatively influences mitochondrial activity.

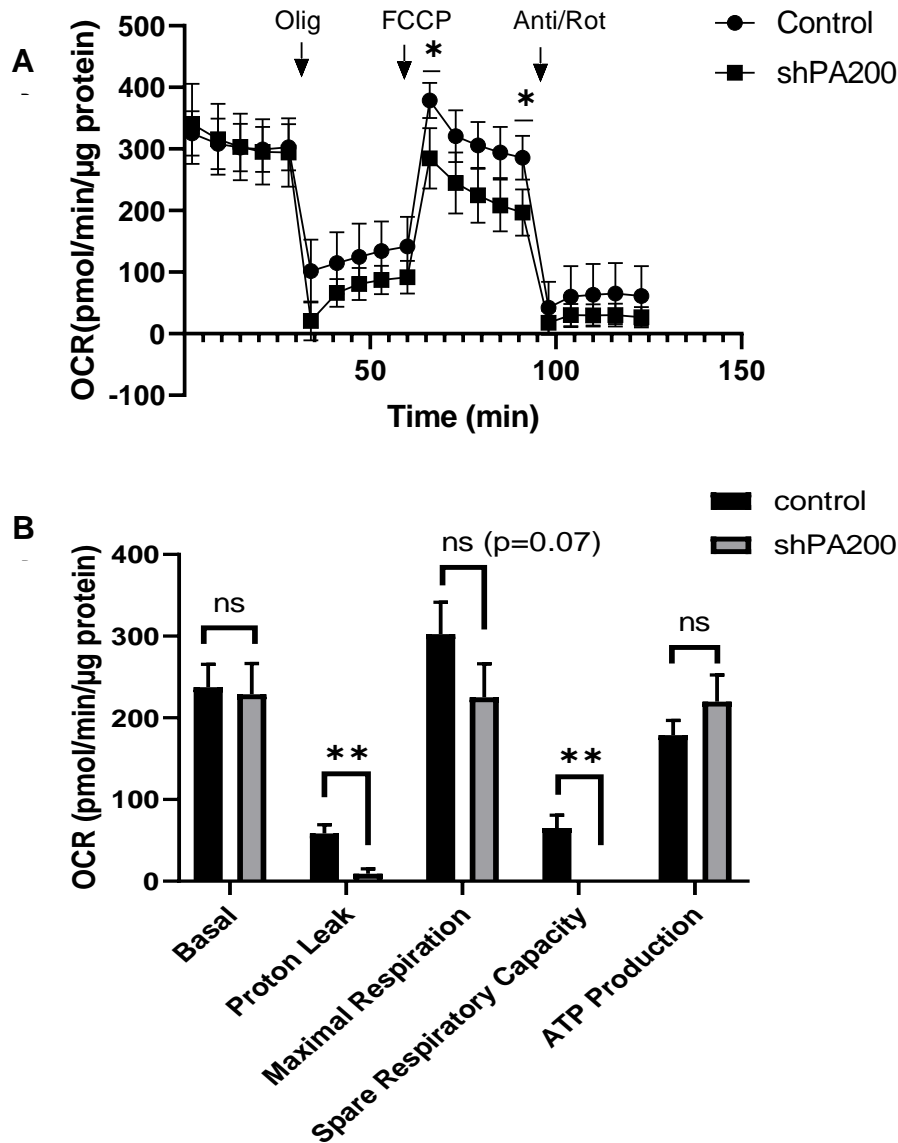


**Figure 21. Mitochondrial bioenergetics profile of control and PA200-deficient cells.** The mitochondrial activity was measured with respect to oxygen consumption rate (OCR) using a Seahorse XF96 analyzer. Control and shPA200 cells were seeded at a density of 35,000 cells/well in XF96 Seahorse plates. The following day, the basal OCR was determined for 30min before the injection of oligomycin (1.5  $\mu$ M); FCCP (1  $\mu$ M); and the cocktail of rotenone/antimycin (1  $\mu$ M). (A) ATP production, basal and maximal respiration. (B) Calculated basal respiration, proton leak respiration, maximal mitochondrial respiratory capacity, spare respiratory capacity, and ATP-coupled respiration. Data were normalized to total protein (pmol/min/ $\mu$ g protein), and were analyzed using Wave Desktop software. Data are presented as mean values  $\pm$  SD ( $n=3$ ), and statistical analysis was performed by unpaired  $t$ -test (\* indicates  $p<0.05$ , \*\* indicates  $p<0.01$ , ns; not significant).

## PA200 knock-down reduces mitochondrial ETC biogenesis

We investigated the protein level of OXPHOS machinery using western blot analysis. Samples were used from total lysates and mitochondrial sub-fractions of both clones (shPA200 and control cells) under normal conditions. Western blot analysis of OXPHOS proteins from a mitochondrial fraction (Fig. 22A) revealed a significant reduction in the protein levels of CI-NDUFB8, CII-SDHB ( $p=0.0648$ ), subunits in shPA200 cells compared to control cells; however, there was no significant change in CV-ATP5A subunit between the two clones (Fig. 22B). CIII-UQCRC2 and CIV-MTCOI were probably affected by the reagents used for mitochondrial extraction especially the CIV-MTCOI subunit, which has a hydrophobic character. Therefore, we investigated the mitochondrial OXPHOS complexes from total lysates as well (Fig. 23A). Western blot analysis showed a significant reduction in all examined OXPHOS complexes subunits; CI-NDUFB8, CII-SDHB, CIII-UQCRC2, and CIV-MTCOI subunits in PA200 deficient cells except CV-ATP5A subunit which did not show any difference in both clones (Fig. 23B-F).

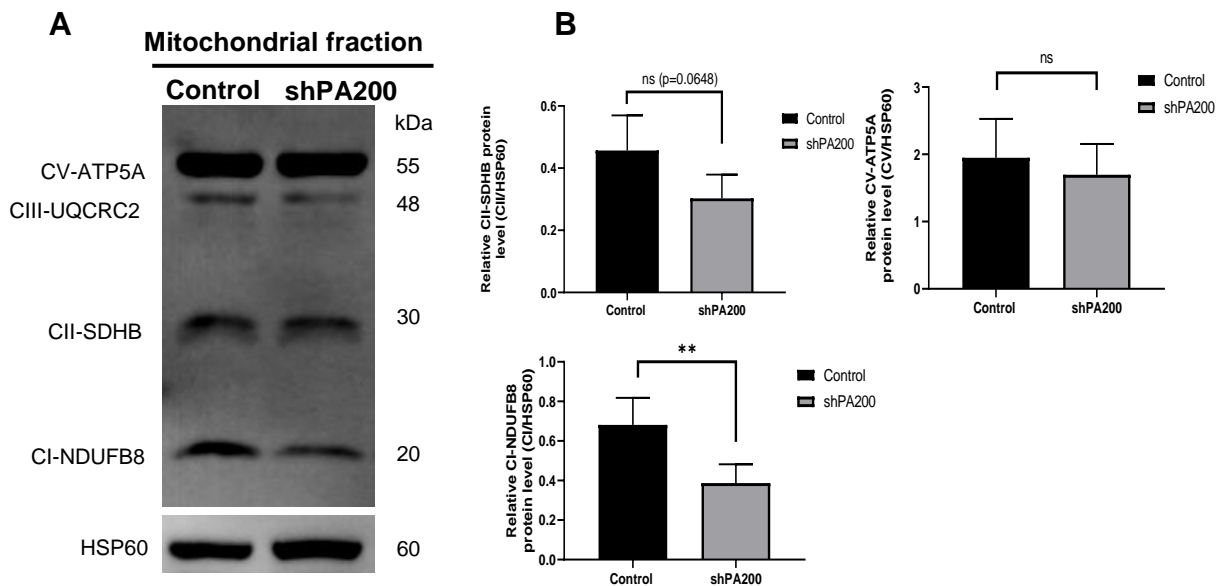


**Figure 22. Reduction in CI-NDUFB8 subunit in mitochondrial fraction of PA200-deficient cells.** Mitochondrial fraction from control and shPA200 cells was analyzed by western blot. (A) Representative western blot of mitochondrial OXPHOS proteins from mitochondrial fraction of control and PA200-deficient cells. (B) Representative bar graphs of statistical analysis of examined OXPHOS subunits. Data were analyzed using Image Lab V 6.1 software and presented as mean values  $\pm$  SD ( $n=4$ ). The statistical analysis was performed by unpaired t-test (\*\* indicates  $p < 0.01$ , ns, not significant).

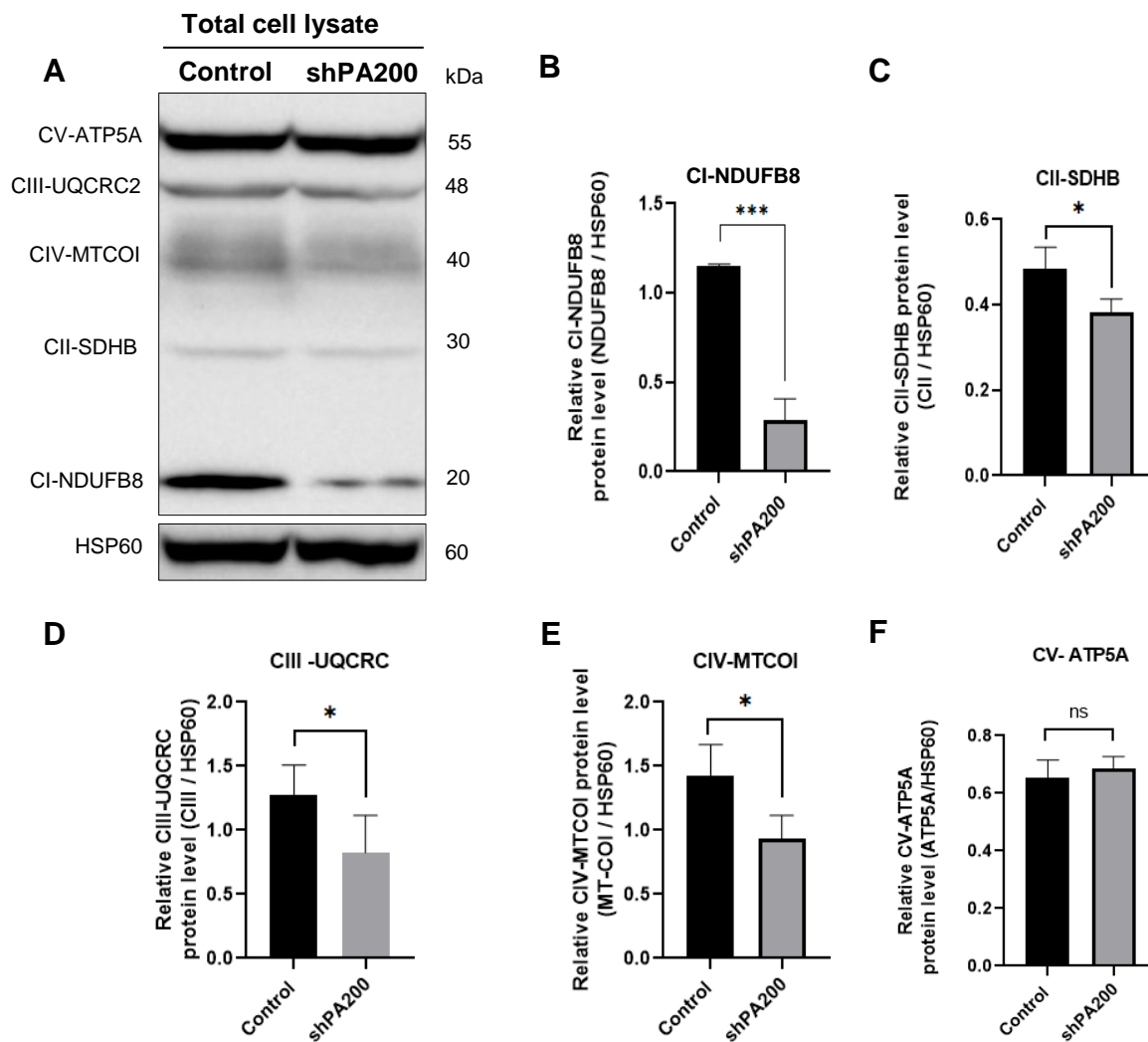


**Figure 23. PA200 knock-down cells exhibit a significant reduction in the protein level of electron transport chain complexes.** Total lysate from control and shPA200 cells at normal conditions (no stress) were analyzed by western blot, the antibody cocktail that detects four subunits of the four ETC complexes; CI-NDUFB8, CII-SDHB, CIII-UQCRC2, CIV-MTCOI, and one subunit for the ATP synthase CV-ATP5A, simultaneously was used. (A) Western blot analysis of mitochondrial OXPHOS proteins from total cell lysate of control and PA200-deficient cells. (B-F) Representative bar graphs of statistical analysis of examined OXPHOS subunits. The density of the protein was normalized to internal control of mitochondrial mass, Hsp 60. Data were analyzed using Image Lab V 6.1 software and presented as mean values  $\pm$  SD ( $n=4$ ). The statistical analysis was performed by unpaired t-test (\* indicates  $p < 0.05$ , \*\*\* indicates  $p < 0.001$ . ns, not significant).

### **Cells stably depleted of PA200 shift from OXPHOS to glycolysis**

Next, we hypothesized that the reduced mitochondrial activity might lead shPA200 cells to be provided by energy from other sources, such as increased glycolysis, especially upon stressed mitochondria. PA200 depletion also leads to downregulation of the negative regulators of glycolytic genes and induces the glycolytic process (Fig. 20D, E, G). Therefore, we determined changes in glycolysis upon PA200 depletion using Seahorse XF analysis. During the real-time ECAR measurement, the shP200 and control cells were subjected to different compounds to investigate the different parameters of cellular glycolysis. First, we determined the baseline of the ECAR for 30min in a glucose-free medium. Next glucose, oligomycin, and 2-DG were sequentially injected. Administrating glucose help to determine glycolysis, while oligomycin treatment blocks ATP production enhancing other sources of energy in the cell, thereby we can determine the glycolytic capacity. Finally, the administration of the glucose analog, 2-DG blocks glycolysis by antagonizing the endogenous glucose, confirmation that the ECAR originates from glycolysis.

Data analysis demonstrates that in PA200 depleted cells, the glycolysis and glycolytic capacity are significantly increased by 42.186% and 26.106%, respectively, compared to control cells (Fig. 24A and B). This data suggests that the loss of PA200 directs cells from oxidative phosphorylation to glycolytic activity as another source of energy, especially under mitochondrial insult.

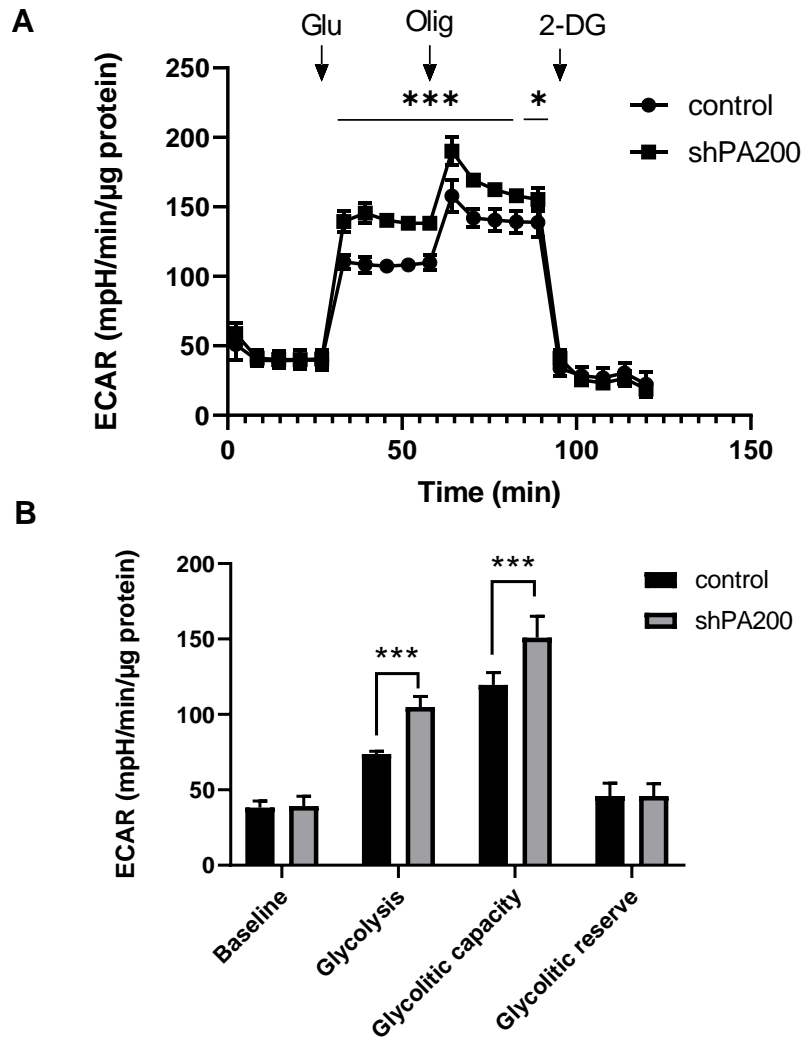


**Figure 24. Increased glycolysis and glycolytic capacity in PA200-deficient cells.** The glycolytic activity was measured using the Seahorse XF 96 analyzer. Glycolysis was assessed by measuring ECAR. PA200-depleted and corresponding control cells were seeded in an XF 96 cell culture microplate at 35,000 cells/well. The basal ECAR was determined for 30 min before the injection of 10 mM glucose (Glu), 1  $\mu$ M oligomycin (Olig), and 50 mM 2-deoxy-d-glucose (2-DG). (A) Glycolytic profile of PA200 depleted cells and control cells. (B) Calculated glycolysis and glycolytic capacity of shPA200 and control cells normalized to total protein (mpH/min/ $\mu$ g protein). Data were analyzed using Wave Desktop software. Data are presented as mean values  $\pm$  SD ( $n=4$ ), and statistical analysis was performed by unpaired  $t$ -test (\* indicates  $p<0.05$ , \*\*\* indicates  $p<0.001$ ).

## **PA200-deficient cells exhibit fused mitochondrial morphology upon selective mitochondrial inhibitor treatment**

Mitochondrial number, structural network, and distribution are subject to change depending on cell type, cell cycle stage, and response to extracellular stimuli (Rambold & Pearce, 2018). Furthermore, the intracellular energy status and the mitochondrial morphology are dependent on each other (Mishra & Chan, 2016; Wai & Langer, 2016). We studied the impact of PA200 depletion on mitochondrial dynamics, in the presence or absence of the mitochondrial inhibitor, oligomycin. We used oligomycin at the concentration of 3  $\mu$ M for 24h based on our previous observations. First, we have chosen oligomycin because it induced more fragmented mitochondria compared to rotenone treatment (Fig. 25), indicative of reduced mitochondrial activity. Second, rotenone treatment showed increased cell death, especially upon loss of PA200, compared to oligomycin treated shPA200 cells (Fig. 11, Fig. 12). Furthermore, oligomycin treatment was described as a tool for the investigation of OXPHOS suppression adaptation in various cancer cell lines (Hao et al., 2010).

Mitochondrial morphology was analyzed using the HCS system. Mitotracker Red CMXRos and Hoechst 33342 were used to stain the mitochondria and nuclei, respectively. The analysis and quantification of mitochondrial morphology were assessed using Harmony 4.8 and PhenoLogic machine learning software. Mitochondria were classified into four classes; long tubular, short tubular, compact tubular, and fragmented mitochondria (Fig. 26). Analysis of Mitochondrial classes revealed that there were no significant changes between the PA200 depleted and the control cells upon vehicle treatment (Fig. 27A and B). When cells were treated with 3  $\mu$ M oligomycin, we observed a significant increase of mitochondrial fragmentation in both cell lines compared to vehicle-treated cells. The effects of oligomycin on mitochondrial fragmentation were significantly higher in control cells compared to shPA200 cells (Fig. 27B). Moreover, the long tubular and the compacted mitochondrial structures were significantly higher in shPA200 cells compared to control cells after 24h treatment with oligomycin. The data suggest that PA200 has a crucial role in the maintenance and proper mitochondrial dynamics.

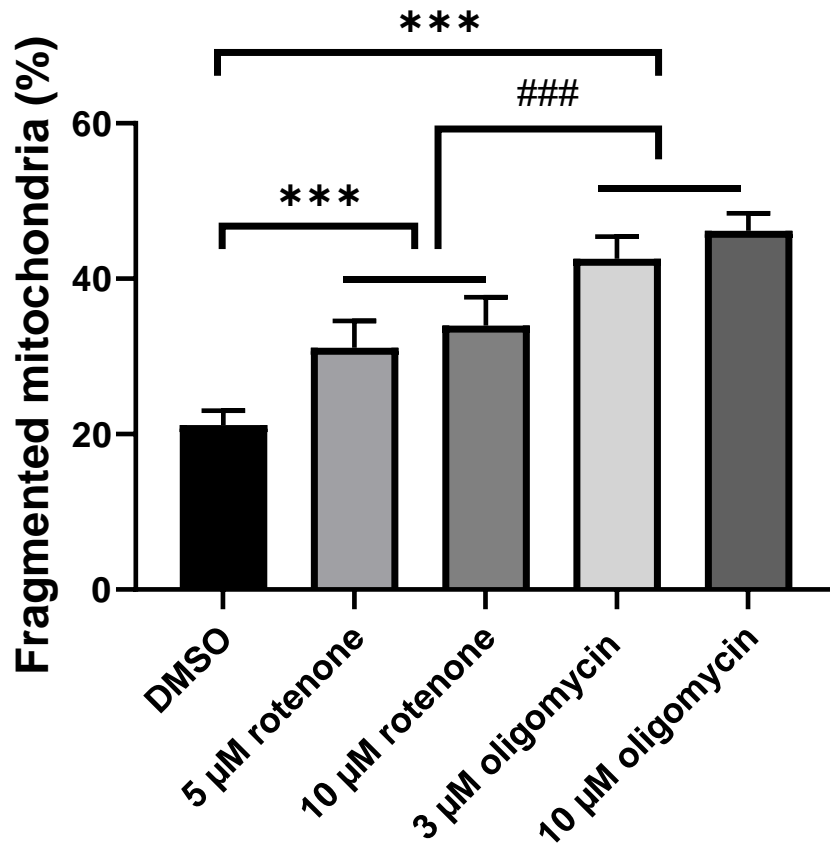


**Figure 25. Oligomycin induces elevated mitochondrial fragmentation compared to other mitochondrial inhibitors in the SH-SY5Y cell line.** Control cells were treated for 24 h either with DMSO or 5 μM and 10 μM rotenone, or 3 μM and 10 μM oligomycin. After 24h treatment, the cells were stained with 50 nM Mitotracker Red CMXRos and 10 μM Hoechst 33342 for 30 minutes. Live cell mitochondrial morphology monitoring was assessed using Opera Phenix High-Content Screening System. Up to 5000 cells were analyzed in each condition of treatment with mitochondrial inhibitors. Images were analyzed using Harmony 4.8 software. Data are presented as mean values  $\pm$  SD ( $n=4$ ), and statistical analysis was performed by Two-way ANOVA test (\*\*\*) indicates  $p<0.001$ . ### indicates  $p<0.001$ ).

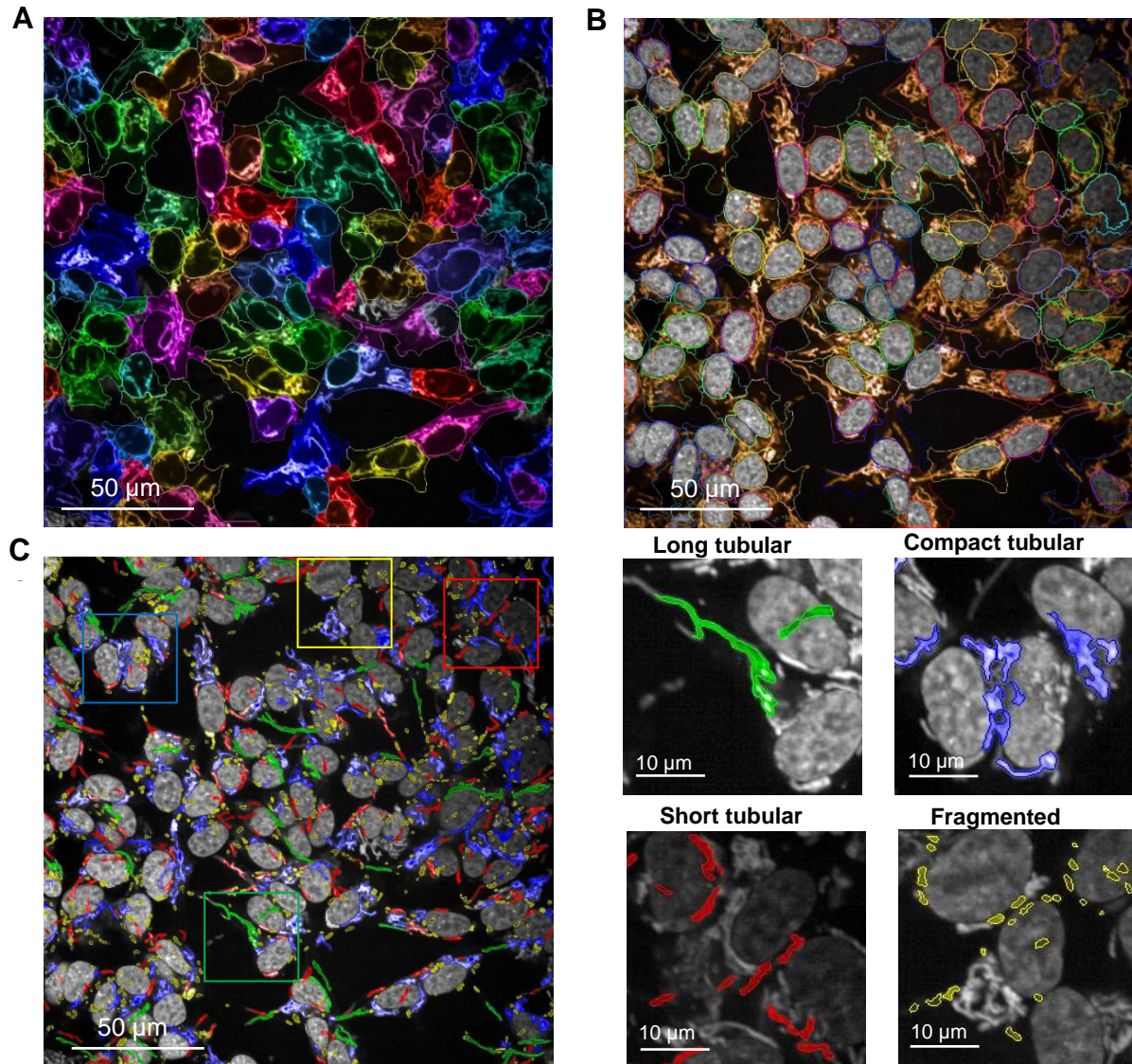


**Figure 26. Classification of Mitochondrial morphology.** Live-cell images were acquired by Opera Phenix High-Content Screening System (63× water objective (NA = 1.15)). The cells were stained with Hoechst 33342 and Mitotracker Red CMXRos to label the nucleus and mitochondria, respectively. shPA200 and control cells constitutively expressed the EGFP to determine the cellular cytosol. (A-B) Images were analyzed using Harmony 4.8 software and different subcellular fluorescence staining was used for cell segmentation (EGFP determines the cytoplasm, Hoechst determines the nuclei, and Mitotracker red determines the mitochondrial compartments). (C) Mitochondria were classified as follows: fragmented, short tubular, long tubular, and compact tubular based on measured properties using the PhenoLOGIC machine learning. % of each mitochondria class = (mitochondria class area / total mitochondria area) x 100. Scale bar = 50μm, inset=10μm.



## Effects of PA200 depletion on genes related to mitochondrial dynamics

Under normal conditions, the loss of PA200 in SH-SY5Y neuroblastoma cells did not affect mitochondrial dynamics (Fig. 27B). However, upon oligomycin treatment, PA200 depleted cells showed a significant reduction of fragmented mitochondria compared to oligomycin-treated control cells (Fig. 27B). The mitochondrial morphology is controlled by heterogeneous groups of proteins (see mitochondrial fission and fusion machinery), which mediate mitochondrial fission and fusion to ensure mitochondrial homeostasis. We investigated the effect of PA200 depletion on the expression pattern of genes involved in mitochondrial fission and fusion upon a vehicle or 3  $\mu$ M oligomycin treatments for 24h, using RT-qPCR. The examined fusion genes were *MFN1*, *MFN2*, and *OPA1*, and the examined fission genes were *MIEF1*, *MIEF2*, *FIS1*, *DNM1L*, and *MPF*. The RT-qPCR data analysis revealed that the majority of genes are down-regulated in both cell lines following oligomycin treatment (Fig. 28A). *OPA1* mRNA level, however, shows a considerable but not significant increase in both clones (Fig. 28A). Interestingly, *MFN1* mRNA expression level was significantly reduced in shPA200 cells compared to control cells upon oligomycin treatment (Fig. 28A).

We also normalized the RT-qPCR data to control cells to see the effect of PA200 depletion on the expression pattern. Data revealed that there were no significant changes in the mRNA expression of the tested genes upon a vehicle or oligomycin treatment compared to control cells, except a slight but significant increase in the fold change of *MFN2*, in the vehicle-treated shPA200 cells (Fig. 28B). Taken together, oligomycin treatment negatively influences gene expression of proteins of mitochondrial dynamics in both control and shPA200 cells. Furthermore, loss of PA200 did not cause significant changes in mRNA expression of mitochondrial fission and fusion proteins compared to control cells, except for *MFN1* after oligomycin treatment (Fig. 28A), and *MFN2* after treatment with vehicle (Fig. 28B).

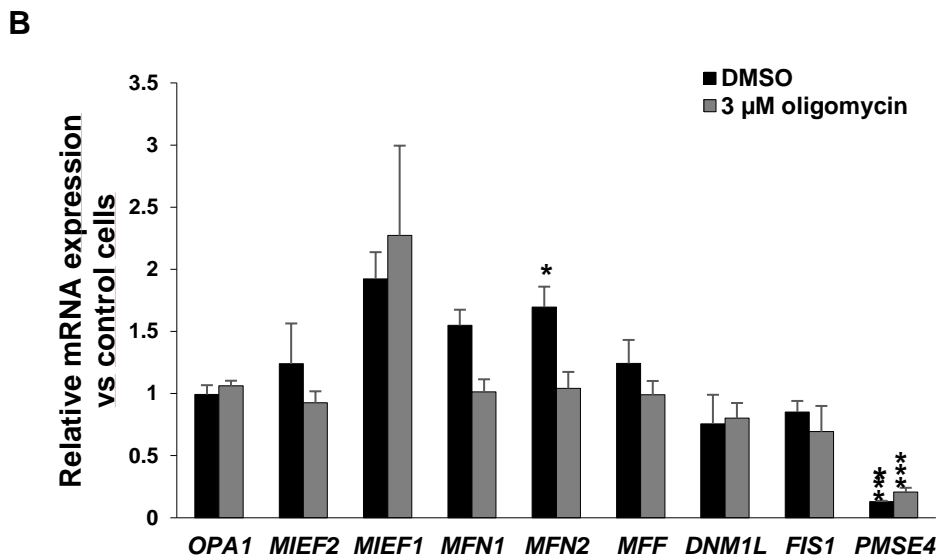
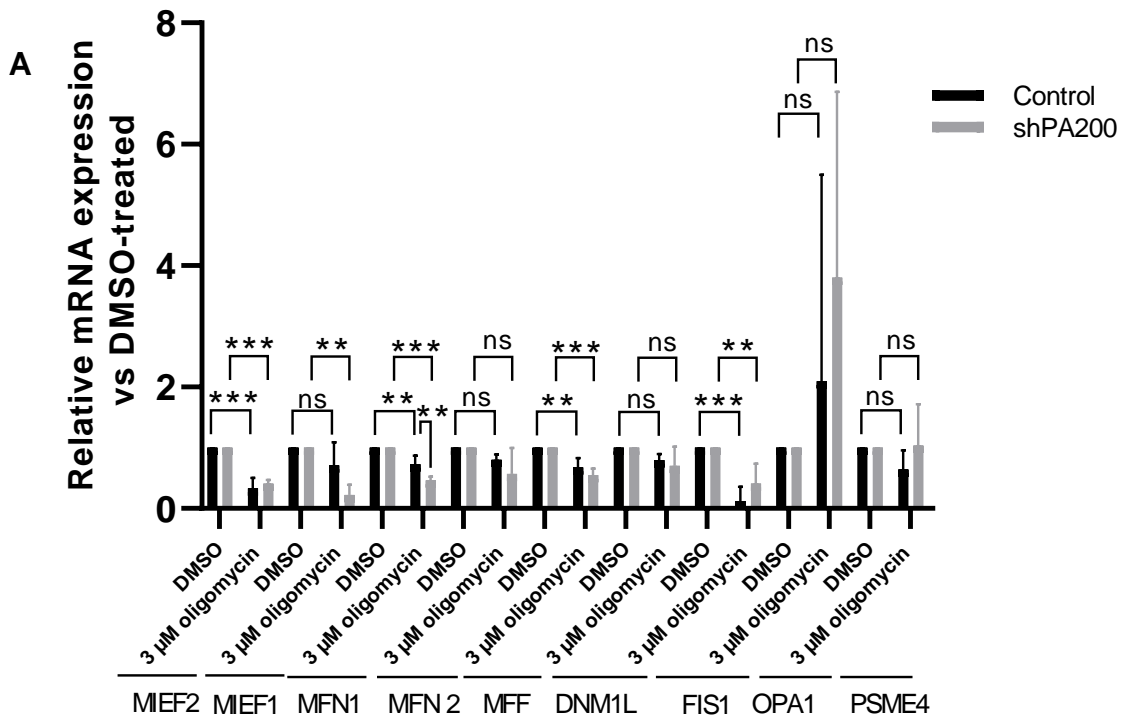


**Figure 28. mRNA expression of mitochondrial fission and fusion genes upon loss of PA200.** Control and shPA200 cells were treated with vehicle or 3μM oligomycin for 24h. The mRNA expression levels of mitochondrial fission and fusion genes were examined by RT-qPCR. (A) The data of RT-qPCR were normalized to vehicle-treated cells. (B) The data of RT-qPCR were normalized to control cells. Data are presented as mean values ± SD. Statistical analysis was performed by Two-Way ANOVA and unpaired student t. test (\* indicates  $p < 0.05$ , \*\* indicates  $p < 0.01$ , \*\*\* indicates  $p < 0.001$ . ns, not significant).

### **PA200-deficient cells demonstrate stabilized L-OPA1 isoform upon oligomycin treatment**

We investigated the key mitochondrial fission and fusion proteins using western-blot analysis (Fig. 29). Overall, the mitochondrial fission and fusion proteins did not show significant changes in shPA200 compared to control cells upon vehicle treatment (Fig. 29A-D). However, 3  $\mu$ M oligomycin treatment significantly reduced the level of L-OPA1 isoform in both clones, compared to vehicle-treated cells (Fig. 29A and B). The effects of oligomycin on L-OPA1 cleavage to S-OPA isoform was significantly higher in control than in shPA200 cells (Fig. 29B), suggesting that PA200 knockdown prevented the oligomycin-induced L-OPA1 cleavage, and thus might lead to more fused mitochondria in shPA200 upon oligomycin treatment (Fig. 27B). OPA1 isoforms in the IMM are controlled by the peptidase OMA1 and the i-AAA protease YME1L (Anand et al., 2013). The cleavage of L-OPA by OMA1 or YME1L depends on extracellular stress that leads to ATP depletion, mitochondrial depolarization, and increased ROS production, which was associated with OMA1 and YME1L activation (Anand et al., 2014; Baker et al., 2014).

To explore the mechanism behind the high cleavage of L-OPA in control, but not shPA200 cells upon oligomycin treatment, we investigated the protein level of OMA1 and YME1L in control and PA200 deficient cells upon vehicle or 3  $\mu$ M oligomycin using western blot analysis. Data reveals that no significant changes in YME1L in both clones were detected either treated with vehicle or 3  $\mu$ M oligomycin (Fig. 29A and D). Interestingly we found a significant reduction of protein level of OMA1 in oligomycin-treated shPA200 compared to oligomycin-treated control cells (Fig. 29A and C). This data suggests that stress-dependent L-OPA1 cleavage is reduced in shPA200 due to the reduction of the protein pool of OMA1 upon oligomycin treatment, compared to oligomycin treated control cells. These results partially explain the increased fused and compacted mitochondrial classes in PA200-deficient cells (Fig. 27B).

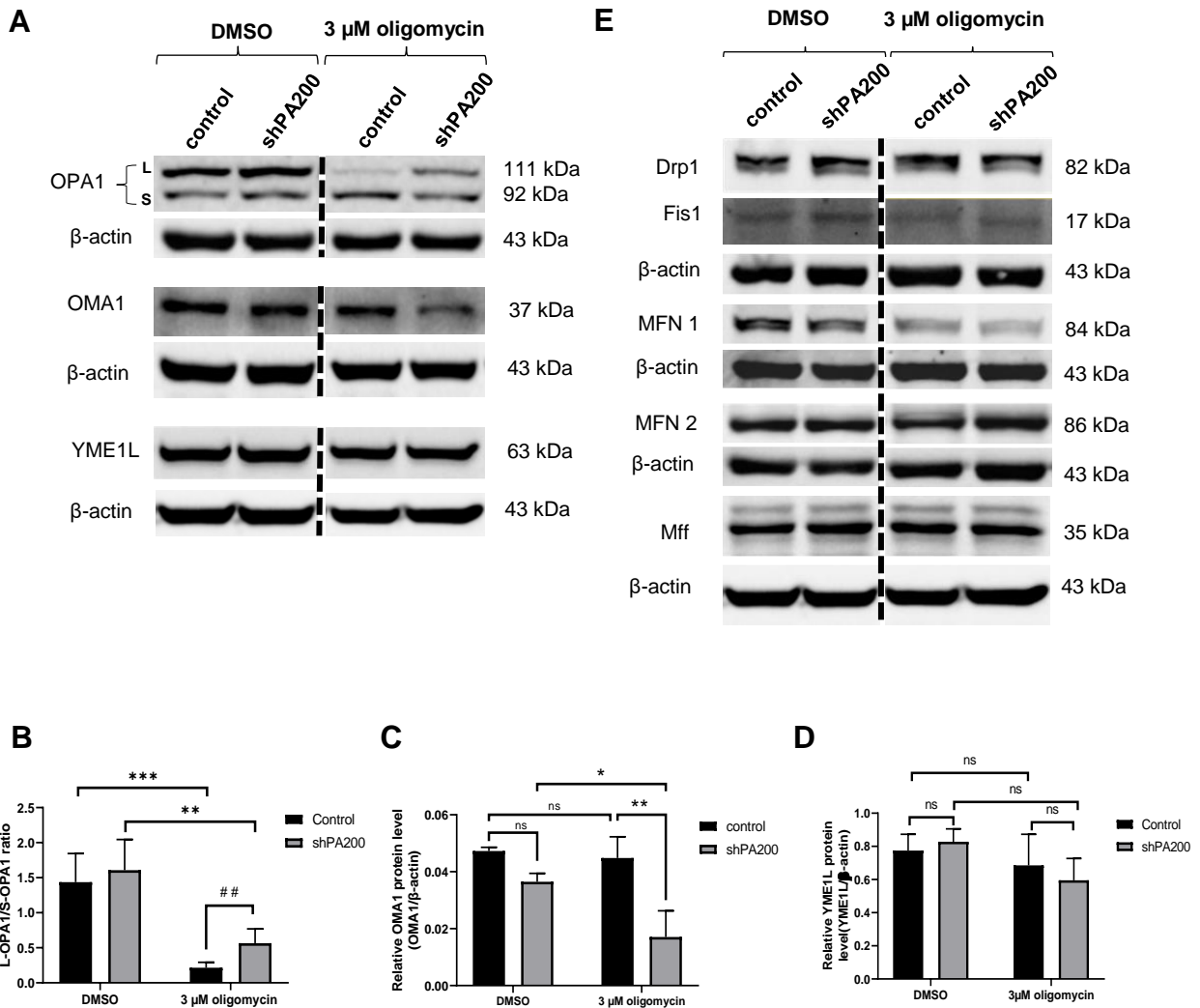


**Figure 29. PA200-deficient cells exhibit reduced stress-induced L-OPA1 cleavage.** Control and PA200-depleted cells were treated either with vehicle or 3  $\mu$ M oligomycin for 24h. Cells were lysed and equal amounts of proteins were separated in SDS-PAGE. Key proteins of mitochondrial dynamics were investigated using; anti-Drp1, anti-Fis1, anti-Mff, anti-Mfn1 and 2, anti-OPA1, anti-OMA1, and anti-YME1L antibodies. (A, E) representative image of western blot analysis. (B) OPA1 statistic bar graph, (C) OMA1 statistic bar graph (D) YME1L statistic bar graph. Images were taken using a ChemiDoc Imager. The pixel intensity was quantified and normalized to internal control  $\beta$ -actin using Image Lab software. Data are presented as mean values  $\pm$  SD (n=4). Statistical analysis was performed by Two-Way ANOVA. (\* indicates  $p < 0.05$ , \*\* indicates  $p < 0.01$ , \*\*\* indicates  $p < 0.001$ , ## indicates  $p < 0.01$ . ns, not significant).

## **Loss of PA200 increases ROS production and oxidized proteins upon mitochondrial stress**

The active mitochondria generate ROS under normal conditions with low rates as part of cellular redox regulation (Loschen et al., 1971). ROS are considered as indicators of mitochondrial status since mitochondria are the main sources of ROS in the cell. Our RNA-seq data analysis demonstrated that loss of PA200 alters the expression of genes related to cellular responses to oxidative stress. Our results also show that PA200-deficient cells exhibit inefficient mitochondrial function and biogenesis. Thus, as a logical step, we studied the possible impact of PA200-depletion on ROS production using flow cytometry analysis.

The total ROS production of control and shPA200 cells were measured in the presence and absence of either vehicle or 3  $\mu$ M oligomycin. Cells were stained with Deep-Red ROS detection dye and the fluorescence intensity was detected from 20,000 PA200-deficient and control cells. FACS analysis revealed a slight but significant reduction in total ROS production in shPA200 compared to control cells in the absence of the treatment (Fig. 30A). We did not see a major difference in ROS production upon vehicle treatment between the two cell lines (Fig. 30B), while, treatment with 3  $\mu$ M oligomycin significantly increased ROS production in shPA200 compared to vehicle-treated cells (Fig. 30B).

ROS induce irreversible structural modification of proteins by giving a rise of carbonyl groups (protein carbonylation) (E. R. Stadtman & Berlett, 1991; E. R. Stadtman & Levine, 2003; E. R. Stadtman, 1990). Oxidized proteins lose their function and promote disease-related protein dysfunction for example in neurodegenerative diseases (Dalle - Donne et al., 2006). We tested the effects of the PA200 knock-down on protein carbonylation. Both cell lines were tested with or without treatment of oligomycin. Cells were lysed and conjugated with DNPH molecules. The derivatized proteins were separated by SDS-PAGE and the oxidized proteins were detected using an anti-DNP antibody. Western blot data analysis showed a slight but significant reduction in protein carbonylation (oxidization) in PA200 knock-down compared to control cells without treatment (Fig. 30C and D). Oligomycin treatment in both PA200-deficient and control cells leads to an increase in oxidized proteins (Fig. 30E). Notably, in PA200 deficient cells, the protein carbonylation is higher compared to oligomycin treated control cells (Fig. 30E). Based on these data, we speculate that PA200 deficient cells can adapt to mitochondrial dysfunction when additional mitochondrial stress is not present, by maintaining low ROS production, thereby

reducing protein oxidation and minimizing intracellular oxidative stress. However, upon mitochondrial insult, such as oligomycin treatment, PA200-deficient cells produce higher level ROS leading to protein oxidation.

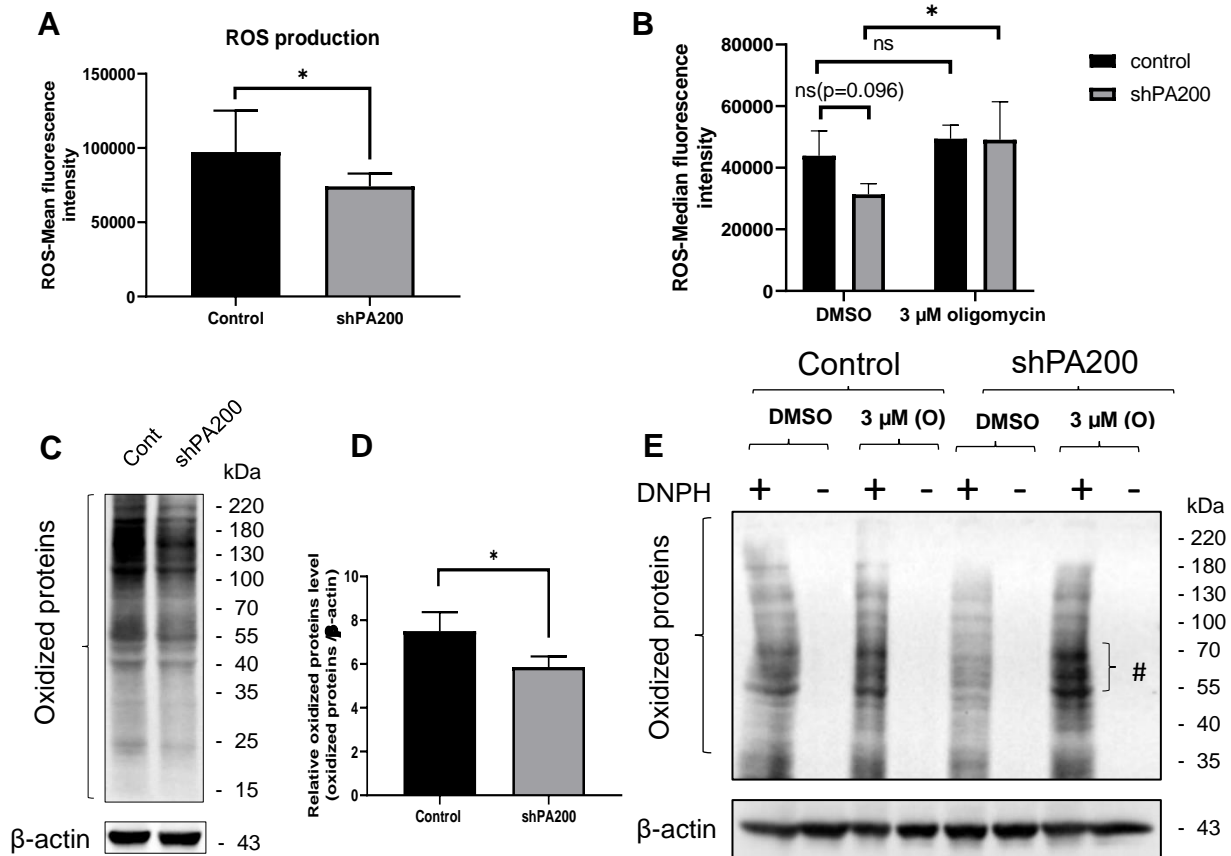


**Figure 30. High ROS production and protein oxidation in PA200-deficient cells upon stress.** Total intracellular ROS in control and PA200 depleted cells were analyzed by flow cytometry. Untreated cells were stained with ROS detection reagent that interacts with free radicals and base on red/ox reactions generates a dye that is detected at the deep-red channel of the flow cytometer. 20,000 cells were analyzed from shPA200 and control cells. (A, B) Statistical histogram of FACS data analysis of ROS dye fluorescence intensity in control and shPA200 cells. Data are presented as mean values  $\pm$  SD ( $n=4$ ). Statistical analysis was performed by unpaired *t*-test and Two-Way ANOVA. (\* indicates  $p<0.05$ , ns, not significant). (C) Representative western blot of protein carbonylation of untreated control and shPA200 cells. (D) Statistical analysis of protein carbonylation in both clones and data normalized to internal control  $\beta$ -actin. Data are presented as mean values  $\pm$  SD ( $n=3$ ). Statistical analysis was performed by unpaired *t*. test. (\* indicates  $p<0.05$ ). (E) Representative western blot of protein carbonylation in control and shPA200 cells upon treatment with vehicle (DMSO) or 3 $\mu$ M oligomycin (O), #; indicates highly oxidized proteins in shPA200 cells upon oligomycin treatment. Images were taken using a ChemiDoc Imager and the pixel intensity was quantified and normalized to internal control,  $\beta$ -actin, using Image Lab software.

## PA200 influences mitochondrial membrane potential ( $\Delta\Psi_m$ )

RNA-seq data revealed that PA200 depletion affects the mRNA expression of genes involved in mitochondrial membrane potential (Fig. 20D and E). We measured  $\Delta\Psi_m$  in PA200-depleted and control cells using FACS. We tested untreated and we challenged cells with the mitochondrial inhibitor, oligomycin.  $\Delta\Psi_m$  in both clones was determined using TMRE staining, which labels only active mitochondria. The fluorescence intensity of TMRE is proportional to mitochondrial membrane polarization. FACS data analysis showed a significant reduction of  $\Delta\Psi_m$  in shPA200 cells, compared to control cells without treatment (Fig. 31A). However, upon 24h treatment with oligomycin,  $\Delta\Psi_m$  significantly increased in both clones, compared to vehicle-treated cells (Fig. 31B). This data supports the mRNA-seq results and suggests that PA200 positively influences  $\Delta\Psi_m$ .

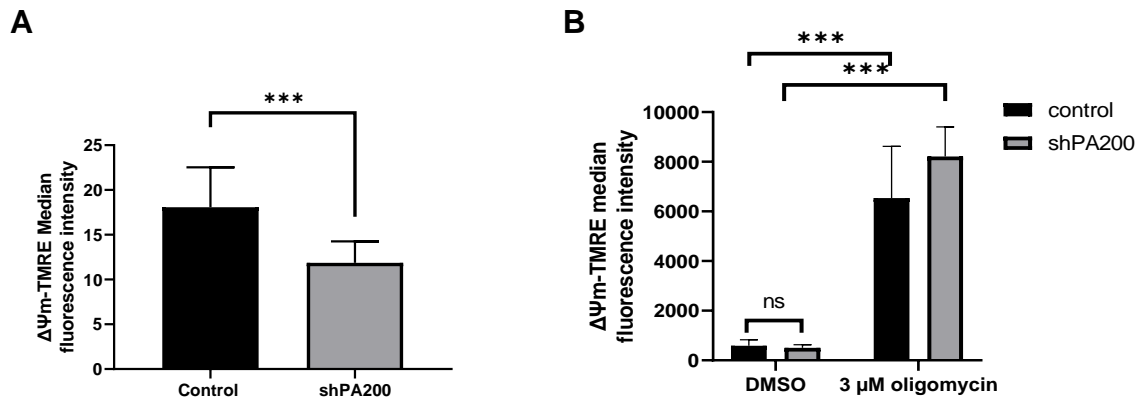


**Figure 31. PA200 deficient cells exhibit lower mitochondrial membrane potential.** The mitochondrial membrane potential of untreated and oligomycin treated shPA200 and control cells was assessed using TMRE. Cells were stained with 100 nM TMRE for 10 min. (A) Statistical bar graph of TMRE-median fluorescence intensity of shPA200 and control cells at normal conditions. (B) Statistical bar graph of median fluorescence intensity of TMRE in PA200-deficient cells and its control that treated either with vehicle or 3  $\mu$ M oligomycin for 24h. Data acquisition was assessed using a flow cytometer analyzer (n=4). Data were analyzed using FlowJo\_V10 software. Data are presented as mean values  $\pm$  SD and statistical analysis was performed by unpaired t-test and ANOVA (\*\*\*) indicates  $p < 0.001$ . ns, not significant).

## DISCUSSION

The proteasome activator, PA200 alternatively binds to 20S core particle and enhances the peptidase activity of the proteasomes. In mammals, PA200 is expressed in all tissues and at a larger extent in testis (Ustrell et al., 2002). PA200 is present in the nucleus, and cytosol either as free form or it binds to 20S proteasome, depending on the cell type and stress conditions (Gomes et al., 2006; Ustrell et al., 2002). The known functions of PA200/BIm10, in addition to its role in proteolysis, are cytoprotection in DNA repair, spermatogenesis, myofibroblast differentiation, mitochondrial function in yeast, and aging (Chen et al., 2020; Huang et al., 2016; Iwanczyk et al., 2006; Khor et al., 2006; Ustrell et al., 2002; Welk et al., 2019).

Based on our preliminary data, we further aimed to explore the role of PA200 in transcriptional control and mitochondrial integrity. We generated stable knockdown of PA200 in the SH-SY5Y cell line using lentiviral technology. We chose SH-SY5Y cells for several reasons, in addition to their human origin and neuronal properties (Klintworth et al., 2007; Lopes et al., 2010; Xicoy et al., 2017). Disease-specific network analysis of SH-SY5Y cells revealed that the genomic integrity of SH-SY5Y cells is highly maintained regarding the pathological pathways of PD and AD, but low for HD (Krishna et al., 2014). The intracellular stress that occurs in disordered neurons in neurodegenerative patients was created in our model by treating the cells with different mitochondrial inhibitors, especially rotenone, which is used to mimic the intracellular condition in the PD model (Betarbet et al., 2000).

The stable depletion of PA200 in SH-SY5Y cells did not show any major differences compared to control cells regarding proliferation and viability; however, cell adhesion was slightly lower in shPA200 compared to control cells. First, we tested the possible role of PA200 in cell viability upon treatment with mitochondrial inhibitors using SRB assay. Our data revealed that all mitochondrial inhibitors led to a significant reduction of cell viability, in both shPA200 and control cells, compared to vehicle-treated cells. Mitochondrial respiratory chain inhibitors such as rotenone, antimycin A, and oligomycin are already known to induce cell death in cultured human lymphoblastoid (Wolvetang et al., 1994). Rotenone showed to induce cell death in the SH-SY5Y cell line (Newhouse et al., 2004), and antimycin-A induced apoptosis in HeLa and HL-60 cells. Interestingly, the effect of rotenone treatment on PA200-deficient cells was more severe on cell viability compared to control cells, suggesting that the loss of PA200 significantly increases cell

death upon rotenone treatment. We confirmed this finding by testing necrosis and apoptosis markers in shPA200 and control cells under the same conditions of treatment. We observed a significant increase in the protein levels of necrotic and apoptotic markers in shPA200 cells upon rotenone treatment, compared to rotenone-treated control cells. Oligomycin and antimycin A treatments did not show any significant differences either in cell viability or apoptosis hallmarks between the two clones.

It is known that the PA200/Blm10 family is recruited to the chromatin upon IR exposure and is involved in the DNA repair process by degradation of acetylated core histones (Qian et al., 2013). PA200 recognizes and binds to acetylated histones by its BRD-like region. Notably, PA200/Blm10 BRD-like domain does not share any sequence homology with any known BRDs (Guan et al., 2020; Qian et al., 2013). Furthermore, deletion of Blm10 in yeast leads to overall changes in the expression pattern of relevant genes encoding for proteins required for cell cycle, chromosome organization, assembly, function, and repair (Doherty et al., 2012). Additionally, structural characteristics of PA200 are typically associated with protein-protein binding (adaptor protein). Based on these findings, we speculated that the mechanism behind the higher sensitization of PA200-deficient cells to rotenone compared to control is due to an overall change in the transcriptional machinery via direct or indirect binding of PA200 to promoters of relevant genes. To verify our hypothesis, we assessed ChIP and ChIP-seq analysis in SH-SY5Y cells upon treatment with mitochondrial inhibitors.

ChIP-seq data analysis revealed that PA200 is a chromatin component in SH-SY5Y cells. Previous reports revealed that PA200 forms nuclear foci upon exposing HeLa cells to IR (Ustrell et al., 2002). Others demonstrated that this accumulation of PA200 in the chromatin upon IR exposure is accompanied by association with 20S proteasomes to ensure the degradation of acetylated histones (Qian et al., 2013). Interestingly, our ChIP-seq data analysis disclosed that PA200 is recruited to TSS regions of genes involved in the cell cycle, primary metabolism, and protein modifications. Furthermore, the binding of PA200 to such promoter regions is changed based on selective mitochondrial inhibitor treatment; for example, upon vehicle treatment PA200 binds to promoter regions of *ATP5E* gene, which encodes for mitochondrial ATP synthase F1 subunit. However, treatment with oligomycin leads to dissociation of PA200 from the *ATP5E* promoter. For the same gene, RT-qPCR data of genes whose promoters are enriched in the anti-PA200 ChIP showed that

the mRNA expression level of *ATP5E* gene was significantly downregulated in shPA200 upon oligomycin treatment compared to vehicle-treated shPA200 cells. *ATP5E* silencing in HEK cells leads to defects in ATP synthase complex and reduction in ATP production (Havlíčková et al., 2010). This data suggests that loss of PA200 affects mitochondrial biogenesis at the transcriptional level, thereby overall influences cellular metabolism. PA200 also binds to promoter regions of genes involved in cell survival, such as *CASP4*, upon oligomycin treatment. RT-qPCR data revealed that *CASP4* mRNA expression was significantly down-regulated in PA200-deficient cells after oligomycin treatment compared to oligomycin-treated control cells. On the other hand, rotenone treatment leads to enrichment of PA200 to promoter regions of genes involved in apoptosis process, such as *CASP5*. *CASP5* mRNA expression was significantly down regulated in rotenone-treated shPA200 cells compared to rotenone-treated control cells. Shuttling of PA200 from one promoter to another, depending on selective mitochondrial stress, is accompanied by changes of expression of many genes that are involved in the cell cycle progression, apoptosis, kinases, and transcription factors upon PA200 depletion. This suggests that PA200 is probably involved in the regulation of transcriptional machinery. Notably, the presence of PA200 in the vicinity of both acetylated and non-acetylated promoter regions supports our hypothesis that PA200 may play a role as a transcription factor or cofactors, but not as proteasome activator that is involved in the degradation of acetylated histones through the BRD-like domain of PA200. The specificity of how this regulation is achieved, and whether PA200 directly binds to DNA or via specific transcription factors requires further investigation.

Flow cytometry and western blot analysis of cell cycle progression support the ChIP-seq data of the enrichment of PA200 on promoter regions of genes involved in cell cycle progression and the possibility that PA200 influences those genes at the transcriptional level. PA200-deficient cells exhibit an increased cell population in the S phase upon oligomycin treatment, compared to vehicle-treated shPA200 cells. In the same context, reports disclosed that the overexpression of Blm10 inhibited cell growth in yeast (Fehlker et al., 2003). Furthermore, the deletion of Blm10 affects the transcription pattern of numerous genes that regulate cell cycle progression (Doherty et al., 2012). Another report has revealed that the PA200-deficient cells are continuously grown at a high rate when extracellular glutamine is limited, while control cells respond by slow growth (Blickwedehl et al., 2012). This data suggests that PA200 plays a crucial role in cell cycle progression either by direct regulation of cell cycle genes, as we showed by ChIP-seq data, or

indirectly by interrupting the cellular metabolism and directing cells to continuous cell cycle as Blickwedehl et al., described.

We also looked at signaling pathways that lead to massive cell death in PA200-deficient cells upon rotenone treatment. It is known that SH-SY5Y cells treated with rotenone activate the JNK/c-Jun pathway leading to cell death (Klintworth et al., 2007; Newhouse et al., 2004). In our study, the loss of PA200 in the SH-SY5Y neuroblastoma cell line leads to strong down-regulation of the *JUN* gene, which is involved in cell death. In our model, c-Jun expression without stress is very low. However, treatment with rotenone leads to induction of the expression of c-Jun and its phosphorylation as a stress response to ensure cell survival. Interestingly, the response to rotenone treatment in shPA200 was significantly lower, compared to rotenone-treated control cells regarding c-Jun protein expression and phosphorylation. This data might explain the massive cell death in PA200-deficient cells upon rotenone treatment. The low expression of c-Jun protein and its phosphorylation in shPA200 upon rotenone treatment reduce the tolerance to extracellular stimuli resulting in increased apoptosis of shPA200 cells. Related to our findings, a report demonstrated that mutations of c-Jun in fibroblasts show enhanced sensitivity to UV and TNF $\alpha$ -induced apoptosis (Wisdom et al., 1999). This data suggested that c-Jun protected cells from apoptosis, while the molecular mechanism by which c-Jun prevents cell apoptosis upon extracellular stimuli is unclear.

Our ChIP-seq data revealed that PA200 is recruited to the promoter region of genes involved in primary metabolic processes. However, these findings needed confirmation by functional assays to reveal the role of PA200 in metabolism. Therefore, we assessed RNA-seq analysis upon stable silencing of PA200 in SH-SY5Y cells and its respective control. RNA-seq data analysis was strongly following ChIP-seq data findings. The RNA-seq has revealed that loss of PA200 leads to an overall transcriptomic change in genes related to apoptosis, metabolism, cell cycle, MAPK signaling pathway, and mitochondrial homeostasis. Similar to our findings, a recent report demonstrated that the PA200 is essential to maintain the transcriptional machinery especially during aging. Furthermore, RNA-seq data analysis from MEF and liver of PA200 knockout mice revealed that PA200 modulates the transcription of genes involved in aging, MAPK signaling, and cell cycle (Chen et al., 2020). In support of the role of PA200 in metabolism and the maintenance of mitochondrial homeostasis, yeast deleted of Blm10 exhibits mitochondrial dysfunction showing

reduction of respiration. Furthermore, this strain is unable to grow on non-fermentable carbon sources, such as glycerol (Tar et al., 2014). Moreover, the expression level of BIm10 increased upon the switch from fermentation to oxidative metabolism (Lopez et al., 2011). In summary, our data suggested that aerobic oxidative phosphorylation might be interrupted by the loss of PA200. These observations in yeast and the results of DEG clustering of RNA-seq data, therefore, pointed us to investigate the metabolic state of cells stably depleted of PA200.

We validated DEGs affected by the depletion of PA200 and found to be involved in metabolism and mitochondrial homeostasis. Seahorse analysis revealed that PA200 cells exhibit defects in mitochondrial activity. Lacking PA200 leads to a significant reduction in the spare respiratory capacity, maximal respiration, and proton leak. Reduction in spare respiratory capacity and maximal respiration indicates that the mitochondria are not able to generate enough energy by oxidative phosphorylation to overcome stress (Desler et al., 2012; Marchetti et al., 2020; Yamamoto et al., 2016). This data shows that loss of PA200 negatively affects oxidative phosphorylation, especially under conditions where cells are in high energy demand. Furthermore, western blot analysis of mitochondrial oxidative phosphorylation complex subunits, in PA200-deficient cells and control cells, show a significant reduction of ETC complexes in shPA200 cells, compared to control cells, especially the CI subunit NDUFB8, which is involved in CI assembly (Vogel et al., 2007). However, the ATP synthase subunit, ATP5E did not change between the two clones, which might explain the similar OCR rate in baseline and ATP production of both clones. The strong reduction of the assembly subunit, NDUFB8 in shPA200 did not affect the ATP production under normal condition and this data is consistent with the finding in a mouse model of AD that shows a reduction in assembly subunit of CI (NDUFB8) without affecting ATP production (Francis et al., 2014). This data suggests that PA200 affects mitochondrial biogenesis and that leads to inefficient mitochondrial function under conditions where cells need high energy. This raised the question of how PA200-deficient cells adapt to mitochondrial dysfunction. The answer primarily appeared in the RNA-seq data. DEGs show that PA200 is a repressor of glycolysis and an activator of negative regulation of glycolysis. As we expected, the glycolytic stress assay revealed that loss of PA200 leads to a significant increase in glycolysis and glycolytic capacity. These data suggest that the interrupted OXPHOS activity in cells stably lacking PA200 drives cells to consume alternative sources of energy, such as glycolysis, to produce more ATP and adapt to

the inefficiency of mitochondrial function. The role of PA200 in the transcriptional machinery is summarized in Figure 32.

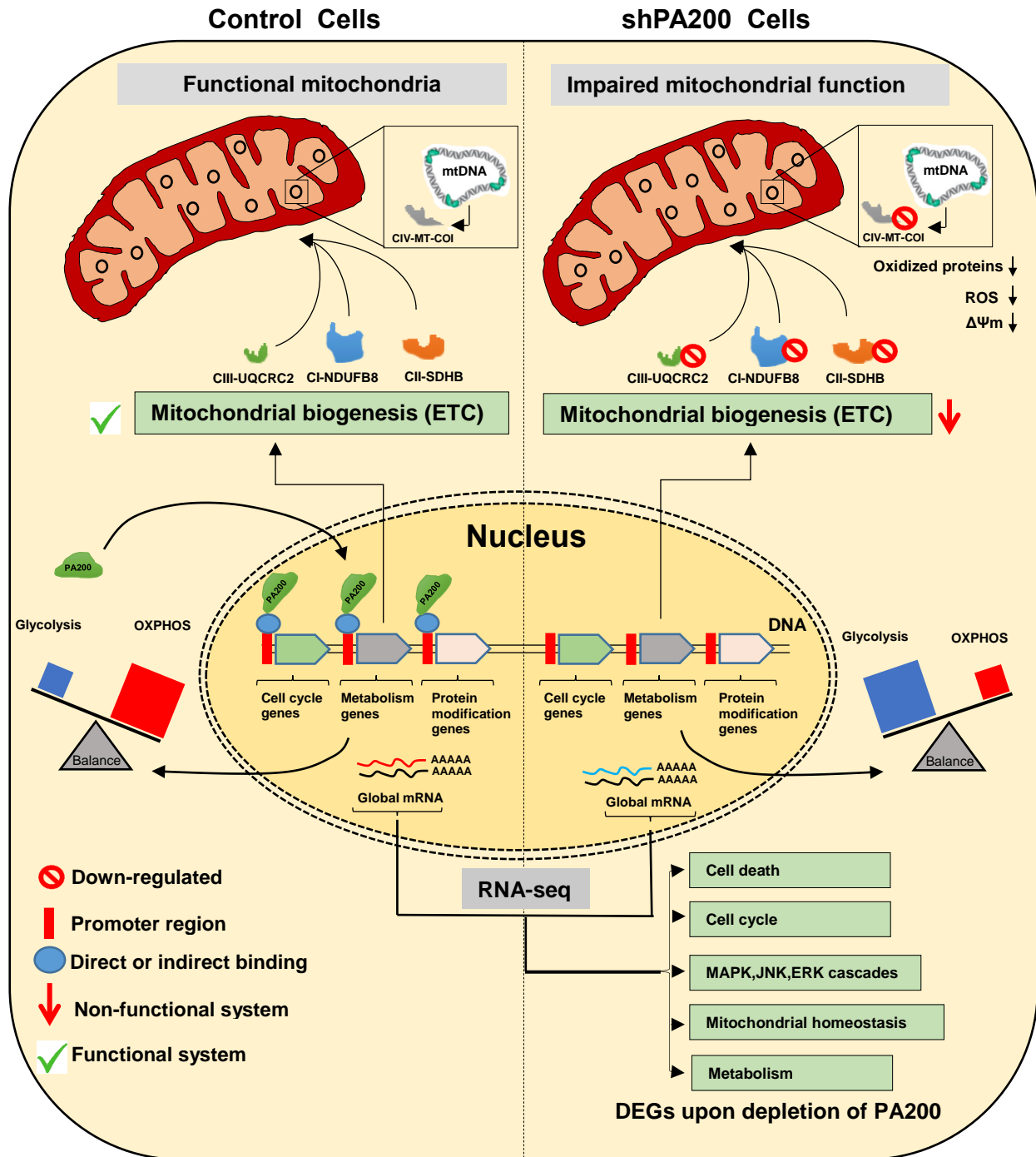


*Figure 32. Representative graphical model summarizing the role of PA200 in the transcriptional machinery.*

The structure of mitochondrial network correlates with the energy status of the cell (Gomes et al., 2011; Jheng et al., 2012; Mitra et al., 2009). We speculated that the impaired mitochondrial activity in PA200-deficient cells has an impact on mitochondrial morphology. Mitochondrial morphology is tightly regulated by proteins with GTPase-activity (Cipolat et al., 2004; Nakamura et al., 2006; Wong et al., 2000). We investigated mitochondrial morphology of PA200-deficient and control cells using Mitotracker Red CMXRos dye by the Opera Phenix HCS system. HCS data analysis revealed that both shPA200 and control cells under physiological conditions did not show any morphological differences in mitochondrial classes, however, when cells were challenged with oligomycin, shPA200 cells exhibited significant increases in long and compact tubular structures. Western blot analysis of key mitochondrial fission and fusion proteins revealed a significant reduction in stress-induced L-OPA1 cleavage in shPA200 cells, compared to control cells. Furthermore, under the same condition OMA1 protease that cleaves L-OPA to S-OPA1 was significantly low in PA200-deficient cells upon oligomycin treatment. This data suggest that the low level of OMA1 protein in shPA200 upon selective mitochondrial stress maintains L-OPA1 isoform and promotes mitochondrial fusion. The role of PA200 in mitochondrial dynamics is summarized in Figure 33.

Our data are also confirmed by a study describing increased glycolysis in mesenchymal cells, which promotes cell survival via Opa1-mediated mitochondrial fusion, regulated by leptin (Yang et al., 2019). Another report has demonstrated that the purposes of mitochondrial fusion are to ensure exchange of metabolites energy restoration, and preventing apoptosis (Gomes et al., 2011; James & Martinou, 2008). Overall, our data suggest that deficiency of PA200 leads to an overall change in the transcriptomic process of relevant genes including metabolism, mitochondrial biogenesis, and homeostasis. Inefficient mitochondrial function in shPA200 cells was counterbalanced by increased glycolysis and elevated mitochondrial fusion upon stress.

During oxidative phosphorylation, ROS are naturally generated from the mitochondria mainly by CI and CIII of the ETC (Harper et al., 2004). The level of ROS is adjusted by an antioxidant mechanism to prevent mitochondrial protein damage and loss of their function. Flow cytometry data shows that loss of PA200 under normal conditions significantly reduces ROS production compared to control cells. However, when cells are treated with oligomycin, ROS are significantly increased in shPA200 cells, compared to vehicle-treated cells, while the level of ROS in control

cells slightly increased, compared to vehicle-treated cells. Low ROS in shPA200 cells under normal conditions might be a result of the reduction of mitochondrial ETC biogenesis, especially the assembly subunit NDUFB8 that contributes directly to oligomerization of CI (Wu et al., 2016). Reports have demonstrated that the decrease in CI activity leads to an increase in ROS production (Verkaart et al., 2007). On the contrary, inhibition of CI assembly by repressing one of the assembly subunits, such as NDUFS3, assembly factor NDUF1, or NDUF13 leads to a reduction in ROS production (Huang et al., 2007; Kamiński et al., 2007). Furthermore, studies demonstrated that treatment of cardiovascular diseases with lovastatin indirectly reduces the protein level of PA200 which is accompanied by minimizing ROS-induced damage in endothelial cells (Wang et al., 2017). Significant increases in ROS production in PA200 depleted cells, but not control cells, upon oligomycin treatment are indicative of more damaged mitochondria in shPA200 cells.

At physiological conditions, the mitochondrial ETC complexes are exposed to ROS-induced ETC protein carbonylation, and progressive mitochondrial dysfunction during normal aging (Choi et al., 2008). We measured low ROS production in shPA200 under normal conditions. Oxyblot assay revealed significantly lower protein oxidation in shPA200 cells compared to control cells. Protein oxidation in PA200-depleted cells treated with oligomycin was higher compared to oligomycin-treated control cells. These data are consistent with ROS status in both cells under the indicated conditions. Together, these findings suggest that loss of PA200 negatively influences ROS production and protein oxidation as an adaptive mechanism of mitochondrial dysfunction preventing ROS-induced ETC oxidation. However, when shPA200 cells are challenged with selective mitochondrial inhibitors, cells were not able to control ROS-induced protein oxidation. One of the explanations might be the interrupted ETC biogenesis in PA200-depleted cells since ETC is the main source of ROS generation. In summary, our findings support a model in which PA200 potentially regulates cellular homeostasis at the transcriptional level and suggest a role for PA200 in the regulation of metabolic changes in response to selective inhibition of ATP synthase in an *in vitro* cellular model.

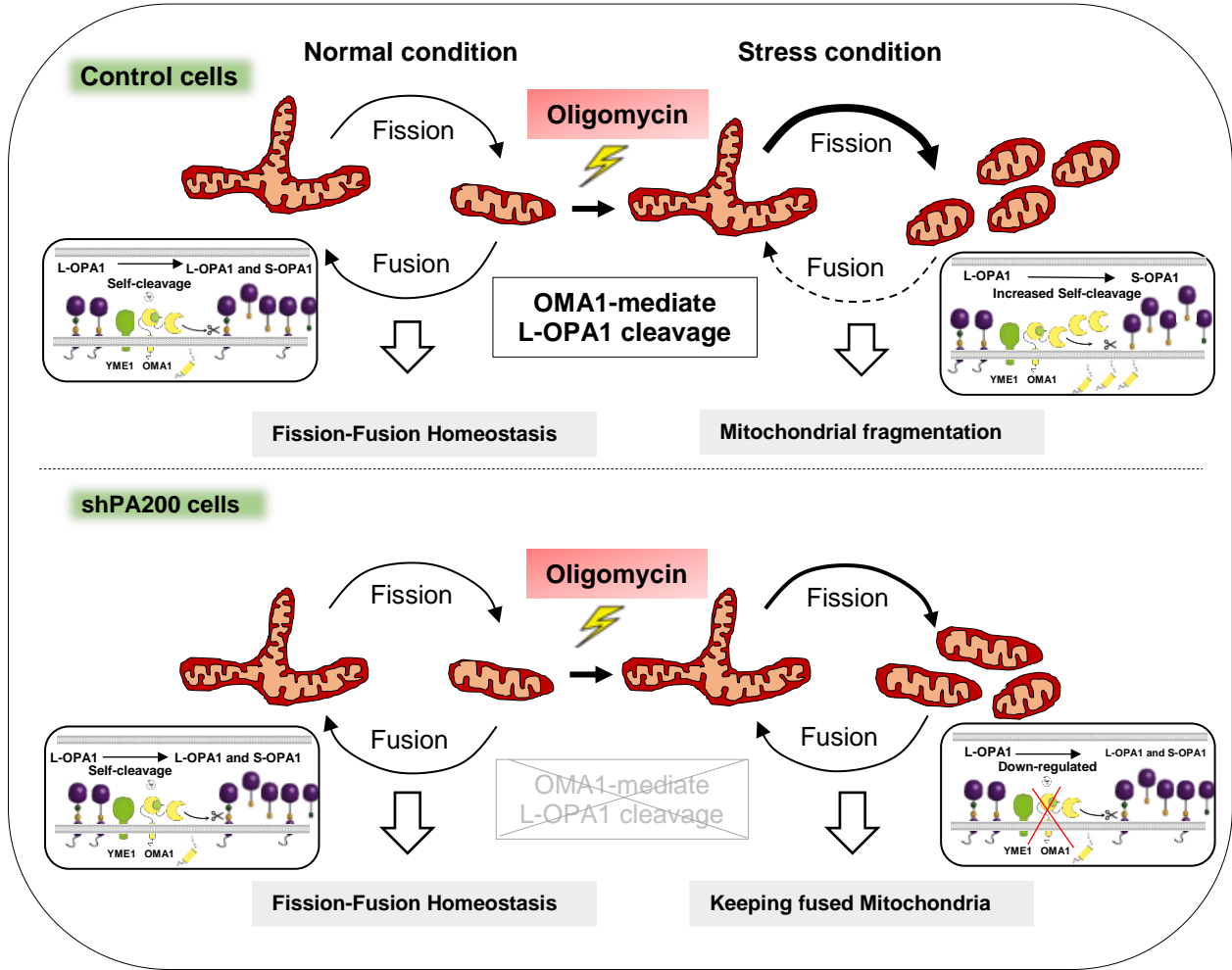


*Figure 33. Graphical model summarizing the role of PA200 in mitochondrial dynamics and metabolic homeostasis upon stress.*

## SUMMARY

The conserved Bln10/PA200 family belongs to the proteasome activators. PA200 alternatively binds to the proteasome core particle (CP) and facilitates peptide degradation in an ATP and ubiquitin-independent manner. PA200 has several important physiological roles, such as DNA repair, spermatogenesis, and aging. However, the exact molecular mechanisms behind these functions are not clear. In the present study, we investigated new promising functions of PA200 and the consequences of PA200 stable depletion at the normal condition and upon mitochondrial stress. First, we investigated the role of PA200 on cell viability and apoptosis with or without mitochondrial stress. We found that PA200 deficient cells are more sensitive to rotenone but not oligomycin and antimycin A treatment. Furthermore, PA200-deficient cells exhibit low expression of c-Jun upon rotenone treatment, thereby; reducing the capacity of PA200 depleted cells to tolerate the rotenone-induced cell death. Second, we performed ChIP followed by ChIP-sequencing analysis to study the possible role of PA200 as a transcription factor or cofactor that regulates the transcription machinery. We demonstrated that PA200 is a chromatin component in SH-SY5Y neuroblastoma cells and it bound to promoter regions of genes involved in the cell cycle, metabolism, and protein modification. Third, we performed an RNA sequencing study. We found that the loss of PA200 has an overall change in the transcriptomic profile of the SH-SY5Y cell line. Functional annotation analysis of differential gene expression (DGEs) revealed that PA200 has a crucial role in cellular functions including apoptosis, metabolism, cell cycle, MAPK signaling pathway, and mitochondrial homeostasis. Furthermore, the extracellular flux analysis of shPA200 and control cells indicates mitochondrial dysfunction and a significant increase in glycolysis in PA200 deficient cells. Further investigations of mitochondrial mass show a significant reduction in mitochondrial ETC biogenesis upon loss of PA200. Finally, mitochondrial morphology analysis shows significant increase in fused mitochondria in shPA200 cells, compared to control cells upon oligomycin treatment due to maintenance of L-OPA1 isoforms. Our new findings provide more information regarding the role of PA200 in eukaryotic cells. The new disclosed functions of PA200 in the maintenance of mitochondrial integrity and cell survival may contribute to the development of new therapy for many diseases related to mitochondrial dysfunction including but not limited to neurodegenerative disease, cardiovascular disease, and aging.

## **KEYWORDS**

Proteasome activator PA200/Blm10 family

Mitochondrial bioenergetics

Mitochondrial dynamics

L-OPA1

OMA1

Mitochondrial inhibitors (rotenone, oligomycin, and antimycin A)

Metabolism

Glycolysis

Cell survival

JNK/c-Jun signaling pathway

Transcriptional machinery

Disease-related to mitochondrial dysfunction

## ACKNOWLEDGMENT

*I would like to thank God for being able to complete my Ph.D. studies with success.*

I am very grateful to my supervisor Dr. Tar Krisztina for guiding and supporting me during the years of my Ph.D. education. I would like to thank the head of Medical Chemistry Department Professor László Virág for the opportunity to work in the Department of Medical Chemistry at the University of Debrecen. I would like to thank Dr. Frank Batista, Pal Boto, Zsolt Regdon, Dr. Agnieszka Robaszkiewicz, Azzam Aladdin, Mónika Szenyikiv, and Rita Czinege for their contribution to my research work

I am grateful to Prof. Viktor Dombrádi and Dr. Karen Uray for constructive discussions. I highly appreciate the professional technical assistance of Andrea Tankáné Farkas, Mihályné Herbály, Erika Gulyás, Dávid Varga, and Kitti Barta. Special thanks to our lab group members Azzam Aladdin and Marvi Ghani for support and sharing work and daily lab life. I am grateful to Dr. Máté Demény, Dr. Endre Kókai, Dr. Katalin Kovács, Zsolt Regdon, and Emese Tóth for the help when I had struggle in my work. Many thanks to all members of Prof. László Virág laboratory for help and sharing technical skills; Dr. Edina Bakondi, Dr. Csaba Hegedús, Dr. Zsuzsanna Polgár, Isotta Sturniolo, Eliza Guti, Zoltán Hajnády, Alexandra Kiss, and Máté Nagy-Pénzes.

I would like to thank my lovely parents for their patience and encouragement all time. Special thanks to my dear wife 'Ibtissem' for her love and support. My sincere and grateful thanks to my little princess Amira. Thanks to my dear brothers: Nadji, Abdallah, Akram, and Saif. I am grateful to my sister Soumia and her sweet family for their encouragement and support.

I would like to thank the Algerian government and the Tempus Public Foundation (TPF) for the funding and financial support.

This Work was supported by the University of Debrecen, Debrecen, Hungary by a Bridging Fund (1G3D BKJ0 BFTK 247), by a 'seedfund' for Dr. Tar Krisztina by the University of Debrecen, Debrecen, Hungary (5N5XBKJ0TARK320), and by the Tempus Foundation, Stipendium Hungaricum (1Q4DBKX5STIP321). Dr Tar Krisztina was a recipient of Lajos Szodoray Fellowship by the University of Debrecen, Debrecen, Hungary.

## REFERENCES

- A. Sazonova, Margarita.V. Sinyov, Vasily.Anastasia I. Ryzhkova Elena V. Galitsyna, Zukhra B. Khasanova, Anton Yu Postnov,Elena I. Yarygina, Alexander N. Orekhov, and I. A. S. (2017). “Role of mitochondrial genome mutations in pathogenesis of carotid atherosclerosis.” *Oxidative Medicine and Cellular Longevity*, 1017. <https://doi.org/10.1155/2018/4575821>
- Abada, A., & Elazar, Z. (2014). Getting ready for building: signaling and autophagosome biogenesis. *EMBO Reports*, 15(8), 839–852. <https://doi.org/10.15252/embr.201439076>
- Afgan, E., Baker, D., Batut, B., Van Den Beek, M., Bouvier, D., Ech, M., Chilton, J., Clements, D., Coraor, N., Grüning, B. A., Guerler, A., Hillman-Jackson, J., Hiltemann, S., Jalili, V., Rasche, H., Soranzo, N., Goecks, J., Taylor, J., Nekrutenko, A., & Blankenberg, D. (2018). The Galaxy platform for accessible, reproducible and collaborative biomedical analyses: 2018 update. *Nucleic Acids Research*, 46(W1), W537–W544. <https://doi.org/10.1093/nar/gky379>
- Ahn, C. S., & Metallo, C. M. (2015). Mitochondria as biosynthetic factories for cancer proliferation. *Cancer and Metabolism*, 3(1), 1–10. <https://doi.org/10.1186/s40170-015-0128-2>
- Aladdin, A., Yao, Y., Yang, C., Kahlert, G., Ghani, M., Király, N., Boratkó, A., Uray, K., Dittmar, G., & Tar, K. (2020). The proteasome activators Blm10/PA200 enhance the proteasomal degradation of N-terminal huntingtin. *Biomolecules*, 10(11), 1–32. <https://doi.org/10.3390/biom10111581>
- Altmann, K., & Westermann, B. (2005). Role of Essential Genes in Mitochondrial Morphogenesis in *Saccharomyces cerevisiae*. *Molecular Biology of the Cell*, 16(November), 5410–5417. <https://doi.org/10.1091/mbc.e05-07-0678>
- Anand, R., Langer, T., & Baker, M. J. (2013). Proteolytic control of mitochondrial function and morphogenesis. *Biochimica et Biophysica Acta - Molecular Cell Research*, 1833(1), 195–204. <https://doi.org/10.1016/j.bbamcr.2012.06.025>
- Anand, R., Wai, T., Baker, M. J., Kladt, N., Schauss, A. C., Rugarli, E., & Langer, T. (2014). The i-AAA protease YME1L and OMA1 cleave OPA1 to balance mitochondrial fusion and fission. *Journal of Cell Biology*, 204(6), 919–929. <https://doi.org/10.1083/jcb.201308006>
- Arias, E., & Cuervo, A. M. (2011). Chaperone-mediated autophagy in protein quality control. *Current Opinion in Cell Biology*, 23(2), 184–189. <https://doi.org/10.1016/j.ceb.2010.10.009>
- Azzu, V., & Brand, M. D. (2010). Degradation of an intramitochondrial protein by the cytosolic proteasome (Journal of Cell Science 123, (578-585)). *Journal of Cell Science*, 123(20), 3616. <https://doi.org/10.1242/jcs.081976>
- Azzu, V., Mookerjee, S. A., & Brand, M. D. (2010). Rapid turnover of mitochondrial uncoupling protein 3. *Biochemical Journal*, 426(1), 13–17. <https://doi.org/10.1042/BJ20091321>
- Baker, M. J., Frazier, A. E., Gulbis, J. M., & Ryan, M. T. (2007). Mitochondrial protein-import machinery: correlating structure with function. *Trends in Cell Biology*, 17(9), 456–464. <https://doi.org/10.1016/j.tcb.2007.07.010>

- Baker, M. J., Lampe, P. A., Stojanovski, D., Korwitz, A., Anand, R., Tatsuta, T., & Langer, T. (2014). Stress-induced OMA1 activation and autocatalytic turnover regulate OPA1-dependent mitochondrial dynamics. *EMBO Journal*, *33*(6), 578–593. <https://doi.org/10.1002/embj.201386474>
- Barton, L. F., Cruz, M., Rangwala, R., Deepe, G. S., & Monaco, J. J. (2002). Regulation of Immunoproteasome Subunit Expression In Vivo Following Pathogenic Fungal Infection. *The Journal of Immunology*, *169*(6), 3046–3052. <https://doi.org/10.4049/jimmunol.169.6.3046>
- Bassing, C. H., Swat, W., & Alt, F. W. (2002). The mechanism and regulation of chromosomal V(D)J recombination. *Cell*, *109*(2 SUPPL. 1), 45–55. [https://doi.org/10.1016/S0092-8674\(02\)00675-X](https://doi.org/10.1016/S0092-8674(02)00675-X)
- Baugh, J. M., Viktorova, E. G., & Pilipenko, E. V. (2009). Proteasomes Can Degrade a Significant Proportion of Cellular Proteins Independent of Ubiquitination. *Journal of Molecular Biology*, *386*(3), 814–827. <https://doi.org/10.1016/j.jmb.2008.12.081>
- Bejarano, E., & Cuervo, A. M. (2010). Chaperone-mediated autophagy. *Proceedings of the American Thoracic Society*, *7*(1), 29–39. <https://doi.org/10.1513/pats.200909-102JS>
- Bereiter-Hahn, J. (1990). Behavior of Mitochondria in the Living Cell. *International Review of Cytology*, *122*(C), 1–63. [https://doi.org/10.1016/S0074-7696\(08\)61205-X](https://doi.org/10.1016/S0074-7696(08)61205-X)
- Betarbet, R., Sherer, T. B., Mackenzie, G., Garcia-osuna, M., Panov, A. V., & Greenamyre, J. T. (2000). Chronic systemic pesticide exposure produces PD symptoms Betarbet. *Nature Neuroscience*, *26*, 1301–1306. <https://doi.org/10.1038/81834>
- Blankenberg, D., Gordon, A., Von Kuster, G., Coraor, N., Taylor, J., Nekrutenko, A., & Team, G. (2010). Manipulation of FASTQ data with galaxy. *Bioinformatics*, *26*(14), 1783–1785. <https://doi.org/10.1093/bioinformatics/btq281>
- Blickwedehl, J., Agarwal, M., Seong, C., Pandita, R. K., Melendy, T., Sung, P., Pandita, T. K., & Bangia, N. (2008). Role for proteasome activator PA200 and postglutamyl proteasome activity in genomic stability. *Proceedings of the National Academy of Sciences of the United States of America*, *105*(42), 16165–16170. <https://doi.org/10.1073/pnas.0803145105>
- Blickwedehl, J., McEvoy, S., Wong, I., Kousis, P., Clements, J., Elliott, R., Cresswell, P., Liang, P., & Bangia, N. (2007). Proteasomes and proteasome activator 200 kDa (PA200) accumulate on chromatin in response to ionizing radiation. *Radiation Research*, *167*(6), 663–674. <https://doi.org/10.1667/RR0690.1>
- Blickwedehl, J., Olejniczak, S., Cummings, R., Sarvaiya, N., Mantilla, A., Chanan-Khan, A., Pandita, T. K., Schmidt, M., Thompson, C. B., & Bangia, N. (2012). The proteasome activator PA200 regulates tumor cell responsiveness to glutamine and resistance to ionizing radiation. *Molecular Cancer Research*, *10*(7), 937–944. <https://doi.org/10.1158/1541-7786.MCR-11-0493-T>
- Bochtler, M., Ditzel, L., Groll, M., Hartmann, C., & Huber, R. (1999). The proteasome. *Annual Review of Biophysics and Biomolecular Structure*, *28*, 295–317. <https://doi.org/10.1146/annurev.biophys.28.1.295>
- Book, A. J., Gladman, N. P., Lee, S. S., Scalf, M., Smith, L. M., & Vierstra, R. D. (2010). Affinity

- purification of the Arabidopsis 26 S proteasome reveals a diverse array of plant proteolytic complexes. *Journal of Biological Chemistry*, 285(33), 25554–25569. <https://doi.org/10.1074/jbc.M110.136622>
- Bragoszewski, P., Gornicka, A., Sztolsztener, M. E., & Chacinska, A. (2013). The Ubiquitin-Proteasome System Regulates Mitochondrial Intermembrane Space Proteins. *Molecular and Cellular Biology*, 33(11), 2136–2148. <https://doi.org/10.1128/mcb.01579-12>
- Burté, F., Carelli, V., Chinnery, P. F., & Yu-Wai-Man, P. (2015). Disturbed mitochondrial dynamics and neurodegenerative disorders. *Nature Reviews Neurology*, 11(1), 11–24. <https://doi.org/10.1038/nrneuro.2014.228>
- Calkins, M. J., Manczak, M., Mao, P., Shirendeb, U., & Reddy, P. H. (2011). Impaired mitochondrial biogenesis, defective axonal transport of mitochondria, abnormal mitochondrial dynamics and synaptic degeneration in a mouse model of Alzheimer’s disease. *Human Molecular Genetics*, 20(23), 4515–4529. <https://doi.org/10.1093/hmg/ddr381>
- Campo, M. L., Kinnally, K. W., & Tedeschi, H. (1992). The effect of antimycin A on mouse liver inner mitochondrial membrane channel activity. *Journal of Biological Chemistry*, 267(12), 8123–8127. [https://doi.org/10.1016/s0021-9258\(18\)42415-5](https://doi.org/10.1016/s0021-9258(18)42415-5)
- Campos, E. I., & Reinberg, D. (2009). Histones: Annotating chromatin. *Annual Review of Genetics*, 43, 559–599. <https://doi.org/10.1146/annurev.genet.032608.103928>
- Carreras, M. C., Franco, M. C., Peralta, J. G., & Poderoso, J. J. (2004). Nitric oxide, complex I, and the modulation of mitochondrial reactive species in biology and disease. *Molecular Aspects of Medicine*, 25(1–2), 125–139. <https://doi.org/10.1016/j.mam.2004.02.014>
- Chaitanya, G. V., Alexander, J. S., & Babu, P. P. (2010). PARP-1 cleavage fragments: Signatures of cell-death proteases in neurodegeneration. *Cell Communication and Signaling*, 8, 1–11. <https://doi.org/10.1186/1478-811X-8-31>
- Chance, B., Sies, H., & Boveris, A. (1979). Hydroperoxide metabolism in mammalian organs. *Physiological Reviews*, 59(3), 527–605. <https://doi.org/10.1152/physrev.1979.59.3.527>
- Chang, C. J., Yin, P. H., Yang, D. M., Wang, C. H., Hung, W. Y., Chi, C. W., Wei, Y. H., & Lee, H. C. (2009). Mitochondrial dysfunction-induced amphiregulin upregulation mediates chemoresistance and cell migration in HepG2 cells. *Cellular and Molecular Life Sciences*, 66(10), 1755–1765. <https://doi.org/10.1007/s00018-009-8767-5>
- Chatenay-Lapointe, M., & Shadel, G. S. (2010). Stressed-out mitochondria get MAD. *Cell Metabolism*, 12(6), 559–560. <https://doi.org/10.1016/j.cmet.2010.11.018>
- Chaudhuri, J., & Alt, F. W. (2004). Class-switch recombination: Interplay of transcription, DNA deamination and DNA repair. *Nature Reviews Immunology*, 4(7), 541–552. <https://doi.org/10.1038/nri1395>
- Chen, L. B., Ma, S., Jiang, T. X., & Qiu, X. B. (2020). Transcriptional upregulation of proteasome activator Blm10 antagonizes cellular aging. *Biochemical and Biophysical Research Communications*, 532(2), 211–218. <https://doi.org/10.1016/j.bbrc.2020.07.003>
- Chen, H., Detmer, S. A., Ewald, A. J., Griffin, E. E., Fraser, S. E., & Chan, D. C. (2003). Mitofusins

- Mfn1 and Mfn2 coordinately regulate mitochondrial fusion and are essential for embryonic development. *Journal of Cell Biology*, 160(2), 189–200. <https://doi.org/10.1083/jcb.200211046>
- Choi, W. S., Kruse, S. E., Palmiter, R. D., & Xia, Z. (2008). Mitochondrial complex I inhibition is not required for dopaminergic neuron death induced by rotenone, MPP+, or paraquat. *Proceedings of the National Academy of Sciences of the United States of America*, 105(39), 15136–15141. <https://doi.org/10.1073/pnas.0807581105>
- Chrissobolis, S., Miller, A. A., Drummond, G. R., Kemp-Harper, B. K., & Sobey, C. G. (2011). Oxidative stress and endothelial dysfunction in cerebrovascular disease. *Frontiers in Bioscience*, 16(5), 1733–1745. <https://doi.org/10.2741/3816>
- Ciechanover, A. (2005). Proteolysis: From the lysosome to ubiquitin and the proteasome. *Nature Reviews Molecular Cell Biology*, 6(1), 79–87. <https://doi.org/10.1038/nrm1552>
- Cilenti, L., Ambivero, C. T., Ward, N., Alnemri, E. S., Germain, D., & Zervos, A. S. (2014). Inactivation of Omi/HtrA2 protease leads to the deregulation of mitochondrial Mulan E3 ubiquitin ligase and increased mitophagy. *Biochimica et Biophysica Acta - Molecular Cell Research*, 1843(7), 1295–1307. <https://doi.org/10.1016/j.bbamcr.2014.03.027>
- Cipolat, S., De Brito, O. M., Dal Zilio, B., & Scorrano, L. (2004). OPA1 requires mitofusin 1 to promote mitochondrial fusion. *Proceedings of the National Academy of Sciences of the United States of America*, 101(45), 15927–15932. <https://doi.org/10.1073/pnas.0407043101>
- Cuervo, A. M. (2011). Chaperone-mediated autophagy: Dice’s “wild” idea about lysosomal selectivity. *Nature Reviews Molecular Cell Biology*, 12(8), 535–541. <https://doi.org/10.1038/nrm3150>
- D. Voges, P. Zwickl, and W. B. (1999). The 26s proteasome: a molecular machine designed for controlled proteolysis. 68, 1015–1068. <https://doi.org/10.1146/annurev.biochem.68.1.1015>
- Dahlmann, B. (2016). Mammalian proteasome subtypes: Their diversity in structure and function. *Archives of Biochemistry and Biophysics*, 591, 132–140. <https://doi.org/10.1016/j.abb.2015.12.012>
- Dalle - Donne, I., Aldini, G., Carini, M., Colombo, R., Rossi, R., & Milzani, A. (2006). Protein carbonylation, cellular dysfunction, and disease progression. <https://doi.org/10.1111/j.1582-4934.2006.tb00407.x>
- Dasgupta, S., Yang, C., Castro, L. M., Tashima, A. K., Ferro, E. S., Moir, R. D., Willis, I. M., & Fricker, L. D. (2016). Analysis of the yeast peptidome and comparison with the human peptidome. *PLoS ONE*, 11(9), 1–26. <https://doi.org/10.1371/journal.pone.0163312>
- Davis, R. J. (1998). Signal transduction by the JNK group of MAP kinases. *Scientist*, 12(11), 13–14. [https://doi.org/10.1016/S0092-8674\(00\)00116-1](https://doi.org/10.1016/S0092-8674(00)00116-1)
- De Brito, O. M., & Scorrano, L. (2008). Mitofusin 2 tethers endoplasmic reticulum to mitochondria. *Nature*, 456(7222), 605–610. <https://doi.org/10.1038/nature07534>

- Deng, Y. T., Huang, H. C., & Lin, J. K. (2010). Rotenone induces apoptosis in MCF-7 human breast cancer cell-mediated ROS through JNK and p38 signaling. *Molecular Carcinogenesis*, 49(2), 141–151. <https://doi.org/10.1002/mc.20583>
- Desler, C., Hansen, T. L., Frederiksen, J. B., Marcker, M. L., Singh, K. K., & Juel Rasmussen, L. (2012). Is there a link between mitochondrial reserve respiratory capacity and aging? *Journal of Aging Research*, 2012. <https://doi.org/10.1155/2012/192503>
- Doelling, J. H., Walker, J. M., Friedman, E. M., Thompson, A. R., & Vierstra, R. D. (2002). The APG8/12-activating enzyme APG7 is required for proper nutrient recycling and senescence in *Arabidopsis thaliana*. *Journal of Biological Chemistry*, 277(36), 33105–33114. <https://doi.org/10.1074/jbc.M204630200>
- Doherty, K. M., Pride, L. D., Lukose, J., Snydsman, B. E., Charles, R., Pramanik, A., Muller, E. G., Botstein, D., & Moore, C. W. (2012). Loss of a 20S proteasome activator in *Saccharomyces cerevisiae* downregulates genes important for genomic integrity, increases DNA damage, and selectively sensitizes cells to agents with diverse mechanisms of action. *G3: Genes, Genomes, Genetics*, 2(8), 943–959. <https://doi.org/10.1534/g3.112.003376>
- Doherty, K., Pramanik, A., Pride, L., Lukose, J., & Moore, C. W. (2004). Expression of the expanded YFL007w ORF and assignment of the gene name BLM10. *Yeast*, 21(12), 1021–1023. <https://doi.org/10.1002/yea.1146>
- Dubiel, W., Pratt, G., Ferrell, K., & Rechsteiner, M. (1992). Purification of an 11 S regulator of the multicatalytic protease. *Journal of Biological Chemistry*, 267(31), 22369–22377. [https://doi.org/10.1016/S0021-9258\(18\)41681-X](https://doi.org/10.1016/S0021-9258(18)41681-X)
- Edelmann, W., Yang, K., Umar, A., Heyer, J., Lau, K., Fan, K., Liedtke, W., & Cohen, P. E. Kane, M F., Lipford, JR., Yu, N., Crouse, G F., W Pollard, J., Kunkel, T., Lipkin, M., Kolodner, R., & Kucherlapati, R. (1997). Mutation in the Mismatch Repair Gene Msh6 Causes Cancer Susceptibility. *Cell*, 91(8), 467–477. [https://doi.org/10.1016/S0092-8674\(00\)80433-X](https://doi.org/10.1016/S0092-8674(00)80433-X)
- Elsasser, S., Chandler-Mitilello, D., Müller, B., Hanna, J., & Finley, D. (2004). Rad23 and Rpn10 serve as alternate ubiquitin receptors for the proteasome. *Journal of Biological Chemistry*, 279(26), 26817–26822. <https://doi.org/10.1074/jbc.M404020200>
- Enenkel, C. (2014). Proteasome dynamics. *Biochimica et Biophysica Acta - Molecular Cell Research*, 1843(1), 39–46. <https://doi.org/10.1016/j.bbamcr.2013.03.023>
- Epple, U. D., Suriapranata, I., Eskelinen, E. L., & Thumm, M. (2001). Aut5/Cvt17p, a putative lipase essential for disintegration of autophagic bodies inside the vacuole. *Journal of Bacteriology*, 183(20), 5942–5955. <https://doi.org/10.1128/JB.183.20.5942-5955.2001>
- Fehlker, M., Wendler, P., Lehmann, A., & Enenkel, C. (2003). Blm3 is part of nascent proteasomes and is involved in a late stage of nuclear proteasome assembly. *EMBO Reports*, 4(10), 959–963. <https://doi.org/10.1038/sj.embor.embor938>
- Finley, D. (2009). Recognition and processing of ubiquitin-protein conjugates by the proteasome. *Annual Review of Biochemistry*, 78, 477–513. <https://doi.org/10.1146/annurev.biochem.78.081507.101607>

- Finley, D., Chen, X., & Walters, K. J. (2016). Gates, Channels, and Switches: Elements of the Proteasome Machine. *Trends Biochem Sci.* 41(1), 77–93. <https://doi.org/10.1016/j.tibs.2015.10.009>.
- Förster, A., Whitby, F. G., & Hill, C. P. (2003). The pore of activated 20S proteasomes has an ordered 7-fold symmetric conformation. *EMBO Journal*, 22(17), 4356–4364. <https://doi.org/10.1093/emboj/cdg436>
- Francis, B. M., Yang, J., Song, B. J., Gupta, S., Maj, M., Bazinet, R. P., Robinson, B., & Mount, H. T. J. (2014). Reduced levels of mitochondrial complex I subunit NDUFB8 and linked complex I + III oxidoreductase activity in the TgCRND8 mouse model of Alzheimer's disease. *Journal of Alzheimer's Disease*, 39(2), 347–355. <https://doi.org/10.3233/JAD-131499>
- Friedman, J. R., Lackner, L. L., West, M., DiBenedetto, J. R., Nunnari, J., & Voeltz, G. K. (2011). ER tubules mark sites of mitochondrial division. *Science*, 334(6054), 358–362. <https://doi.org/10.1126/science.1207385>
- Gaczynska, M., Rock, K. L., & Goldberg, A. L. (1993).  $\gamma$ -Interferon and expression of MHC genes regulate peptide hydrolysis by proteasomes. *Nature*, 365(6443), 264–267. <https://doi.org/10.1038/365264a0>
- Galluzzi, L., Baehrecke, E. H., Ballabio, A., Boya, P., Bravo-San Pedro, J. M., Cecconi, F., Choi, A. M., Chu, C. T., Codogno, P., Colombo, M. I., Cuervo, A. M., Debnath, J., Deretic, V., Dikic, I., Eskelinen, E., Fimia, G. M., Fulda, S., Gewirtz, D. A., Green, D. R., ... Kroemer, G. (2017). Molecular definitions of autophagy and related processes. *The EMBO Journal*, 36(13), 1811–1836. <https://doi.org/10.15252/embj.201796697>
- Gaucher, J., Reynoird, N., Montellier, E., Boussouar, F., Rousseaux, S., & Khochbin, S. (2010). From meiosis to postmeiotic events: The secrets of histone disappearance. *FEBS Journal*, 277(3), 599–604. <https://doi.org/10.1111/j.1742-4658.2009.07504.x>
- Giannoccaro, M. P., La Morgia, C., Rizzo, G., & Carelli, V. (2017). Mitochondrial DNA and primary mitochondrial dysfunction in Parkinson's disease. *Movement Disorders*, 32(3), 346–363. <https://doi.org/10.1002/mds.26966>
- Glick, D., Barth, S., & Macleod, K. F. (2010). Autophagy: Cellular and molecular mechanisms. *Journal of Pathology*, 221(1), 3–12. <https://doi.org/10.1002/path.2697>
- Glickman, M. H., Rubin, D. M., Coux, O., Wefes, I., Pfeifer, G., Cjeka, Z., Baumeister, W., Fried, V. A., & Finley, D. (1998). A subcomplex of the proteasome regulatory particle required for ubiquitin-conjugate degradation and related to the COP9-signalosome and eIF3. *Cell*, 94(5), 615–623. [https://doi.org/10.1016/S0092-8674\(00\)81603-7](https://doi.org/10.1016/S0092-8674(00)81603-7)
- Gomes, L. C., Benedetto, G. Di, & Scorrano, L. (2011). During autophagy mitochondria elongate, are spared from degradation and sustain cell viability. *Nature Cell Biology*, 13(5), 589–598. <https://doi.org/10.1038/ncb2220>
- Gomes, A. V., Zong, C., Edmondson, R. D., Li, X., Stefani, E., Zhang, J., Jones, R. C., Thyparambil, S., Wang, G. W., Qiao, X., Bardag-Gorce, F., & Ping, P. (2006). Mapping the murine cardiac 26S proteasome complexes. *Circulation Research*, 99(4), 362–371. <https://doi.org/10.1161/01.RES.0000237386.98506.f7>

- Green, K., Brand, M. D., & Murphy, M. P. (2004). Prevention of Mitochondrial Oxidative Damage as a Therapeutic Strategy in Diabetes. *Diabetes*, 53(February), 1-9. <https://doi.org/10.2337/diabetes.53.2007.S110>
- Groettrup, M., Kirk, C. J., & Basler, M. (2010). Proteasomes in immune cells: More than peptide producers? *Nature Reviews Immunology*, 10(1), 73–78. <https://doi.org/10.1038/nri2687>
- Groll, M., Bajorek, M., Köhler, A., Moroder, L., Rubin, D. M., Huber, R., Glickman, M. H., & Finley, D. (2000). A gated channel into the proteasome core particle. *Nature Structural Biology*, 7(11), 1062–1067. <https://doi.org/10.1038/80992>
- Groll, M., Ditzel, L., Lowe, J., Stock, D., Bochtler, M., Bartunik, H. D., & Huber, R. (1997). Structure of 20S proteasome from yeast at 2.4 Å resolution. *Nature*, 386(April), 463–471. <https://www-nature-com.er.lib.k-state.edu/articles/386463a0.pdf>
- Gu, M., Cooper, J. M., Taanman, J. W., & Schapira, A. H. V. (1998). Mitochondrial DNA transmission of the mitochondrial defect in Parkinson's disease. *Annals of Neurology*, 44(2), 177–186. <https://doi.org/10.1002/ana.410440207>
- Guan, H., Wang, Y., Yu, T., Huang, Y., Li, M., Saeed, A. F. U. H., Perculija, V., Li, D., Xiao, J., Wang, D., Zhu, P., & Ouyang, S. (2020). Cryo-EM structures of the human PA200 and PA200-20S complex reveal regulation of proteasome gate opening and two PA200 apertures. *PLoS Biology*, 18(3), 1–24. <https://doi.org/10.1371/journal.pbio.3000654>
- Gunter, T. E., Yule, D. I., Gunter, K. K., Eliseev, R. A., & Salter, J. D. (2004). Calcium and mitochondria. *FEBS Letters*, 567(1), 96–102. <https://doi.org/10.1016/j.febslet.2004.03.071>
- Gutman, M., Thomas P. Singer, John E. Casida, (1969). *Role of multiple binding sites in the inhibition of NADH oxidase by piericidin and rotenone*, 34(4), 615–622.
- Han, Y. H., Kim, S. H., Kim, S. Z., & Park, W. H. (2008). Intracellular GSH levels rather than ROS levels are tightly related to AMA-induced HeLa cell death. *Chemico-Biological Interactions*, 171(1), 67–78. <https://doi.org/10.1016/j.cbi.2007.08.011>
- Han, S. Y., Jeong, Y. J., Choi, Y., Hwang, S. K., Bae, Y. S., & Chang, Y. C. (2018). Mitochondrial dysfunction induces the invasive phenotype, and cell migration and invasion, through the induction of AKT and AMPK pathways in lung cancer cells. *International Journal of Molecular Medicine*, 42(3), 1644–1652. <https://doi.org/10.3892/ijmm.2018.3733>
- Hao, W., Chang, C. P. B., Tsao, C. C., & Xu, J. (2010). Oligomycin-induced bioenergetic adaptation in cancer cells with heterogeneous bioenergetic organization. *Journal of Biological Chemistry*, 285(17), 12647–12654. <https://doi.org/10.1074/jbc.M109.084194>
- Harper, M. E., Bevilacqua, L., Hagopian, K., Weindruch, R., & Ramsey, J. J. (2004). Ageing, oxidative stress, and mitochondrial uncoupling. *Acta Physiologica Scandinavica*, 182(4), 321–331. <https://doi.org/10.1111/j.1365-201X.2004.01370.x>
- Hatefi, Y. (1985). The mitochondrial electron transport and oxidative phosphorylation system. *Ann. Rev. Biochem.* 54. 1015-69. <https://doi.org/10.1146/annurev.bi.54.070185.005055>
- Havlíčková, V., Kaplanová, V., Nůšková, H., Drahotka, Z., & Houštěk, J. (2010). Knockdown of F1 epsilon subunit decreases mitochondrial content of ATP synthase and leads to

- accumulation of subunit c. *Biochimica et Biophysica Acta - Bioenergetics*, 1797(6–7), 1124–1129. <https://doi.org/10.1016/j.bbabi.2009.12.009>
- Heidari, M. M., Mirfakhradini, F. S., Tayefi, F., Ghorbani, S., Khatami, M., & Hadadzadeh, M. (2020). Novel Point Mutations in Mitochondrial MT-CO2 Gene May Be Risk Factors for Coronary Artery Disease. *Applied Biochemistry and Biotechnology*, 191(3), 1326–1339. <https://doi.org/10.1007/s12010-020-03275-0>
- Heo, J. M., Livnat-Levanon, N., Taylor, E. B., Jones, K. T., Dephore, N., Ring, J., Xie, J., Brodsky, J. L., Madeo, F., Gygi, S. P., Ashrafi, K., Glickman, M. H., & Rutter, J. (2010). A Stress-Responsive System for Mitochondrial Protein Degradation. *Molecular Cell*, 40(3), 465–480. <https://doi.org/10.1016/j.molcel.2010.10.021>
- Hiltunen, J. K., Schonauer, M. S., Autio, K. J., Mittelmeier, T. M., Kastaniotis, A. J., & Dieckmann, C. L. (2009). Mitochondrial fatty acid synthesis type II: More than just fatty acids. *Journal of Biological Chemistry*, 284(14), 9011–9015. <https://doi.org/10.1074/jbc.R800068200>
- Hinkie, P. C., Arun Kumar, M., Resetar, A., & Harris, D. L. (1991). Mechanistic Stoichiometry of Mitochondrial Oxidative Phosphorylation. *Biochemistry*, 30(14), 3576–3582. <https://doi.org/10.1021/bi00228a031>
- Ho, Y., Ho, Y., Gruhler, A., Gruhler, A., Heilbut, A., Heilbut, A., Bader, G. D., Moore, L., Moore, L., Adams, S. L., Adams, S. L., Millar, A., Millar, A., Taylor, P., Taylor, P., Bennett, K., Bennett, K., Boutilier, K., Boutilier, K., ... Tyers, M. (2002). Systematic identification of protein complexes in *Saccharomyces cerevisiae* by mass spectrometry. *Nature*, 415(6868), 180–183. <https://doi.org/10.1038/415180a>
- Hoffman, L., Pratt, G., & Rechsteiner, M. (1992). Multiple forms of the 20 S multicatalytic and the 26 S ubiquitin/ATP- dependent proteases from rabbit reticulocyte lysate. *Journal of Biological Chemistry*, 267(31), 22362–22368.
- Huang, G., Chen, Y., Lu, H., & Cao, X. (2007). Coupling mitochondrial respiratory chain to cell death: An essential role of mitochondrial complex I in the interferon- $\beta$  and retinoic acid-induced cancer cell death. *Cell Death and Differentiation*, 14(2), 327–337. <https://doi.org/10.1038/sj.cdd.4402004>
- Huang, L., Haratake, K., Miyahara, H., & Chiba, T. (2016). Proteasome activators, PA28 $\gamma$  and PA200, play indispensable roles in male fertility. *Scientific Reports*, 6(October 2015), 2–10. <https://doi.org/10.1038/srep23171>
- Huber, E. M., & Groll, M. (2017). The Mammalian Proteasome Activator PA28 Forms an Asymmetric  $\alpha\beta_3$  Complex. *Structure*, 25(10), 1473–1480.e3. <https://doi.org/10.1016/j.str.2017.07.013>
- Ingerman, E., Perkins, E. M., Marino, M., Mears, J. A., McCaffery, J. M., Hinshaw, J. E., & Nunnari, J. (2005). Dnm1 forms spirals that are structurally tailored to fit mitochondria. *Journal of Cell Biology*, 170(7), 1021–1027. <https://doi.org/10.1083/jcb.200506078>
- Ishihara, N., Fujita, Y., Oka, T., & Mihara, K. (2006). Regulation of mitochondrial morphology through proteolytic cleavage of OPA1. *EMBO Journal*, 25(13), 2966–2977. <https://doi.org/10.1038/sj.emboj.7601184>

- Iwanczyk, J., Sadre-Bazzaz, K., Ferrell, K., Kondrashkina, E., Formosa, T., Hill, C. P., & Ortega, J. (2006). Structure of the Bln10-20 S Proteasome Complex by Cryo-electron Microscopy. Insights into the Mechanism of Activation of Mature Yeast Proteasomes. *Journal of Molecular Biology*, *363*(3), 648–659. <https://doi.org/10.1016/j.jmb.2006.08.010>
- Jagannathan, S., Vad, N., Vallabhapurapu, S., Vallabhapurapu, S., Anderson, K. C., & Driscoll, J. J. (2015). MiR-29b replacement inhibits proteasomes and disrupts aggresome+autophagosome formation to enhance the antimyeloma benefit of bortezomib. *Leukemia*, *29*(3), 727–738. <https://doi.org/10.1038/leu.2014.279>
- James, D. I., & Martinou, J. C. (2008). Mitochondrial Dynamics and Apoptosis: A Painful Separation. *Developmental Cell*, *15*(3), 341–343. <https://doi.org/10.1016/j.devcel.2008.08.011>
- Jelinsky, S. A., Estep, P., Church, G. M., & Samson, L. D. (2000). Regulatory Networks Revealed by Transcriptional Profiling of Damaged *Saccharomyces cerevisiae* Cells: Rpn4 Links Base Excision Repair with Proteasomes. *Molecular and Cellular Biology*, *20*(21), 8157–8167. <https://doi.org/10.1128/mcb.20.21.8157-8167.2000>
- Jeon, H. B., Choi, E. S., Yoon, J. H., Hwang, J. H., Chang, J. W., Lee, E. K., Choi, H. W., Park, Z. Y., & Yoo, Y. J. (2007). A proteomics approach to identify the ubiquitinated proteins in mouse heart. *Biochemical and Biophysical Research Communications*, *357*(3), 731–736. <https://doi.org/10.1016/j.bbrc.2007.04.015>
- Jheng, H.-F., Tsai, P.-J., Guo, S.-M., Kuo, L.-H., Chang, C.-S., Su, I.-J., Chang, C.-R., & Tsai, Y.-S. (2012). Mitochondrial Fission Contributes to Mitochondrial Dysfunction and Insulin Resistance in Skeletal Muscle. *Molecular and Cellular Biology*, *32*(2), 309–319. <https://doi.org/10.1128/mcb.05603-11>
- Jiang, T.-X., Ma, S., Han, X., Luo, Z.-Y., Zhu, Q.-Q., Chiba, T., Xie, W., Chen, S.-R., Lin, K., & Qiu, X.-B. (2020). Proteasome activator PA200 maintains stability of histone marks during transcription and aging. 1–62. <https://doi.org/10.1101/2020.04.28.067132>
- Johnston-Carey, H. K., Pomatto, L. C. D., & Davies, K. J. A. (2016). The Immunoproteasome in oxidative stress, aging, and disease. *Critical Reviews in Biochemistry and Molecular Biology*, *51*(4), 268–281. <https://doi.org/10.3109/10409238.2016.1172554>
- Jornayvaz, F. R., & Shulman, G. I. (2010). Regulation of mitochondrial biogenesis. *Essays in Biochemistry*, *47*, 69–84. <https://doi.org/10.1042/BSE0470069>
- Juríková, M., Danihel, L., Polák, Š., & Varga, I. (2016). Ki67, PCNA, and MCM proteins: Markers of proliferation in the diagnosis of breast cancer. *Acta Histochemica*, *118*(5), 544–552. <https://doi.org/10.1016/j.acthis.2016.05.002>
- Kajava, A. V., Gorbea, C., Ortega, J., Rechsteiner, M., & Steven, A. C. (2004). New HEAT-like repeat motifs in proteins regulating proteasome structure and function. *Journal of Structural Biology*, *146*(3), 425–430. <https://doi.org/10.1016/j.jsb.2004.01.013>
- Kamer, K. J., & Mootha, V. K. (2015). The molecular era of the mitochondrial calcium uniporter. *Nature Reviews Molecular Cell Biology*, *16*(9), 545–553. <https://doi.org/10.1038/nrm4039>
- Kamiński, M., Kießling, M., Süß, D., Krammer, P. H., & Gülow, K. (2007). Novel Role for

- Mitochondria: Protein Kinase C $\theta$ -Dependent Oxidative Signaling Organelles in Activation-Induced T-Cell Death. *Molecular and Cellular Biology*, 27(10), 3625–3639. <https://doi.org/10.1128/mcb.02295-06>
- Karbowski, M., Neutzner, A., & Youle, R. J. (2007). The mitochondrial E3 ubiquitin ligase MARCH5 is required for Drp1 dependent mitochondrial division. *Journal of Cell Biology*, 178(1), 71–84. <https://doi.org/10.1083/jcb.200611064>
- Kasahara, A., & Scorrano, L. (2014). Mitochondria: From cell death executioners to regulators of cell differentiation. *Trends in Cell Biology*, 24(12), 761–770. <https://doi.org/10.1016/j.tcb.2014.08.005>
- Kaushik, S., & Cuervo, A. M. (2012). Chaperone-mediated autophagy: A unique way to enter the lysosome world. *Trends in Cell Biology*, 22(8), 407–417. <https://doi.org/10.1016/j.tcb.2012.05.006>
- Khan, S., van den Broek, M., Schwarz, K., de Giuli, R., Diener, P.-A., & Groettrup, M. (2001). Immunoproteasomes Largely Replace Constitutive Proteasomes During an Antiviral and Antibacterial Immune Response in the Liver. *The Journal of Immunology*, 167(12), 6859–6868. <https://doi.org/10.4049/jimmunol.167.12.6859>
- Khor, B., Bredemeyer, A. L., Huang, C.-Y., Turnbull, I. R., Evans, R., Maggi, L. B., White, J. M., Walker, L. M., Carnes, K., Hess, R. A., & Sleckman, B. P. (2006). Proteasome Activator PA200 Is Required for Normal Spermatogenesis. *Molecular and Cellular Biology*, 26(8), 2999–3007. <https://doi.org/10.1128/mcb.26.8.2999-3007.2006>
- Kish-Trier, E., & Hill, C. P. (2013). Structural biology of the proteasome. *Annual Review of Biophysics*, 42(1), 29–49. <https://doi.org/10.1146/annurev-biophys-083012-130417>
- Klintworth, H., Newhouse, K., Li, T., Choi, W. S., Faigle, R., & Xia, Z. (2007). Activation of c-Jun N-terminal protein kinase is a common mechanism underlying paraquat- and rotenone-induced dopaminergic cell apoptosis. *Toxicological Sciences*, 97(1), 149–162. <https://doi.org/10.1093/toxsci/kfm029>
- Koshiba, T., Detmer, S. A., Kaiser, J. T., Chen, H., McCaffery, J. M., & Chan, D. C. (2004). Structural basis of mitochondrial tethering by mitofusin complexes. *Science*, 305(5685), 858–862. <https://doi.org/10.1126/science.1099793>
- Krishna, A., Biryukov, M., Trefois, C., Antony, P. M. A., Hussong, R., Lin, J., Heinäniemi, M., Glusman, G., Köglberger, S., Boyd, O., van den Berg, B. H. J., Linke, D., Huang, D., Wang, K., Hood, L., Tholey, A., Schneider, R., Galas, D. J., Balling, R., & May, P. (2014). Systems genomics evaluation of the SH-SY5Y neuroblastoma cell line as a model for Parkinson's disease. *BMC Genomics*, 15(1), 1–21. <https://doi.org/10.1186/1471-2164-15-1154>
- Labbé, K., Murley, A., & Nunnari, J. (2014). Determinants and functions of mitochondrial behavior. *Annual Review of Cell and Developmental Biology*, 30(1), 357–391. <https://doi.org/10.1146/annurev-cellbio-101011-155756>
- Langmead, B., Trapnell, C., Pop, M., & Salzberg, S. L. (2009). Ultrafast and memory-efficient alignment of short DNA sequences to the human genome. *Genome Biology*, 10(3). <https://doi.org/10.1186/gb-2009-10-3-r25>

- Lee, H., & Yoon, Y. (2016). Mitochondrial fission and fusion. *Biochemical Society Transactions*, 44(6), 1725–1735. <https://doi.org/10.1042/BST20160129>
- Lehmann, A., Jechow, K., & Enenkel, C. (2008). Blm10 binds to pre-activated proteasome core particles with open gate conformation. *EMBO Reports*, 9(12), 1237–1243. <https://doi.org/10.1038/embor.2008.190>
- Levy-Barda, A., Lerenthal, Y., Davis, A. J., Chung, Y. M., Essers, J., Shao, Z., Van Vliet, N., Chen, D. J., Hu, M. C. T., Kanaar, R., Ziv, Y., & Shiloh, Y. (2011). Involvement of the nuclear proteasome activator PA28 $\gamma$  in the cellular response to DNA double-strand breaks. *Cell Cycle*, 10(24), 4300–4310. <https://doi.org/10.4161/cc.10.24.18642>
- Li, W. W., Li, J., & Bao, J. K. (2012). Microautophagy: Lesser-known self-eating. *Cellular and Molecular Life Sciences*, 69(7), 1125–1136. <https://doi.org/10.1007/s00018-011-0865-5>
- Libby, P., Bornfeldt, K. E., & Tall, A. R. (2016). Atherosclerosis: Successes, Surprises, and Future Challenges. *Circulation Research*, 118(4), 531–534. <https://doi.org/10.1161/CIRCRESAHA.116.308334>
- Liesa, M., Palacín, M., & Zorzano, A. (2009). Mitochondrial dynamics in mammalian health and disease. *Physiological Reviews*, 89(3), 799–845. <https://doi.org/10.1152/physrev.00030.2008>
- Lin, C., Li, H., Liu, J., Hu, Q., Zhang, S., Zhang, N., Liu, L., Dai, Y., Cao, D., Li, X., Huang, B., Lu, J., & Zhang, Y. (2020). Arginine hypomethylation-mediated proteasomal degradation of histone H4—an early biomarker of cellular senescence. *Cell Death and Differentiation*, 27(9), 2697–2709. <https://doi.org/10.1038/s41418-020-0562-8>
- Liu, J., Killilea, D. W., & Ames, B. N. (2002). Age-associated mitochondrial oxidative decay: Improvement of carnitine acetyltransferase substrate-binding affinity and activity in brain by feeding old rats acetyl-L-carnitine and/or R- $\alpha$ -lipoic acid. *Proceedings of the National Academy of Sciences of the United States of America*, 99(4), 1876–1881. <https://doi.org/10.1073/pnas.261709098>
- Liu, X., Kim, C. N., Yang, J., Jemmerson, R., & Wang, X. (1996). Induction of apoptotic program in cell-free extracts: Requirement for dATP and cytochrome c. *Cell*, 86(1), 147–157. [https://doi.org/10.1016/S0092-8674\(00\)80085-9](https://doi.org/10.1016/S0092-8674(00)80085-9)
- Livak, K. J., & Schmittgen, T. D. (2001). Analysis of relative gene expression data using real-time quantitative PCR and the 2- $\Delta\Delta$ CT method. *Methods*, 25(4), 402–408. <https://doi.org/10.1006/meth.2001.1262>
- Lopes, F. M., Schröder, R., Júnior, M. L. C. da F., Zanotto-Filho, A., Müller, C. B., Pires, A. S., Meurer, R. T., Colpo, G. D., Gelain, D. P., Kapczinski, F., Moreira, J. C. F., Fernandes, M. da C., & Klamt, F. (2010). Comparison between proliferative and neuron-like SH-SY5Y cells as an in vitro model for Parkinson disease studies. *Brain Research*, 1337, 85–94. <https://doi.org/10.1016/j.brainres.2010.03.102>
- Lopez, A. D., Tar, K., Krügel, U., Dange, T., Ros, I. G., & Schmidt, M. (2011). Proteasomal degradation of Sfp1 contributes to the repression of ribosome biogenesis during starvation and is mediated by the proteasome activator Blm10. *Molecular Biology of the Cell*, 22(5), 528–540. <https://doi.org/10.1091/mbc.E10-04-0352>

- Loschen, G., Flohé, L., & Chance, B. (1971). Respiratory chain linked H<sub>2</sub>O<sub>2</sub> production in pigeon heart mitochondria. *FEBS Letters*, *18*(2), 261–264. [https://doi.org/10.1016/0014-5793\(71\)80459-3](https://doi.org/10.1016/0014-5793(71)80459-3)
- Löwe, J., Stock, D., Jap, B., Zwickl, P., Baumeister, W., & Huber, R. (1995). Crystal structure of the 20S proteasome from the archaeon *T. acidophilum* at 3.4 Å resolution. *Science*, *268*(5210), 533–539. <https://doi.org/10.1126/science.7725097>
- Madamanchi, N. R., & Runge, M. S. (2007). Mitochondrial dysfunction in atherosclerosis. *Circulation Research*, *100*(4), 460–473. <https://doi.org/10.1161/01.RES.0000258450.44413.96>
- Majeski, A. E., & Fred Dice, J. (2004). Mechanisms of chaperone-mediated autophagy. *International Journal of Biochemistry and Cell Biology*, *36*(12), 2435–2444. <https://doi.org/10.1016/j.biocel.2004.02.013>
- Manor, U., Bartholomew, S., Golani, G., Christenson, E., Kozlov, M., Higgs, H., Spudich, J., & Lippincott-Schwartz, J. (2015). A mitochondria-anchored isoform of the actin-nucleating spire protein regulates mitochondrial division. *ELife*, *4*(AUGUST2015), 1–27. <https://doi.org/10.7554/eLife.08828>
- Marchetti, P., Fovez, Q., Germain, N., Khamari, R., & Kluza, J. (2020). Mitochondrial spare respiratory capacity: Mechanisms, regulation, and significance in non-transformed and cancer cells. *FASEB Journal*, *34*(10), 13106–13124. <https://doi.org/10.1096/fj.202000767R>
- Margineantu, D. H., Emerson, C. B., Diaz, D., & Hockenbery, D. M. (2007). Hsp90 inhibition decreases mitochondrial protein turnover. *PLoS ONE*, *2*(10). <https://doi.org/10.1371/journal.pone.0001066>
- Maupin-Furlow, J. (2012). Proteasomes and protein conjugation across domains of life. *Nature Reviews Microbiology*, *10*(2), 100–111. <https://doi.org/10.1038/nrmicro2696>
- McBride, H. M., Neuspiel, M., & Wasiak, S. (2006). Mitochondria: More Than Just a Powerhouse. *Current Biology*, *16*(14), 551–560. <https://doi.org/10.1016/j.cub.2006.06.054>
- McNaught, K. S. P., Olanow, C. W., Halliwell, B., Isacson, O., & Jenner, P. (2001). Failure of the ubiquitin proteasome system in Parkinson's disease. *Nature Reviews Neuroscience*, *2*(8), 589–594. <https://doi.org/10.1038/35086067>
- Minina, E. A., Moschou, P. N., & Bozhkov, P. V. (2017). Limited and digestive proteolysis: crosstalk between evolutionary conserved pathways. *New Phytologist*, *215*(3), 958–964. <https://doi.org/10.1111/nph.14627>
- Mishra, P., & Chan, D. C. (2016). Metabolic regulation of mitochondrial dynamics. *Journal of Cell Biology*, *212*(4), 379–387. <https://doi.org/10.1083/jcb.201511036>
- Mitchell. (1961). Coupling of Phosphorylation to Electron and Hydrogen Transfer by a Chemi-Osmotic type of Mechanism. *Nature*. *191*, 144–148. <https://doi.org/10.1038/191144a0>
- Mitra, K., Wunder, C., Roysam, B., Lin, G., & Lippincott-Schwartz, J. (2009). A hyperfused mitochondrial state achieved at G1-S regulates cyclin E buildup and entry into S phase. *Proceedings of the National Academy of Sciences of the United States of America*, *106*(29),

11960–11965. <https://doi.org/10.1073/pnas.0904875106>

- Mizushima, N., Levine, B., Cuervo, A. M., & Klionsky, D. J. (2008). Autophagy fights disease through cellular self-digestion. *Nature*, *451*(7182), 1069–1075. <https://doi.org/10.1038/nature06639>
- Mortimore, G. E., & Reeta Pösö, A. (1986). The lysosomal pathway of intracellular proteolysis in liver: Regulation by amino acids. *Advances in Enzyme Regulation*, *25*(C), 257–276. [https://doi.org/10.1016/0065-2571\(86\)90018-X](https://doi.org/10.1016/0065-2571(86)90018-X)
- Müller, O., Sattler, T., Flötenmeyer, M., Schwarz, H., Mayer, A., Miiller, O., Sattler, T., Flitenmeyer, M., & Schwarz, H. (2016). Autophagic Tubes: Vacuolar Invaginations Involved in Lateral Membrane Sorting and Inverse Vesicle Budding. *The Journal of Cell Biology*, *151*(3), 519–528. <https://doi.org/10.1083/jcb.151.3.519>
- Murata, S., Kawahara, H., Tohma, S., Yamamoto, K., Kasahara, M., Nabeshima, Y. I., Tanaka, K., & Chiba, T. (1999). Growth retardation in mice lacking the proteasome activator PA28 $\gamma$ . *Journal of Biological Chemistry*, *274*(53), 38211–38215. <https://doi.org/10.1074/jbc.274.53.38211>
- Murata, S., Sasaki, K., Kishimoto, T., Niwa, S., Hayashi, H., Takahama, Y., & Tanaka, K. (2007). Regulation of CD8<sup>+</sup> T Cell Development by Thymus-Specific Proteasomes by Thymus-Specific Proteasomes. *Science* *316*(June), 1349–1353. <https://doi.org/10.1126/science.1141915>.
- Myung, J., Kim, K. B., & Crews, C. M. (2001). The ubiquitin-proteasome pathway and proteasome inhibitors. *Medicinal Research Reviews*, *21*(4), 245–273. <https://doi.org/10.1002/med.1009>
- Nakamura, N and Hirose, S. (2008). Regulation of Mitochondrial Morphology by USP30, a Deubiquitinating Enzyme Present in the Mitochondrial Outer Membrane. *Molecular Biology of the Cell*, *19*(May), 1903–1911. <https://doi.org/10.1091/mbc.e07-11-1103>
- Nakamura, N., Kimura, Y., Tokuda, M., Honda, S., & Hirose, S. (2006). MARCH-V is a novel mitofusin 2- and Drp1-binding protein able to change mitochondrial morphology. *EMBO Reports*, *7*(10), 1019–1022. <https://doi.org/10.1038/sj.embor.7400790>
- Nedelsky, N. B., Todd, P. K., & Taylor, J. P. (2008). Autophagy and the ubiquitin-proteasome system: Collaborators in neuroprotection. *Biochimica et Biophysica Acta - Molecular Basis of Disease*, *1782*(12), 691–699. <https://doi.org/10.1016/j.bbadis.2008.10.002>
- Newhouse, K., Hsuan, S. L., Chang, S. H., Cai, B., Wang, Y., & Xia, Z. (2004). Rotenone-induced apoptosis is mediated by p38 and JNK MAP kinases in human dopaminergic SH-SY5Y cells. *Toxicological Sciences*, *79*(1), 137–146. <https://doi.org/10.1093/toxsci/kfh089>
- Olichon, A., Baricault, L., Gas, N., Guillou, E., Valette, A., Belenguer, P., & Lenaers, G. (2003). Loss of OPA1 perturbs the mitochondrial inner membrane structure and integrity, leading to cytochrome c release and apoptosis. *Journal of Biological Chemistry*, *278*(10), 7743–7746. <https://doi.org/10.1074/jbc.C200677200>
- Orlowski, M., & Wilk, S. (2000). Catalytic activities of the 20 S proteasome, a multicatalytic proteinase complex. *Archives of Biochemistry and Biophysics*, *383*(1), 1–16. <https://doi.org/10.1006/abbi.2000.2036>

- Ortega, J., Heymann, J. B., Kajava, A. V., Ustrell, V., Rechsteiner, M., & Steven, A. C. (2005). The axial channel of the 20 S proteasome opens upon binding of the PA200 activator. *Journal of Molecular Biology*, *346*(5), 1221–1227. <https://doi.org/10.1016/j.jmb.2004.12.049>
- Park, Y. Y., Lee, S., Karbowski, M., Neutzner, A., Youle, R. J., & Cho, H. (2010). Loss of MARCH5 mitochondrial E3 ubiquitin ligase induces cellular senescence through dynamin-related protein 1 and mitofusin 1. *Journal of Cell Science*, *123*(4), 619–626. <https://doi.org/10.1242/jcs.061481>
- Peng, J., Schwartz, D., Elias, J. E., Thoreen, C. C., Cheng, D., Marsischky, G., Roelofs, J., Finley, D., & Gygi, S. P. (2003). A proteomics approach to understanding protein ubiquitination. *Nature Biotechnology*, *21*(8), 921–926. <https://doi.org/10.1038/nbt849>
- Pernas, L., & Scorrano, L. (2016). Mito-Morphosis: Mitochondrial Fusion, Fission, and Cristae Remodeling as Key Mediators of Cellular Function. *Annual Review of Physiology*, *78*, 505–531. <https://doi.org/10.1146/annurev-physiol-021115-105011>
- Peth, A., Besche, H. C., & Goldberg, A. L. (2009). Ubiquitinated Proteins Activate the Proteasome by Binding to Usp14/Ubp6, which Causes 20S Gate Opening. *Molecular Cell*, *36*(5), 794–804. <https://doi.org/10.1016/j.molcel.2009.11.015>
- Pickart, C. M., & Cohen, R. E. (2004). Proteasomes and their kin: Proteases in the machine age. *Nature Reviews Molecular Cell Biology*, *5*(3), 177–187. <https://doi.org/10.1038/nrm1336>
- Pickering, A. M., & Davies, K. J. A. (2012). Differential roles of proteasome and immunoproteasome regulators Pa28 $\alpha\beta$ , Pa28 $\gamma$  and Pa200 in the degradation of oxidized proteins. In *Archives of Biochemistry and Biophysics* (Vol. 523, Issue 2, pp. 181–190). <https://doi.org/10.1016/j.abb.2012.04.018>
- Piecznik, S. R., & Neustadt, J. (2007). Mitochondrial dysfunction and molecular pathways of disease. *Experimental and Molecular Pathology*, *83*(1), 84–92. <https://doi.org/10.1016/j.yexmp.2006.09.008>
- Piquereau, J., Caffin, F., Novotova, M., Lemaire, C., Veksler, V., Garnier, A., Ventura-Clapier, R., & Joubert, F. (2013). Mitochondrial dynamics in the adult cardiomyocytes: Which roles for a highly specialized cell? *Frontiers in Physiology*, *4* MAY(May), 1–12. <https://doi.org/10.3389/fphys.2013.00102>
- Pittman, D. L., Cobb, J., Schimenti, K. J., Wilson, L. A., Cooper, D. M., Brignull, E., Handel, M. A., & Schimenti, J. C. (1998). Meiotic prophase arrest with failure of chromosome synapsis in mice deficient for Dmc1, a germline-specific RecA homolog. *Molecular Cell*, *1*(5), 697–705. [https://doi.org/10.1016/S1097-2765\(00\)80069-6](https://doi.org/10.1016/S1097-2765(00)80069-6)
- Qian, M. X., Pang, Y., Liu, C. H., Haratake, K., Du, B. Y., Ji, D. Y., Wang, G. F., Zhu, Q. Q., Song, W., Yu, Y., Zhang, X. X., Huang, H. T., Miao, S., Chen, L. Bin, Zhang, Z. H., Liang, Y. N., Liu, S., Cha, H., Yang, D., ... Qiu, X. B. (2013). XAcetylation-mediated proteasomal degradation of core histones during DNA repair and spermatogenesis. *Cell*, *153*(5), 1012. <https://doi.org/10.1016/j.cell.2013.04.032>
- Quirós, P. M., Ramsay, A. J., Sala, D., Fernández-Vizarra, E., Rodríguez, F., Peinado, J. R., Fernández-García, M. S., Vega, J. A., Enríquez, J. A., Zorzano, A., & López-Otín, C. (2012).

- Loss of mitochondrial protease OMA1 alters processing of the GTPase OPA1 and causes obesity and defective thermogenesis in mice. *EMBO Journal*, 31(9), 2117–2133. <https://doi.org/10.1038/emboj.2012.70>
- Radad, K., Rausch, W. D., & Gille, G. (2006). Rotenone induces cell death in primary dopaminergic culture by increasing ROS production and inhibiting mitochondrial respiration. *Neurochemistry International*, 49(4), 379–386. <https://doi.org/10.1016/j.neuint.2006.02.003>
- Rambold, A. S., & Pearce, E. L. (2018). Mitochondrial Dynamics at the Interface of Immune Cell Metabolism and Function. *Trends in Immunology*, 39(1), 6–18. <https://doi.org/10.1016/j.it.2017.08.006>
- Ramírez, F., Ryan, D. P., Grüning, B., Bhardwaj, V., Kilpert, F., Richter, A. S., Heyne, S., Dündar, F., & Manke, T. (2016). deepTools2: a next generation web server for deep-sequencing data analysis. *Nucleic Acids Research*, 44(W1), W160–W165. <https://doi.org/10.1093/nar/gkw257>
- Rechsteiner, M. (1998). The 26 S Proteasome. *Ubiquitin and the Biology of the Cell*, 147–189. [https://doi.org/10.1007/978-1-4899-1922-9\\_6](https://doi.org/10.1007/978-1-4899-1922-9_6)
- Rechsteiner, M., & Hill, C. P. (2005). Mobilizing the proteolytic machine: Cell biological roles of proteasome activators and inhibitors. *Trends in Cell Biology*, 15(1), 27–33. <https://doi.org/10.1016/j.tcb.2004.11.003>
- Rivett, A. J. (1998). Intracellular distribution of proteasomes. *Current Opinion in Immunology*, 10(1), 110–114. [https://doi.org/10.1016/S0952-7915\(98\)80040-X](https://doi.org/10.1016/S0952-7915(98)80040-X)
- Rosenzweig, R., Bronner, V., Zhang, D., Fushman, D., & Glickman, M. H. (2012). Rpn1 and Rpn2 coordinate ubiquitin processing factors at proteasome. *Journal of Biological Chemistry*, 287(18), 14659–14671. <https://doi.org/10.1074/jbc.M111.316323>
- Sadre-Bazzaz, K., Whitby, F. G., Robinson, H., Formosa, T., & Hill, C. P. (2010). Structure of a Blm10 Complex Reveals Common Mechanisms for Proteasome Binding and Gate Opening. *Molecular Cell*, 37(5), 728–735. <https://doi.org/10.1016/j.molcel.2010.02.002>
- Sahu, I., & Glickman, M. H. (2021). Structural insights into substrate recognition and processing by the 20s proteasome. *Biomolecules*, 11(2), 1–15. <https://doi.org/10.3390/biom11020148>
- Sano, S., Inoue, S., Tanabe, Y., Sumiya, C., & Koike, S. (1959). Significance of mitochondria for porphyrin and heme biosynthesis. *Science*, 129(3344), 275–276. <https://doi.org/10.1126/science.129.3344.275>
- Sattler, T., & Mayer, A. (2000). Cell-free reconstitution of microautophagic vacuole invagination and vesicle formation. *The Journal of cell biology*, 151(3), 529–538. <https://doi.org/10.1083/jcb.151.3.529>
- Schapira, A. H. V., Cooper, J. M., Dexter, D., Clark, J. B., Jenner, P., & Marsden, C. D. (1990). Mitochondrial Complex I Deficiency in Parkinson's Disease. *Journal of Neurochemistry*, 54(3), 823–827. <https://doi.org/10.1111/j.1471-4159.1990.tb02325.x>
- Schmidt, M., Haas, W., Crosas, B., Santamaria, P. G., Gygi, S. P., Walz, T., & Finley, D. (2005). The HEAT repeat protein Blm10 regulates the yeast proteasome by capping the core particle.

- Nature Structural and Molecular Biology*, 12(4), 294–303. <https://doi.org/10.1038/nsmb914>
- Schultz, L. B., Chehab, N. H., Malikzay, A., & Halazonetis, T. D. (2000). p53 binding protein 1 (53BP1) is an early participant in the cellular response to DNA double-strand breaks. *Journal of Cell Biology*, 151(7), 1381–1390. <https://doi.org/10.1083/jcb.151.7.1381>
- Schwartz, A. L., & Ciechanover, A. (1999). The Ubiquitin-Proteasome Pathway and Pathogenesis. *Ann. Rev. Med.*, 50, 57–74.
- Seemüller, E., Lupas, A., Stock, D., Löwe, J., Huber, R., & Baumeister, W. (1995). Proteasome from *Thermoplasma acidophilum*: A threonine protease. *Science*, 268(5210), 579–582. <https://doi.org/10.1126/science.7725107>
- Sharma A., Singh K., Almasan A. (2012) Histone H2AX Phosphorylation: A Marker for DNA Damage. In: Bjergbæk L. (eds) DNA Repair Protocols. Methods in Molecular Biology (Methods and Protocols), vol 920. Humana Press, Totowa, NJ. [https://doi.org/10.1007/978-1-61779-998-3\\_40](https://doi.org/10.1007/978-1-61779-998-3_40)
- Shigenaga, M. K., Hagen, T. M., & Ames, B. N. (1994). Oxidative Damage and Mitochondrial Decay in Aging. *National Academy of Sciences S.* 91(23), 10771–10778. <https://doi.org/10.1073/pnas.91.23.10771>.
- Sickmann, A., Reinders, J., Wagner, Y., Joppich, C., Zahedi, R., Meyer, H. E., Schönfisch, B., Perschil, I., Chacinska, A., Guiard, B., Rehling, P., Pfanner, N., & Meisinger, C. (2003). The proteome of *Saccharomyces cerevisiae* mitochondria. *Proceedings of the National Academy of Sciences of the United States of America*, 100(23), 13207–13212. <https://doi.org/10.1073/pnas.2135385100>
- Sies, H. (1993). Strategies of antioxidant defense. *European Journal of Biochemistry*, 215(2), 213–219. <https://doi.org/10.1111/j.1432-1033.1993.tb18025.x>
- Silva, G. M., Netto, L. E. S., Simões, V., Santos, L. F. A., Gozzo, F. C., Demasi, M. A. A., Oliveira, C. L. P., Bicev, R. N., Klitzke, C. F., Sogayar, M. C., & Demasi, M. (2012). Redox control of 20S proteasome gating. *Antioxidants and Redox Signaling*, 16(11), 1183–1194. <https://doi.org/10.1089/ars.2011.4210>
- Sixt, S. U., & Dahlmann, B. (2008). Extracellular, circulating proteasomes and ubiquitin - Incidence and relevance. *Biochimica et Biophysica Acta - Molecular Basis of Disease*, 1782(12), 817–823. <https://doi.org/10.1016/j.bbadis.2008.06.005>
- Song, Z., Ghochani M, McCaffery, M., Frey, T G., & Chan, D C. (2009). Mitofusins and OPA1 Mediate Sequential Steps in Mitochondrial Membrane Fusion. *Molecular Biology of the Cell*, 20, 3525–3532. <https://doi.org/10.1091/mbc.e09-03-0252>
- Stadtman, E. R., & Berlett, B. S. (1991). Fenton chemistry: Amino acid oxidation. *Journal of Biological Chemistry*, 266(26), 17201–17211. [https://doi.org/10.1016/s0021-9258\(19\)47359-6](https://doi.org/10.1016/s0021-9258(19)47359-6)
- Stadtman, E. R., & Levine, R. L. (2003). Free radical-mediated oxidation of free amino acids and amino acid residues in proteins. *Amino Acids*, 25(3–4), 207–218. <https://doi.org/10.1007/s00726-003-0011-2>

- Stadtman, Earl R. (1990). Metal ion-catalyzed oxidation of proteins: Biochemical mechanism and biological consequences. *Free Radical Biology and Medicine*, 9(4), 315–325. [https://doi.org/10.1016/0891-5849\(90\)90006-5](https://doi.org/10.1016/0891-5849(90)90006-5)
- Stadtmueller, B. M., & Hill, C. P. (2011). Proteasome activators. *Molecular Cell*, 41(1), 8–19. <https://doi.org/10.1016/j.molcel.2010.12.020>
- Stokin, G. B., Lillo, C., Falzone, T. L., Brusch, R. G., Rockenstein, E., Mount, S. L., Raman, R., Davies, P., Masliah, E., Williams, D. S., & Goldstein, L. S. B. (2005). Axonopathy and transport deficits early in the pathogenesis of Alzheimer's diseases. *Science*, 307(5713), 1282–1288. <https://doi.org/10.1126/science.1105681>
- Sugiura, A., Nagashima, S., Tokuyama, T., Amo, T., Matsuki, Y., Ishido, S., Kudo, Y., McBride, H. M., Fukuda, T., Matsushita, N., Inatome, R., & Yanagi, S. (2013). MITOL regulates endoplasmic reticulum-mitochondria contacts via Mitofusin2. *Molecular Cell*, 51(1), 20–34. <https://doi.org/10.1016/j.molcel.2013.04.023>
- Swerdlow, R. H. (2018). Mitochondria and Mitochondrial Cascades in Alzheimer's Disease. *Journal of Alzheimer's Disease*, 62(3), 1403–1416. <https://doi.org/10.3233/JAD-170585>
- Swerdlow, R. H., Parks, J. K., Miller, S. W., Tuttle, J. B., Trimmer, P. A., Sheehan, J. P., Bennett, J. P., Davis, R. E., & Parker, W. D. (1996). Origin and functional consequences of the complex I defect in Parkinson's disease. *Annals of Neurology*, 40(4), 663–671. <https://doi.org/10.1002/ana.410400417>
- Tanahashi, N., Murakami, Y., Minami, Y., Shimbara, N., Hendil, K. B., & Tanaka, K. (2000). Hybrid Proteasomes. *Journal of Biological Chemistry*, 275(19), 14336–14345. <https://doi.org/10.1074/jbc.275.19.14336>
- Tanaka, A., Cleland, M. M., Xu, S., Narendra, D. P., Suen, D. F., Karbowski, M., & Youle, R. J. (2010). Proteasome and p97 mediate mitophagy and degradation of mitofusins induced by Parkin. *Journal of Cell Biology*, 191(7), 1367–1380. <https://doi.org/10.1083/jcb.201007013>
- Tar, K., Dange, T., Yang, C., Yao, Y., Bulteau, A. L., Salcedo, E. F., Braigen, S., Bouillaud, F., Finley, D., & Schmidt, M. (2014). Proteasomes associated with the blm10 activator protein antagonize mitochondrial fission through degradation of the fission protein dnm1. *Journal of Biological Chemistry*, 289(17), 12145–12156. <https://doi.org/10.1074/jbc.M114.554105>
- Tatsuta, T. (2009). Protein quality control in mitochondria. *Journal of Biochemistry*, 146(4), 455–461. <https://doi.org/10.1093/jb/mvp122>
- Thibaudeau, T. A., & Smith, D. M. (2019). A practical review of proteasome pharmacology. *Pharmacological Reviews*, 71(2), 170–197. <https://doi.org/10.1124/pr.117.015370>
- Tilokani, L., Nagashima, S., Paupe, V., & Prudent, J. (2018). Mitochondrial dynamics: Overview of molecular mechanisms. *Essays in Biochemistry*, 62(3), 341–360. <https://doi.org/10.1042/EBC20170104>
- Tomko, R. J., & Hochstrasser, M. (2013). Molecular architecture and assembly of the eukaryotic proteasome. *Annual Review of Biochemistry*, 82, 415–445. <https://doi.org/10.1146/annurev-biochem-060410-150257>

- Tondera, D., Czauderna, F., Paulick, K., Schwarzer, R., Kaufmann, J., & Santel, A. (2005). The mitochondrial protein MTP18 contributes to mitochondrial fission in mammalian cells. *Journal of Cell Science*, *118*(14), 3049–3059. <https://doi.org/10.1242/jcs.02415>
- Toste Rêgo, A., & da Fonseca, P. C. A. (2019a). Characterization of Fully Recombinant Human 20S and 20S-PA200 Proteasome Complexes. *Molecular Cell*, *76*(1), 138-147.e5. <https://doi.org/10.1016/j.molcel.2019.07.014>
- Toste Rêgo, A., & da Fonseca, P. C. A. (2019b). Characterization of Fully Recombinant Human 20S and 20S-PA200 Proteasome Complexes. *Molecular Cell*, *76*(1), 138-147.e5. <https://doi.org/10.1016/j.molcel.2019.07.014>
- Trushina, E., Nemetlu, E., Zhang, S., Christensen, T., Camp, J., Mesa, J., Siddiqui, A., Tamura, Y., Sesaki, H., Wengenack, T. M., Dzeja, P. P., & Poduslo, J. F. (2012). Defects in mitochondrial dynamics and metabolomic signatures of evolving energetic stress in mouse models of familial alzheimer's disease. *PLoS ONE*, *7*(2). <https://doi.org/10.1371/journal.pone.0032737>
- Tsukuda, T., Fleming, A. B., Nickoloff, J. A., & Osley, M. A. (2005). Chromatin remodelling at a DNA double-strand break site in *Saccharomyces cerevisiae*. *Nature*, *438*(7066), 379–383. <https://doi.org/10.1038/nature04148>
- Uechi, H., Hamazaki, J., & Murata, S. (2014). Characterization of the testis-specific proteasome subunit  $\alpha 4s$  in mammals. *Journal of Biological Chemistry*, *289*(18), 12365–12374. <https://doi.org/10.1074/jbc.M114.558866>
- Ustrell, V., Hoffman, L., Pratt, G., & Rechsteiner, M. (2002). Pa200, a nuclear proteasome activator involved in DNA repair. *EMBO Journal*, *21*(13), 3516–3525. <https://doi.org/10.1093/emboj/cdf333>
- Ustrell, V., Pratt, G., Gorbea, C., & Rechsteiner, M. (2005). Purification and assay of proteasome activator PA200. *Methods in Enzymology*, *398*, 321–329. [https://doi.org/10.1016/S0076-6879\(05\)98026-9](https://doi.org/10.1016/S0076-6879(05)98026-9)
- Vafai, S. B., & Mootha, V. K. (2012). Mitochondrial disorders as windows into an ancient organelle. *Nature*, *491*(7424), 374–383. <https://doi.org/10.1038/nature11707>
- Van Ark, G., & Berden, J. A. (1977). Binding of HQNO to beef-heart sub-mitochondrial particles. *BBA - Bioenergetics*, *459*(1), 119–137. [https://doi.org/10.1016/0005-2728\(77\)90014-7](https://doi.org/10.1016/0005-2728(77)90014-7)
- Vecoli, C., Borghini, A., Pulignani, S., Mercuri, A., Turchi, S., Carpeggiani, C., Picano, E., & Andreassi, M. G. (2018). Prognostic value of mitochondrial DNA4977 deletion and mitochondrial DNA copy number in patients with stable coronary artery disease. *Atherosclerosis*, *276*, 91–97. <https://doi.org/10.1016/j.atherosclerosis.2018.07.015>
- Verkaart, S., Koopman, W. J. H., Cheek, J., van Emst-de Vries, S. E., van den Heuvel, L. W. P. J., Smeitink, J. A. M., & Willems, P. H. G. M. (2007). Mitochondrial and cytosolic thiol redox state are not detectably altered in isolated human NADH:ubiquinone oxidoreductase deficiency. *Biochimica et Biophysica Acta - Molecular Basis of Disease*, *1772*(9), 1041–1051. <https://doi.org/10.1016/j.bbadis.2007.05.004>

- Vichai, V., & Kirtikara, K. (2006). Sulforhodamine B colorimetric assay for cytotoxicity screening. *Nature Protocols*, *1*(3), 1112–1116. <https://doi.org/10.1038/nprot.2006.179>
- Vogel, R. O., Smeitink, J. A. M., & Nijtmans, L. G. J. (2007). Human mitochondrial complex I assembly: A dynamic and versatile process. *Biochimica et Biophysica Acta - Bioenergetics*, *1767*(10), 1215–1227. <https://doi.org/10.1016/j.bbabi.2007.07.008>
- Vyas, S., Zaganjor, E., & Haigis, M. C. (2016). Mitochondria and Cancer. *Cell*, *166*(3), 555–566. <https://doi.org/10.1016/j.cell.2016.07.002>
- Wai, T., & Langer, T. (2016). Mitochondrial Dynamics and Metabolic Regulation. *Trends in Endocrinology and Metabolism*, *27*(2), 105–117. <https://doi.org/10.1016/j.tem.2015.12.001>
- Wallace, D. C. (2005). A mitochondrial paradigm of metabolic and degenerative diseases, aging, and cancer: A dawn for evolutionary medicine. *Annual Review of Genetics*, *39*, 359–407. <https://doi.org/10.1146/annurev.genet.39.110304.095751>
- Walsh, C. T., Tu, B. P., & Tang, Y. (2018). Eight Kinetically Stable but Thermodynamically Activated Molecules that Power Cell Metabolism. *Chemical Reviews*, *118*(4), 1460–1494. <https://doi.org/10.1021/acs.chemrev.7b00510>
- Wang, F., Ma, H., Liang, W. J., Yang, J. J., Wang, X. Q., Shan, M. R., Chen, Y., Jia, M., Yin, Y. L., Sun, X. Y., Zhang, J. N., Peng, Q. S., Chen, Y. G., Liu, L. Y., Li, P., Guo, T., & Wang, S. X. (2017). Lovastatin upregulates microRNA-29b to reduce oxidative stress in rats with multiple cardiovascular risk factors. *Oncotarget*, *8*(6), 9021–9034. <https://doi.org/10.18632/oncotarget.14462>
- Wang, J., Xiong, S., Xie, C., Markesbery, W. R., & Lovell, M. A. (2005). Increased oxidative damage in nuclear and mitochondrial DNA in Alzheimer's disease. *Journal of Neurochemistry*, *93*(4), 953–962. <https://doi.org/10.1111/j.1471-4159.2005.03053.x>
- Wang, X., & Robbins, J. (2014). Proteasomal and lysosomal protein degradation and heart disease. *Journal of Molecular and Cellular Cardiology*, *71*, 16–24. <https://doi.org/10.1016/j.yjmcc.2013.11.006>
- Wei, Y. H., Lu, C. Y., Lee, H. C., Pang, C. Y., & Ma, Y. S. (1998). Oxidative damage and mutation to mitochondrial DNA and age-dependent decline of mitochondrial respiratory function. *Annals of the New York Academy of Sciences*, *854*, 155–170. <https://doi.org/10.1111/j.1749-6632.1998.tb09899.x>
- Welk, V., Meul, T., Lukas, C., Kammerl, I. E., Mulay, S. R., Schamberger, A. C., Semren, N., Fernandez, I. E., Anders, H. J., Günther, A., Behr, J., Eickelberg, O., Korfei, M., & Meiners, S. (2019). Proteasome activator PA200 regulates myofibroblast differentiation. *Scientific Reports*, *9*(1), 1–11. <https://doi.org/10.1038/s41598-019-51665-0>
- Whitehall, J. C., & Greaves, L. C. (2020). Aberrant mitochondrial function in ageing and cancer. *Biogerontology*, *21*(4), 445–459. <https://doi.org/10.1007/s10522-019-09853-y>
- Wisdom, R., Johnson, R. S., & Moore, C. (1999). c-Jun regulates cell cycle progression and apoptosis by distinct mechanisms. *EMBO Journal*, *18*(1), 188–197. <https://doi.org/10.1093/emboj/18.1.188>

- Wolvetang, E. J., Johnson, K. L., Krauer, K., Ralph, S. J., & Linnane, A. W. (1994). Mitochondrial respiratory chain inhibitors induce apoptosis. *FEBS Letters*, 339(1–2), 40–44. [https://doi.org/10.1016/0014-5793\(94\)80380-3](https://doi.org/10.1016/0014-5793(94)80380-3)
- Wong, E. D., Wagner, J. A., Gorsich, S. W., McCaffery, J. M., Shaw, J. M., & Nunnari, J. (2000). The dynamin-related GTPase, Mgm1p, is intermembrane space protein required for maintenance of fusion competent mitochondria. *Journal of Cell Biology*, 151(2), 341–352. <https://doi.org/10.1083/jcb.151.2.341>
- Woo, H. P., Yong, W. H., Suh, H. K., & Sung, Z. K. (2007). An ROS generator, antimycin A, inhibits the growth of HeLa cells via apoptosis. *Journal of Cellular Biochemistry*, 102(1), 98–109. <https://doi.org/10.1002/jcb.21280>
- Wu, M., Gu, J., Guo, R., Huang, Y., & Yang, M. (2016). Structure of Mammalian Respiratory Supercomplex I<sub>1</sub>III<sub>2</sub>IV<sub>1</sub>. *Cell*, 167(6), 1598–1609.e10. <https://doi.org/10.1016/j.cell.2016.11.012>
- Xicoy, H., Wieringa, B., & Martens, G. J. M. (2017). The SH-SY5Y cell line in Parkinson's disease research: a systematic review. *Molecular Neurodegeneration*, 12(1), 1–11. <https://doi.org/10.1186/s13024-017-0149-0>
- Xu, S., Cherek, E., Das, S., Li, S., Roelofs, B. A., Ge, S. X., Polster, B. M., Boyman, L., Lederer, W. J., Wang, C., & Karbowski, M. (2016). Mitochondrial E3 ubiquitin ligase MARCH5 controls mitochondrial fission and cell sensitivity to stress-induced apoptosis through regulation of MiD49 protein. *Molecular Biology of the Cell*, 27(2), 349–359. <https://doi.org/10.1091/mbc.E15-09-0678>
- Yamamoto, H., Morino, K., Mengistu, L., Ishibashi, T., Kiriya, K., Ikami, T., & Maegawa, H. (2016). Amla Enhances Mitochondrial Spare Respiratory Capacity by Increasing Mitochondrial Biogenesis and Antioxidant Systems in a Murine Skeletal Muscle Cell Line. *Oxidative Medicine and Cellular Longevity*, 2016. <https://doi.org/10.1155/2016/1735841>
- Yang, F., Li, B., Yang, Y., Huang, M., Liu, X., Zhang, Y., Liu, H., Zhang, L., Pan, Y., Tian, S., Wu, Y., Wang, L., & Yang, L. (2019). Leptin enhances glycolysis via OPA1-mediated mitochondrial fusion to promote mesenchymal stem cell survival. *International Journal of Molecular Medicine*, 44(1), 301–312. <https://doi.org/10.3892/ijmm.2019.4189>
- Yang, L., Achreja, A., Yeung, T. L., Mangala, L. S., Jiang, D., Han, C., Baddour, J., Marini, J. C., Ni, J., Nakahara, R., Wahlig, S., Chiba, L., Kim, S. H., Morse, J., Pradeep, S., Nagaraja, A. S., Haemmerle, M., Kyunghee, N., Derichsweiler, M., ... Nagraath, D. (2016). Targeting Stromal Glutamine Synthetase in Tumors Disrupts Tumor Microenvironment-Regulated Cancer Cell Growth. *Cell Metabolism*, 24(5), 685–700. <https://doi.org/10.1016/j.cmet.2016.10.011>
- Yang, Z., & Klionsky, D. J. (2010). Mammalian autophagy: Core molecular machinery and signaling regulation. *Current Opinion in Cell Biology*, 22(2), 124–131. <https://doi.org/10.1016/j.ceb.2009.11.014>
- Yao, T., & Cohen, R. E. (2002). A cryptic protease couples deubiquitination and degradation by the proteasome. *Nature* 419, 403–407. *Molecular. Nature*, 419(September), 406–407. <https://doi.org/10.1038/nature00962.1>

- Yonashiro, R., Ishido, S., Kyo, S., Fukuda, T., Goto, E., Matsuki, Y., Ohmura-Hoshino, M., Sada, K., Hotta, H., Yamamura, H., Inatome, R., & Yanagi, S. (2006). A novel mitochondrial ubiquitin ligase plays a critical role in mitochondrial dynamics. *EMBO Journal*, *25*(15), 3618–3626. <https://doi.org/10.1038/sj.emboj.7601249>
- Yonashiro, R., Sugiura, A., Miyachi, M., Fukuda, T., Matsushita, N., Inatome, R., Ogata, Y., Suzuki, T., Dohmae, N., & Yanagi, S. (2009). Mitochondrial Ubiquitin Ligase MITOL Ubiquitinates Mutant SOD1 and Attenuates Mutant SOD1-induced Reactive Oxygen Species Generation. *Molecular Biology of the Cell*, *20*, 4524–4530. <https://doi.org/10.1091/mbc.e09-02-0112>
- Yuan, X., Miller, M., & Belote, J. M. (1996). Duplicated proteasome subunit genes in *Drosophila melanogaster* encoding testes-specific isoforms. *Genetics*, *144*(1), 147–157. <https://doi.org/10.1093/genetics/144.1.147>
- Zannini, L., Lecis, D., Buscemi, G., Carlessi, L., Gasparini, P., Fontanella, E., Lisanti, S., Barton, L., & Delia, D. (2008). REG $\gamma$  proteasome activator is involved in the maintenance of chromosomal stability. *Cell Cycle*, *7*(4), 504–512. <https://doi.org/10.4161/cc.7.4.5355>
- Zhang, Y., Liu, T., Meyer, C. A., Eeckhoute, J., Johnson, D. S., Bernstein, B. E., Nussbaum, C., Myers, R. M., Brown, M., Li, W., & Shirley, X. S. (2008). Model-based analysis of ChIP-Seq (MACS). *Genome Biology*, *9*(9). <https://doi.org/10.1186/gb-2008-9-9-r137>
- Zorzano, A., & Claret, M. (2015). Implications of mitochondrial dynamics on neurodegeneration and on hypothalamic dysfunction. *Frontiers in Aging Neuroscience*, *7*(JUN), 1–17. <https://doi.org/10.3389/fnagi.2015.00101>

## **APPENDIX**

The thesis is based on the following publications:



Registry number: DEENK/102/2021.PL  
Subject: PhD Publication List

Candidate: Abdennour Douida  
Doctoral School: Doctoral School of Molecular Medicine

### List of publications related to the dissertation

1. **Douida, A.**, Batista, F., Botó, P., Regdon, Z., Robaszkiewicz, A., Tar, K.: Cells Lacking PA200 Adapt to Mitochondrial Dysfunction by Enhancing Glycolysis via Distinct Opa1 Processing. *Int. J. Mol. Sci.* 22 (4), 1-22, 2021.  
DOI: <http://dx.doi.org/10.3390/ijms22041629>  
IF: 4.556 (2019)
2. **Douida, A.**, Batista, F., Robaszkiewicz, A., Botó, P., Aladdin, A., Szenyiv, M., Czinege, R., Virág, L., Tar, K.: The proteasome activator PA200 regulates expression of genes involved in cell survival upon selective mitochondrial inhibition in neuroblastoma cells. *J. Cell. Mol. Med.* 24 (12), 6716-6730, 2020.  
DOI: <http://dx.doi.org/10.1111/jcmm.15323>  
IF: 4.486 (2019)

**Total IF of journals (all publications): 9,042**

**Total IF of journals (publications related to the dissertation): 9,042**

The Candidate's publication data submitted to the iDEa Tudóstér have been validated by DEENK on the basis of the Journal Citation Report (Impact Factor) database.

17 March, 2021

